



FLOODSTAND-deliverable:

**Pressure losses and flow velocities in flow through manholes
and cross-ducts**

Author	Mikael Stening
Organisation	Aalto University (TKK)
Revision	1.2.1
Deliverable No.	D2.3

Date	7 December 2010
------	-----------------



Document identification sheet	
FLOODSTAND	Integrated Flooding Control and Standard for Stability and Crises Management
FP7-RTD- 218532	
Title: Pressure losses and flow velocities in flow through manholes and cross-ducts	
Other report identifications:	
Investigating partners: AALTO (TKK)	
Author: Mikael Stening	
Reviewed by: Juha Järvelä, Harri Koivusalo	
<input type="checkbox"/> Outline <input type="checkbox"/> Draft <input checked="" type="checkbox"/> Final Version number: 1.2.1 Revision date: 7 December 2010 Next version due: Number of pages: 103	<input checked="" type="checkbox"/> A deliverable <input type="checkbox"/> Part of a deliverable <input type="checkbox"/> Cover document for a part of a deliverable <input type="checkbox"/> Deliverable cover document <input type="checkbox"/> Other Deliverable number: D2.3 Work Package: WP2 Deliverable due at month: 14
Accessibility:	Available from: December 2010
<input checked="" type="checkbox"/> Public <input type="checkbox"/> Restricted <input type="checkbox"/> Confidential (consortium only) <input type="checkbox"/> Internal (accessibility defined for the final version)	Distributed to:
	Discloses when restricted:
	Comments: This deliverable can be downloaded from the web-page: http://floodstand.tkk.fi/Info/public_download.html Note! Correction of an error in figure 63 has been implemented in this revision 1.2.1 of deliverable D2.3.
<p>Abstract: Laboratory experiments were conducted to examine the discharge coefficients of manholes and cross-ducts. In addition, flow velocities in the vicinity of a cross-duct girder were examined. The tested objects were a full-scale manhole, a 1:2 scale model manhole, a 1:3 scale model cross-duct and a 1:3 scale model girder with two manholes.</p> <p>In free flow the scale models had higher discharge coefficients than the full-scale manhole, but the relationship was opposite in submerged flow. Structural stiffeners were found to increase the value of the discharge coefficient. The influence of flow velocity and the web-frame was small.</p> <p>The experimentally obtained discharge coefficients for the cross-duct were smaller than the corresponding values derived with the standard computational method recommended by the International Maritime Organization (IMO). The results suggested that the geometry of the girders and the influence of stiffeners should be taken into account when determining a discharge coefficient for a cross-duct.</p>	

Acknowledgements

The research leading to these results has received funding from the European Union's Seventh Framework Programme (FP7/2007-2013) under grant agreement n° 218532. The financial support is gratefully appreciated.

Disclaimer

Neither the European Commission nor any person acting on behalf of the FLOODSTAND Consortium is responsible for the use, which might be made of the following information. The views expressed in this report are those of the authors and do not necessarily reflect those of the European Commission and other members of the FLOODSTAND Consortium.

Copyright © 2010 FP7 FLOODSTAND project consortium
 Reproduction is authorized provided the source is acknowledged

PREFACE

This report, deliverable D2.3, is the result of Task 2.3, “Experimental studies on pressure losses”. It is one of the several reports of Work Package 2, “Flooding progression modelling”, of the project “Integrated Flooding Control and Standard for Stability and Crises Management”, abbreviated as FLOODSTAND¹. The Collaborative project FLOODSTAND, Grant Agreement number: 218532 (SCP7-GA-2009-218532) belongs to the seventh Framework Program (FP7). It is funded by the European Commission within the group of Small or medium scale focused research projects.

This one volume report, deliverable D2.3, “Pressure losses and flow velocities in flow through manholes and crossducts”, includes a description of the scientific research carried out in Task 2.3 and its results. The work related to this study was carried out at the Water Engineering Group and at the Marine Technology Group of the Aalto University School of Science and Technology. The research was mainly carried out by the author, Mr. Mikael Stening², who carried out the experimental tests with the assistance of Mr Antti Louhio². The former carried out the analysis, leading to the results and wrote the report. Dr Juha Järvelä² was the Task Leader of Task 2.3. He was involved in the early planning phase of Task 2.3, but acted also actively in the co-operative and supervisory tasks at the later stages of the task. He acted also as a reviewer of this report. In the last task he was accompanied with professor Harri Koivusalo². The model was designed and built in the workshop of Marine Technology Group by the team consisting of Mr Risto Ripatti³, who prepared all the cross-duct model drawings and Mr Jarmo Leinonen³ and Mr Pentti Tukia³, who built the model, under the supervision of Mr Keijo Hanhiova³ (who also participated in the early planning of the tests). Mr Risto Jalonen³ participated in the work of Task 2.3, where his role included: being a contact person between all persons and organisations involved, some planning, participating in Task-level meetings, many discussions and some commenting, too.

Mrs Anna-Lea Routi, Mr Markku Kajosaari (STX Finland Oy) and Mr Henning Luhman (Meyer Werft GmbH) took part in the early planning phase of Task 2.3 and participated meetings and discussions related to it. A full size manhole cut in a steel plate to be tested and some information related to typical cross-duct structures in a large passenger ship being of assistance for the planning and design of the cross-duct model were delivered by STX Finland. Dr Pekka Ruponen (Napa Ltd) participated in Task 2.3 in the role as the assisting technical manager of the project FLOODSTAND, mainly in the early planning phase of Task 2.3, but also by giving valuable comments to the refined test plans and the manuscript of this report. He acted actively also by participating many Task-level meetings and discussions related to this.

I want to present my thanks to all the organizations listed and especially all the persons mentioned, who have contributed, with all their well-performed efforts and co-operation, to the work in this Task 2.3 to make it successful.

Risto Jalonen
Project manager
Coordinator of project FLOODSTAND,
Work Package Manager (WPM) of WP2

¹ The project FLOODSTAND is funded by the European Commission 7th Framework Program under contract SCP7-GA-218532. The project was started in March 2009 and the project duration is 36 months. The partners on the project FLOODSTAND are:

Aalto University (ex. **Teknillinen korkeakoulu**, which has been merged to Aalto University since 1.1.2010 as the School of Science and Technology), **Finland**; **STX Finland Oy, Finland**; Centre National de la Recherche Scientifique, France; Centrum Techniki Okretowej Spolka Akcyjna, Poland; Det Norske Veritas AS, Norway; BMT Group Limited, United Kingdom; Stichting Maritiem Research Instituut Nederland, The Netherlands; MEC Insenerilahendused, Estonia; **MEYER WERFT GmbH, Germany**; **Napa Ltd, Finland**; SSPA Sweden AB, Sweden; SF-Control Oy; Finland; National Technical University of Athens - Ship Design Laboratory, Greece; Bureau Veritas – Registre International de Classification de Navires et d Aeronefs SA, France; Safety At Sea Limited, United Kingdom; Maritime and Coastguard Agency, United Kingdom; University of Strathclyde, United Kingdom

² At the time of the work related to Task 2.3 in project FLOODSTAND (218532) he was working at the Water Engineering Group of the Aalto University School of Science and Technology.

³ At the time of the work related to Task 2.3 in project FLOODSTAND (218532) he was working at the Marine Technology Group of the Aalto University School of Science and Technology.

Table of contents

Executive Summary	6
List of Symbols.....	7
Glossary	8
1 Introduction.....	9
1.1 Background.....	9
1.2 Different approaches to solve the problem	10
1.3 Objectives and scope of the study	12
2 Discharge coefficient variation.....	13
2.1 General computational considerations.....	13
2.2 Opening form and scale effects.....	15
2.3 Distance between girders and number of openings on girders.....	17
2.4 Incomplete contraction of the jet due to the approach channel	17
2.5 Tail water level	19
2.6 Influence of flow velocity and other uncertain factors	20
2.7 Summary of discharge coefficient variation	21
3 Methods	23
3.1 Laboratory studies	23
3.1.1 Flume and water circulation system.....	23
3.1.2 Measurement considerations and arrangements.....	24
3.1.3 Description of the test objects	25
3.2 Discharge equations for different flow conditions.....	27
3.2.1 Free flow.....	28
3.2.2 Submerged orifice flow	30
3.2.3 Submerged weir flow and partly submerged orifice flow	32
3.3 Other computational aspects	35
3.3.1 Scale similarity formula.....	35
3.3.2 Inclination.....	35
3.3.3 Discharge coefficient of a duct	36
3.3.4 Scale effect correction factor	37

4	Test cases	37
4.1	Full-scale manhole	38
4.2	Scale model manhole	39
4.3	Scale model girders.....	39
4.3.1	Velocity measurements.....	41
4.4	Scale model cross-duct.....	44
5	Errors and uncertainty of measurements and computations	45
5.1	Calibration and measurement accuracy.....	46
5.2	Statistical distribution of measured values.....	48
5.3	Statistical comparison of results.....	49
5.4	Pressure losses due to the flume.....	49
5.5	Other sources of error	50
6	Results and discussion	51
6.1	Single manholes and girders	51
6.1.1	Free flow.....	51
6.1.2	Partly and completely submerged flow	56
6.1.3	Flow velocities in submerged flow through a girder.....	66
6.2	Cross-duct	72
6.2.1	Comparison of measured and computed discharge coefficients...	77
6.3	Remarks on the applicability of the results	81
7	Conclusions and recommendations	82
8	References	83
	Appendix I: Photographs from the experiments	86

Executive Summary

The survivability of passenger ships in damaged condition is assessed with flooding simulation tools. The reliability of these tools depends on the availability of proper discharge coefficients for various flow obstacles. The present investigation was motivated by the fact that there was a gap in the knowledge about discharge coefficients for typical openings in ships and the factors which affect their values. Associated hydraulic phenomena can be examined either on the basis of experiments or with computational fluid dynamics (CFD). Experimental data are, however, needed to verify CFD simulations. Therefore laboratory experiments were carried out to examine pressure losses and flow velocities in flow through manholes and cross-ducts, and to gain knowledge about the properties which affect the discharge coefficient. The purpose of this deliverable is to report the experimentally obtained results and recommendations.

The experiments were carried out in a laboratory flume at the Water Engineering Group of the Aalto University School of Science and Technology. The tested objects were a full-scale manhole, a 1:2 scale model manhole, a 1:3 scale model cross-duct and a 1:3 scale model cross-duct girder with two manholes. The influence of the length and the inclination of the cross-duct, the structural stiffeners, and the web-frame were examined. Discharge and level of submergence were varied in the tests.

The discharge coefficient for the full-scale manhole was typically 0.58-0.59 when the jet discharged into air. The corresponding values for the scale models were up to 5% higher. In submerged flow, the discharge coefficient for the full-scale manhole and the scale model manhole and girders were in the ranges of 0.67-0.70 and 0.63-0.67, respectively. Structural stiffeners were found to increase significantly the value of the discharge coefficient. The influence of the flow velocity and the web-frame was small.

Experimentally obtained discharge coefficients for cross-ducts were compared to estimates obtained with the standard computational methods of the International Maritime Organization (IMO). The computational methods were found to overestimate the discharge coefficients. The results suggested that the geometry of the girders and the influence of stiffeners should be taken into account when determining the discharge coefficient for a cross-duct.

List of Symbols

A	flow area of cross section, [m ²]
A_O	cross-sectional area of the opening(s), [m ²]
$b(z)$	width of the manhole at a certain height z from the bottom of the opening
C_D	discharge coefficient, $C_D = Q_A/Q_T$. The discharge coefficient is sometimes referred to as the speed reduction factor
D	hydraulic diameter $D = 4A/P$, [m]
d_z	depth of flow, [m]
F_R	Froude number, $F_R = \frac{u}{\sqrt{gd_z}}$
h_D	downstream elevation head, [m]
h_D^*	downstream elevation head at the opening, $h_D^* < h_D$, [m]
h_O	height of the opening, i.e. the manhole, [m]
h_u	upstream elevation head, [m]
g	acceleration due to gravity, $g = 9.81$ [m/s ²]
H_U	total upstream head (velocity head included), [m]
h_V	head over the measurement weir, [m]
k_L	pressure loss coefficient
P	wetted perimeter of cross section, [m]
ρ	height of the lower edge of the opening from the flume bed, [m]
ρ_x	pressure (not examined in this study), [Pa]
Q_A	actual discharge measured over the laboratory 90° V-notch weir, [m ³ /s]
Q_T	computed theoretical discharge of an ideal fluid, [m ³ /s]
Re_O	orifice Reynolds number $Re_O = uD^2/(vd)$
u_U	average actual upstream flow velocity, [m/s]
u_T	theoretical velocity at a certain height of the opening [m/s]
μ	viscosity, for water $\mu = 1.040 \cdot 10^{-3}$ [Ns/m ²]
ν	kinematic viscosity $\nu = \mu/\rho$, in this study $\nu = 1.04 \cdot 10^{-6}$ [m ² /s]
ρ	density, for water with 0% salinity $\rho = 1000$ [kg/m ³]

Glossary

ADV	Acoustic Doppler Velocimetre. Measurement device used for flow velocity measurements.
CFD	Computational Fluid Dynamics
Cross-duct	Cross-flooding duct typically in the double bottom of a ship. The purpose of the duct is to lead water from one side of the ship to the other in the case of an accident.
Discharge coefficient	Coefficient used in non-viscous flow theory to correct ideal fluid computations for the properties of real fluids.
Downstream side	Compartment into which water flows through an opening.
Energy loss	Synonym for pressure loss.
Flooding simulation	Computational tool used to estimate the flooding time of a vessel.
Free flow	Flow condition, in which the jet discharges into air.
Girder	Dividing wall of a cross-duct with openings for water to pass through.
Head	Term used to describe the energy water possesses in [m]. The total head consists of elevation head (e.g. h_U or h_D), velocity head and pressure head.
Ideal flow	Flow of an ideal fluid, i.e. a fluid which is not affected by viscosity, friction and turbulence.
IMO	International Maritime Organization
MSC	Maritime Safety Committee, a committee of the IMO
Pressure loss	Head loss when water flows from one point to another.
Stationary flow	Flow condition, in which the same amount of water enters and exits a compartment. The flow velocity and the heads are theoretically constant with time.
Stiffener	Steel beam, which makes a construction stiffer and more durable.
Submerged flow	Flow condition, in which the jet discharges into water.
Unsteady flow	Flow condition, in which the flow velocity and the heads change with time.
Upstream side	Compartment from which water flows through an opening.
Web-frame	Plate with manholes placed in the longitudinal direction (of the cross-duct) inside the cross-duct.
Wing tank	Compartment on the side of a ship.

1 Introduction

1.1 Background

Flooding is considered a major risk to people onboard ships. Current safety regulations require various flow computations (e.g. Söding 2002). The time dependent survivability of ships in damaged conditions is estimated with flooding simulation tools.

Flooding simulations are based on either viscous or non-viscous flow theory. The application of viscous flow theory in ship scale flooding simulations is currently considered too slow. Current vessel flooding simulation tools are therefore based on non-viscous flow theory (Ruponen 2007, p. 21). In non-viscous flow theory, the computed ideal discharge needs to be corrected for the viscosity, the friction and the turbulence of real fluids. These effects are taken into account by multiplying the ideal discharge with an empirical discharge coefficient, C_D . Recent studies prove that current flooding simulation tools provide reasonable estimates when the affecting parameters are properly taken into account (Ruponen 2006b). A main challenge is to find proper discharge coefficients for different openings.

Discharge coefficients for typical openings such as round, rectangular and triangular openings can be found in hydraulic engineering manuals. There is, however, a lack of experimental data on the discharge coefficients of some important types of openings on ships. This study was focused on the discharge coefficients of a manhole and a cross flooding duct, which consists of a corridor divided by several girders with manholes (Figure 1).

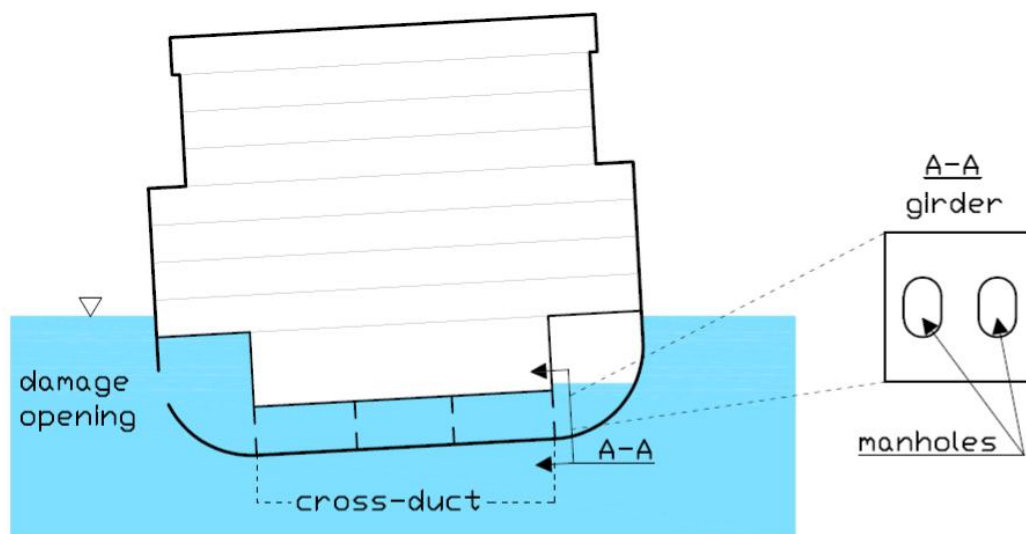


Figure 1. A schematic cross-sectional drawing of a cross-flooding arrangement in a passenger ship. Manholes are not only installed in cross-ducts, but also in many other places on the ship.

A manhole is an opening with a size large enough for an adult individual to pass through the hole. Manholes in ships make construction and maintenance work possible in places which otherwise would be inaccessible. Manholes also serve as passages later during inspections.

Cross-flooding ducts, or simply cross-ducts, are installed in ship double bottoms in order to allow water to pass between the wing tanks of the ship. This decreases the heel angle of the ship in the case of an accident (Figure 1). In most state-of-the-art flooding simulations the cross-duct is treated as a single structure with one discharge coefficient, which is computed on the basis of discharge coefficients of single manholes. Other components that might affect the discharge coefficient are typically neglected.

Only a few studies exist on the pressure losses of a cross-duct (e.g. Vredeveltdt and Journée 1991). One of the most current studies on a cross-duct is the CFD (Computational Fluid Dynamics) based study by Pittaluga and Giannini (2006). It is highly important to acquire new experimental data about the subject, not at least in order to provide verifying data for future CFD analyses.

There is some confusion about the many different object and environment properties, which affect the discharge coefficient. Discharge coefficient variation was therefore first examined on a general level on the basis of literature. Laboratory flume experiments were conducted in order to acquire new data on the behaviour of the discharge coefficient of a manhole and a cross-duct in different flow conditions.

1.2 Different approaches to solve the problem

The discharge properties of any object can be examined in two ways:

- 1) By applying a CFD model
- 2) By conducting hydraulic experiments

CFD analyses are typically Finite Volume Models (FVM) based on viscous flow theory. CFD computations are a lucrative method for hydrodynamic engineering problems, because they make it possible to construct test cases, which would be difficult to achieve experimentally. However, it has been pointed out that there is a need of to experimentally verify the results achieved with CFD analyses in order to know their trustworthiness (e.g. Ruponen 2007, p. 32). Experiments and CFD analyses should complement each other.

The other possible way to examine the discharge properties is to conduct full-scale or scale model experiments, and compare the measured results with

computations based on non-viscous flow theory. Field measurements, i.e. measurements with a real full-scale test object, are preferable, but in practice often difficult or even impossible to conduct. Experiments are therefore usually performed with a scale model in a laboratory environment, where it is possible to control and measure the actual discharge Q_A . One of the downsides with scale model experiments is that the scale affects the results. Experiments are, however, still widely considered the most reliable way to acquire information about hydraulic phenomena.

There are two main types of experiments, which can be used to study pressure losses in flow through a manhole or a cross-duct. One way is to attach the test object to a wing tank and then quickly lower the system into a large water tank. Water starts to flow through the test object into the tank, where the water level is monitored (Figure 2). The time to fill up the tank is recorded, and an equation provided in the IMO A.266(VIII) or MSC.245(83) resolution is applied to compute the average discharge coefficient of the test object.

The head and the corresponding discharge decrease as a function of time, i.e. the flow is unsteady. Parameters of interest are the size of the wing tank and the depth of the test object. These properties vary depending on the ship and its draught and heel angle. Modifications of this approach are applied in studies by Ikeda and Takayama (2005) and Vreedeveltdt and Journée (1991), which are described in section 2.6.

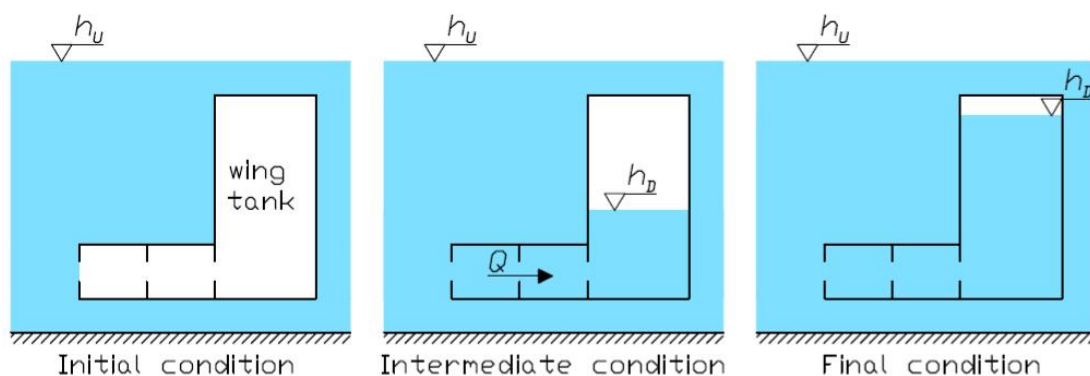


Figure 2. An example of an experiment for the determination of the average discharge coefficient in unsteady flow conditions. The time to reach a certain water level inside the tank is measured. The wing tank can either be ventilated or air-proof, as depicted.

The other experiment type is to examine the test object in a laboratory flume, where the actual discharge Q_A can be measured. In such tests the discharge coefficient can be determined for different discharges and up- and downstream water level combinations (Figure 3). The up- and downstream elevation heads h_U and h_D are measured and the corresponding ideal discharge Q_T is computed.

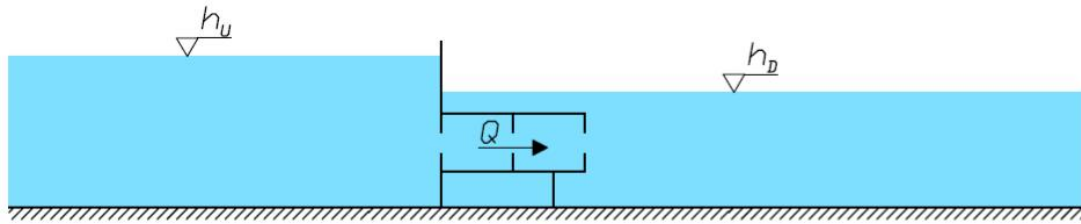


Figure 3. The discharge coefficient can be determined in stationary flow conditions in a laboratory flume. The actual discharge Q_A and the corresponding up- and downstream heads h_U and h_D are measured.

In this type of experiments the flow is stationary, which means that the discharge, flow velocities and relative positions of the upstream and downstream heads are nearly constant. This approach or test type was applied in this study. The theory and equations which are used to compute the ideal discharge are presented in section 3.

1.3 Objectives and scope of the study

The goal of the study is to improve knowledge on the flow properties in different flow conditions through manholes and cross-ducts. The specific objectives are:

- 1) Determination of the factors that cause variation in the discharge coefficient value on the basis of literature. When possible, these factors were taken into account and analysed in the laboratory flume tests.
- 2) Determination of the discharge coefficient of a manhole in different flow conditions using laboratory experiments.
 - 2.a) Discharge coefficients for free flow through a manhole.
 - 2.b) Discharge coefficients for submerged flow through manhole.
 - 2.c) Discharge coefficients for a partly submerged manhole.
- 3) Estimation of the potential scale effects related to the tests.
- 4) Determination of the discharge coefficients of a typical cross-duct.
 - 4.a) Influence of the number of girders
 - 4.b) Influence of other components inside the cross-duct
 - 4.c) Evaluation of the standard computational discharge coefficient estimation methods for cross-ducts (IMO) on the basis of test results.
- 5) To gather experimental data about the flow velocity field in the vicinity of the manholes of a girder for the verification of CFD computations.

The laboratory experiments are limited to stationary flow with relatively low heads. The influence of air compression falls outside the scope of this study.

2 Discharge coefficient variation

The discharge coefficient is often assumed constant, but in fact its value is affected by many environmental conditions and object properties. The aim of this chapter is to give an overview of the possible causes behind discharge coefficient variation on the basis of a literature review. The significance of these causes and the possibility to examine them in the experiments of this study are discussed.

2.1 General computational considerations

All computations in this study were based on non-viscous flow theory. The fundamental equations are the continuity equation (1) and the Bernoulli equation (2), which is one form of the energy equation (Blevins 1984, p. 29):

$$Q = u_1 A_1 = u_2 A_2, \quad (1)$$

$$h_1 + \frac{u_1^2}{2g} + \frac{p_1}{\rho g} = h_2 + \frac{u_2^2}{2g} + \frac{p_2}{\rho g} + \frac{1}{2} k_L u_2^2, \quad (2)$$

where Q is the discharge, A_x is the cross-sectional area, u_x the flow velocity, h_x is the vertical distance from a reference level and p_x is the external pressure at two locations, noted by their sub-indexes. The last term describes the pressure loss in the opening, which depends on the pressure loss coefficient k_L and the mean flow velocity through the opening (e.g. Pittaluga and Giannini 2006, p. 20). Equation (2) can sometimes be simplified by assuming atmospheric external pressure ($p_1 = p_2$).

The pressure loss coefficient k_L is introduced in order to take all the non-ideal properties of real fluids into account. Real fluids, such as water, are affected by viscosity, friction and turbulence. The pressure loss coefficient needs to be determined in experiments.

Flow obstacles, such as walls with openings, are the most important sources of pressure losses. The pressure loss at a flow obstacle can be divided into contraction losses and expansion losses (Walshaw 1979, p. 315-320). Pressure losses due to contraction of the jet are relatively small (Walshaw and Jobson 1979, p. 78). Most of the total pressure losses occur when the jet diverges at the opening. The sudden expansion of the jet creates turbulent eddies, in which energy is converted into heat and noise (Bos 1989, p. 63) (Figure 4).

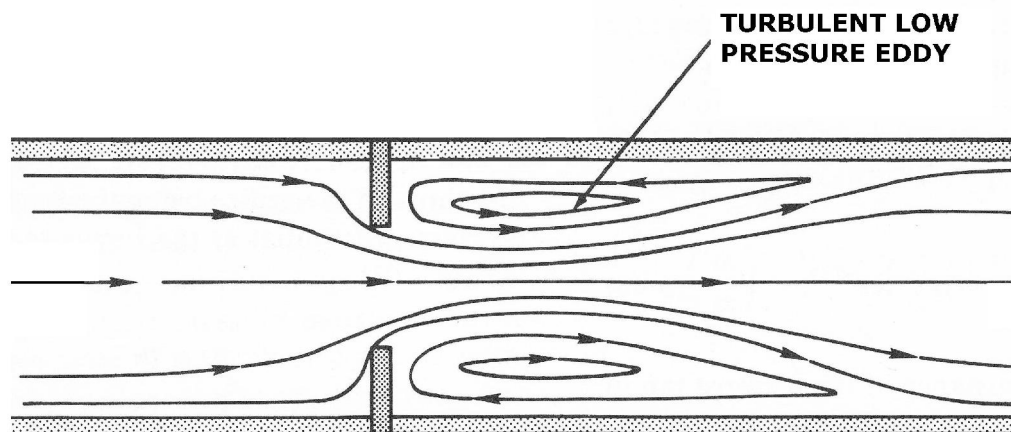


Figure 4. Turbulent pipe flow through an orifice plate causes eddies on the downstream side on all sides of the jet. The flow through a manhole in a narrow compartment is similar. Most of the energy losses occur in these eddies. The picture is modified from Blevins (1984, p. 81).

Wall and bed friction contribute to pressure losses, but their influence is quite small in laboratory conditions. Frictional pressure losses can be estimated with the Manning's equation or by measurements, as in this study. When the flow is modular and has free surfaces, a small amount of energy is also lost in a hydraulic jump downstream of the opening (Bos 1985, p. 71).

The pressure loss coefficient k_L is obtained from the discharge coefficient, C_D , which by definition is the quotient of the actual discharge Q_A and the corresponding theoretical discharge of an ideal fluid, Q_T (e.g. Clemmens et. al. 2001, p. 229):

$$C_D = \frac{Q_A}{Q_T} \quad (3)$$

The quotient of equation (3) is sometimes referred to as the effective discharge coefficient or the speed reduction factor (e.g. IMO A.266(VIII)). In this study it is simply called the discharge coefficient. The discharge coefficient is often presented as the product of the relative contraction and velocity decrease:

$$C_D = C_C C_V, \quad (4)$$

where C_C is the contraction coefficient and C_V is the velocity coefficient. The contraction coefficient is defined as the cross surface area of the jet at its narrowest section, called vena contracta, divided with the area of the opening (e.g. Walshaw and Jobson 1979, p. 83). The velocity coefficient C_V is the quotient of the real velocity at the vena contracta and the corresponding theoretical velocity of an ideal fluid. The value of the discharge coefficient is

primarily explained by contraction, whereas the velocity coefficient usually has values in the range of 0.95-0.99 (Walshaw and Jobson 1979, p. 84).

The relationship between the pressure loss coefficient and the discharge coefficient is according to the IMO Resolution A.266(VIII):

$$C_D = \frac{1}{\sqrt{1 + k_L}} = \frac{1}{\sqrt{1 + \sum k_i}}, \quad (5)$$

where the constants k_i are pressure loss coefficients for individual components i of the system. The number 1 in the square root takes the outlet losses into account (Söding 2002). In the resolution MSC.245(83), which is a revised version of IMO A.266(VIII), the same equation does not contain the number 1 in the square root. However, it is mentioned in appendix 2 of resolution MSC.245(83) that 1 should be added to the sum in order to consider the outlet losses. The number 1 should always be applied when values for k_L are computed on the basis of determined discharge coefficients.

The discharge coefficient value for a cross-duct can be measured either over the entire cross-duct or estimated with equation (5) on the basis of measurements over single girders. Consequently, the number of flow obstacles is a major factor that affects the discharge coefficient. However, it should be pointed out that equation (5) does not consider the interaction between single components, and therefore its application causes some inaccuracy in the results. The application of equation (5) is explained more in detail in section 3.3.3.

2.2 Opening form and scale effects

Important properties related to the opening form are the geometrical shape, the sharpness of the opening edges and the length of the crest or throat (e.g. Walshaw and Jobson 1979, p. 83; Bos 1985, p. 16). A rounded opening, for instance, causes a smaller contraction of the jet than a sharp edged opening, and consequently it has a higher discharge coefficient (Figure 5). The discharge coefficients of sharp edged orifices with common forms, such as circles and rectangles, are typically close to 0.6 (e.g. Bos 1989, p. 271).

It is possible to visually observe the influence of the opening form when the jet through the opening discharges into air. The opening edges can be considered sharp when the only contact between the jet and the opening is at the upstream edge of the opening. Similar observations cannot be made when the jet discharges into water. It is possible that the contraction caused by the edges of an opening is not similar when the jet discharges into water instead of air.

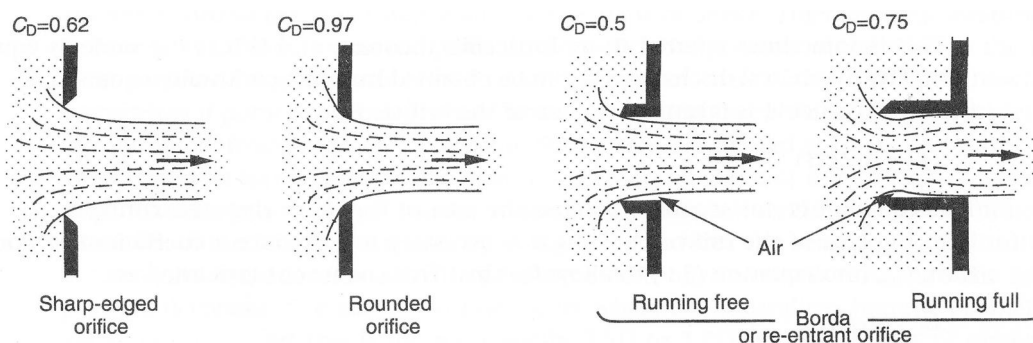


Figure 5. A text book example of typical opening forms and their influence on the discharge coefficient, when the jet discharges into air (Hamill 2001, p. 134). The contraction of the jet is not depicted very realistically in the figure.

The flow through scale models is never completely similar to flow through the corresponding real structure. There are several potential reasons for the differences, which are often lumped together and simply called scale effects. Scale effects are a source of uncertainty in scale model tests, but their influence can be limited by selecting a sufficiently large scale for the model. On the other hand, a larger scale means that the relative discharges that can be used in the laboratory will be smaller.

The cross-sectional opening form also affects the discharge coefficient. Rectangular and circular openings, for instance, do not have equal discharge coefficients. The discharge coefficient for free flow through a circular opening depends strongly on the upstream head h_U (Bos 1989, p. 169) (Figure 7B). The influence of the manhole's geometrical form on the discharge coefficient was clearly visible in this study (see section 6.1.1).

Katayama and Ikeda (2005) conducted experiments with two rectangular openings. The larger opening was 60 mm high and 210 mm wide and the smaller was geometrically similar but to 1:2.5 scale. The average discharge coefficients in their research were 0.58 and 0.70 for the large and small models, respectively, when the jet discharged into air. In submerged flow conditions the corresponding C_D values were 0.53 and 0.60 (Katayama and Ikeda 2005).

Ruononen (2006a, p. 25) used a hydraulic model to evaluate the discharge coefficients of some small scale openings, through which the jet discharged into air. The discharge coefficients for rectangular openings with the dimensions 100 mm x 100 mm, 40 mm x 60 mm and 25 mm x 25 mm were found to be 0.72, 0.78 and 0.83, respectively. Consequently, opening form and scale effects should not be neglected in the analysis and generalization of experimental research should be made with care.

2.3 Distance between girders and number of openings on girders

Pittaluga and Giannini (2006) conducted CFD computations for a 12 m long cross-duct and found that the distance between the girders affected the pressure loss coefficient related to each space between two adjacent girders, i.e. also the pressure loss coefficients of the girders themselves. The flow was stationary with a constant head of 5.0 m and 7.5 m. They presented following regression equations for the pressure loss coefficients related to each space between two adjacent girders (MSC.245(83) appendix 2):

$$k_S(L_i) = \begin{cases} 0.0424L_i^3 - 0.3593L_i^2 + 1.1401L_i - 0.356, & 1 \leq L_i \leq 4 \\ 1.17, & L_i > 4 \end{cases} \quad (6)$$

when there are two manholes on the girders and

$$k_S(L_i) = \begin{cases} -0.0986L_i^3 + 0.6873L_i^2 - 1.0212L_i + 0.7386, & 1 \leq L_i \leq 4 \\ 1.34, & L_i > 4 \end{cases} \quad (7)$$

when there are one manhole on each girder. L_i is the spacing between the girders in meters. The pressure loss for the entrance is included in the value of k_S , but $k = 1$ has to be added to take the outlet losses into account (MSC.245(83)).

According to equations (6) and (7), a shorter distance between the girders yields a higher discharge coefficient for each space between two adjacent girders. As the distance between the girders gets shorter, the jet expands less in the compartments of the cross-duct and the expansion and contraction losses are consequently smaller.

With a distance longer than $L_i = 2.5$ m between the girders, the discharge coefficient of a compartment with one manhole on each girder is lower than for a compartment with two manholes on each girder. The relation is opposite when $L_i \leq 2.5$ m. The phenomenon probably has to do with contraction and streamline curvature.

2.4 Incomplete contraction of the jet due to the approach channel

The flow through the opening will not be fully contracted if the approach channel walls and bed are close to the opening. The reason for this is that the streamlines are straightened and arrive less obliquely towards the opening (Figure 6A). This increases their component of momentum normal to the opening, which increases the discharge (Walshaw and Jobson 1979, p. 111). Consequently, the discharge coefficient is higher if the flow is affected by the vicinity of the flume bed and sidewalls (equation (4)).

The flow through an opening is fully contracted when the walls and the bed of the approach channel are sufficiently remote from the opening (Figure 6B). In order for the flow through an orifice to be fully contracted, the distance from the opening edges to the flume walls and bed is recommended to be greater than the radius of the orifice (Bos 1989, p. 271).

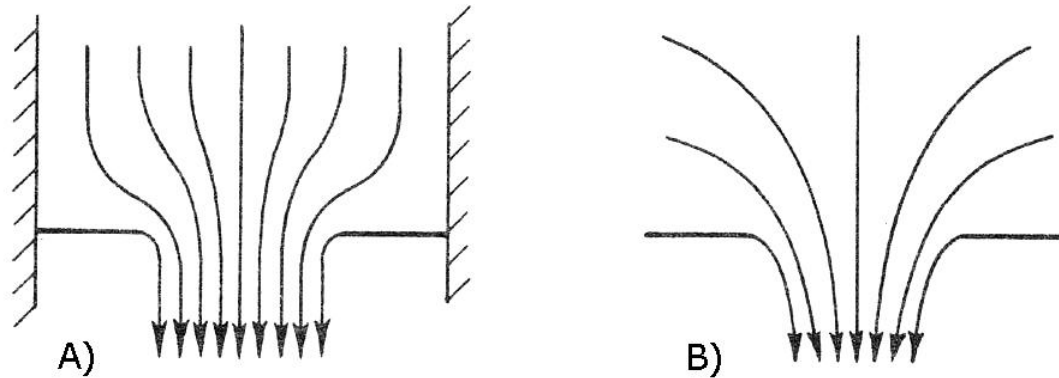


Figure 6. A) The flow through the opening is not fully contracted due to the vicinity of the approach channel sidewalls. B) The flow through the opening is fully contracted, which results in a lower discharge coefficient (Walshaw and Jobson 1979, p. 111).

Many of the more advanced discharge equations for sharp crested weirs, such as the Carter-Kindsvater, Hamilton-Smith and Swiss S.I.A equations, take the vicinity of the sidewalls into account (e.g. Ackers et al. 1980, p. 59-63). These equations are developed for rectangular weirs. The same principles, however, also apply to other openings. The influence of incomplete side contraction of the jet on the discharge coefficient of a rectangular sharp crested weir is shown in Figure 7A.

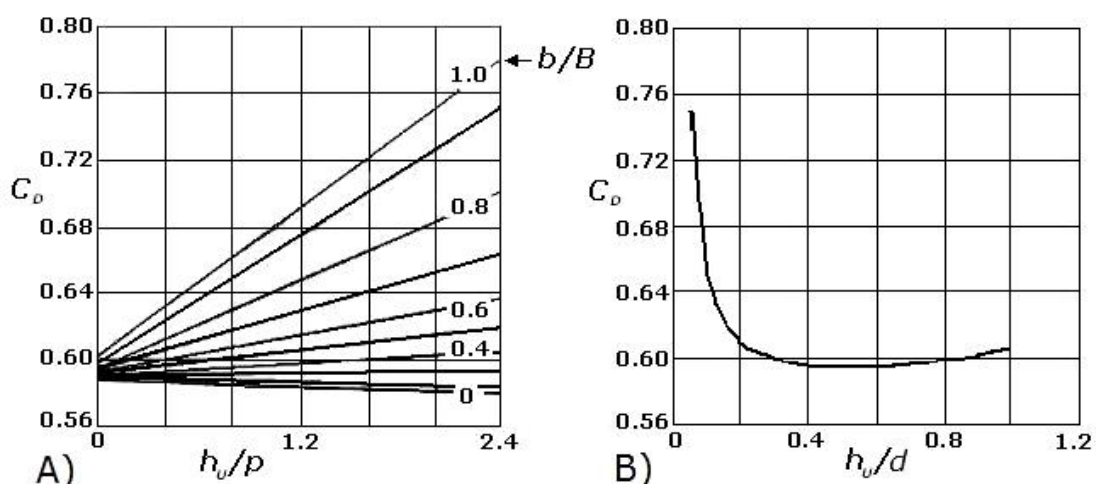


Figure 7. A) The influence of incomplete side contraction on the discharge coefficient of a rectangular sharp crested weir is stronger for high upstream heads. Parameters b , B and p are the width of the weir, width of the approach channel and height of the weir crest, respectively. B) The discharge coefficient for fully contracted flow through a circular sharp crested weir with the diameter d shows

the influence of the geometrical shape of the opening. The figures are based on research by Carter and Kindsvater (Bos 1989, p. 157, 169).

The possible influence of the flume bed and sidewalls should be taken into account in experiments and the application of experiment results. The degree of contraction has great influence on the discharge coefficients for individual girders of a cross-duct.

2.5 Tail water level

A downstream water level below the opening does not affect the flow, which means that the flow through the opening is supercritical. When the downstream water level is raised, it will at some level start to affect the flow through the opening. This water level is called the modular limit (e.g. Clemmens et al. 2001, p. 30). When the downstream water level is above the modular limit, a part of the flow will be in a subcritical condition. In such conditions the flow is typically expressed as a function of the downstream head divided with the upstream head h_D/h_U (Blevins 1984, p. 202). This ratio is sometimes referred to as the submergence ratio (e.g. Clemmens et al. 2001, p. 30) or the degree of submergence (e.g. Tullis and Neilson 2009). The modular limit of long throated flumes can be close to 90% of the upstream head (Clemmens et al. 2001, p. 31), whereas it is 0% for some openings.

When the downstream water level is between the lower and the upper edge of the opening, the determination of the discharge is generally considered uncertain and difficult (e.g. Villemonte 1947). Some research has been conducted for specific types of submerged weirs. These include ogee-crest weirs (Tullis and Neilson 2008), spillway gates (Tullis and Swain 1998), labyrinth sharp-crested weirs (Tullis et al. 2007) and straight sharp-crested weirs (Villemonte 1947). All studies point out the increased uncertainty related to submerged weir flow measurements and computations. In some references on flow measuring devices, it is even recommended to avoid submerged weir conditions for measurement purposes (e.g. Clemmens et al. 2001, p. 229). However, submerged weir flow and partly submerged orifice flow cases are common flow conditions in flooding of ships and they cannot therefore be neglected.

The flow through the opening becomes fully submerged when the downstream water level rises above the upper edge of the opening. In such conditions the ratio between the downstream water level h_D and the opening height h_O can affect the discharge coefficient. In many submerged sluice gate equations the discharge depends not only on the head difference, but also on the relation between h_D and h_O (e.g. Sepúlveda et al. 2009). Nielsen and Weber (2000)

carried out experiments with a rectangular partly contracted opening and found that the discharge coefficient decreased from 0.85 to 0.60 when the ratio h_D/h_O was increased from 1.4 to 2.5, respectively. Such a strong dependency is, however, probably exceptional.

The size of the downstream compartment has some influence on the discharge coefficient when the downstream water level is above the lower edge of the opening. One reason for this is that the water level at the downstream side of the opening is lower than the average water level in the downstream compartment. The difference between the downstream water levels is considerable when the downstream compartment is small compared to the discharge (see section 3.2.3).

2.6 Influence of flow velocity and other uncertain factors

Flooding simulations typically assume that the compartments before and after the opening are infinitely large from a hydraulic point of view (Ruponen 2007, p. 31). This means that the flow velocities in the compartments are negligible. In compartments, which are small compared to the discharge through the opening, the velocity head will affect the flow. The influence of the velocity head on the discharge coefficient was, however, quite small for most flow configurations examined in this study.

It is possible that the velocity itself, i.e. not just the velocity potential, has an influence on the discharge coefficient. In the study by Pittaluga and Giannini (2006) an increase of the head from 5 m to 7.5 m caused a small increase in the value of C_D when the distance between the girders was 3 m. The increase had no influence on the discharge coefficient when the distance between the girders was 4 m.

Vredeveltdt and Journée (1991) conducted model tests with a cross-duct connected to wing tanks on each side and computed pressure loss coefficients with the IMO A.266(VIII) equation. According to their results, an increase in the discharge causes a decrease in the pressure loss coefficient, i.e. an increase in the discharge coefficient value. Vredeveltdt and Journée (1991) speculated that the variation of k_L might be caused by the non-stationary properties of the flow. Chanson et al. (2002), on the other hand, examined unsteady flow through an orifice into air and found the discharge coefficient to be constant.

In the theory on pipe flow it is well known that the Reynolds number and, consequently, the flow velocity affect C_D . A cross-duct with girders can be compared to a regular pipe or duct with orifice plates, even though the analogue

has some flaws. The discharge coefficient in pipe flow through an orifice plate is typically expressed as a function of the orifice Reynolds number, Re_o (Blevins 1984, p. 81-82):

$$Re_o = Re \frac{D}{d} = \frac{uD^2}{\nu d}, \quad (8)$$

where u is the flow velocity and D and d are the hydraulic diameters of the duct and the opening, respectively. The hydraulic diameter is defined as

$$D = \frac{4A}{P}, \quad (9)$$

where A is the cross section area of the flow and P is the wetted perimeter. According to the pipe flow theory the influence of flow velocity on the discharge coefficient is the opposite compared to the studies by Vredeveltdt and Journée (1991) and Pittaluga and Giannini (2006). At low orifice Reynolds numbers there is a considerable decrease in the discharge coefficient as the velocity increases. The relative influence of flow velocity decreases as Re_o increases and becomes almost negligible when $Re_o > 10^6$ (Reader-Harris et al. 1995).

In the case of an accident, the flow through openings of cross-ducts in ship double bottoms can be driven by heads up to 10 m. For such heads the typical Reynolds numbers for flow through the cross-duct would be in the order of 10^6 , which means that $Re_o \gg 10^4$. Consequently, according to the duct flow theory, the possible range of velocities in ship flooding situations should not affect the value of the discharge coefficient. Flow velocity and the corresponding head difference must, however, be regarded as a potential source of discharge coefficient variation, until the opposite is proven.

There are a few uncertain flow factors, which are related to this study specifically. The compartments and girders of cross-ducts are for structural purposes equipped with stiffeners (see Figure 25 in section 4.4). Such structural details are usually not taken into consideration and, consequently, there is no literature on the influence of stiffeners on the flow.

Flooding simulations take inclination into account, but it is usually not assumed to affect the discharge coefficient. The heel angle was zero in the CFD analyses by Pittaluga and Giannini (2006). The influence of inclination on the discharge coefficient has not been verified sufficiently in experiments.

2.7 Summary of discharge coefficient variation

An overview of the possible causes for discharge coefficient variation is presented in Table 1 (next page). Some of the phenomena and variables in the

table are linked to each other. The discharge coefficient of any opening is the sum of several complicated phenomena. Some of these phenomena were examined in this study. Most of the listed phenomena are not taken into account in flooding simulations, which are based on simplifying assumptions.

Table 1. Summary of the certain and potential phenomena and properties that affect the discharge coefficient of manholes and cross-ducts.

Phenomenon or variable	Certainty of effects	Influence on C_D	Examined in this study
Number of girders	Fact	An increased in the number of girders decreases C_D	Yes
Opening form	Fact	Depends on several factors	Yes. The influence of girder stiffeners was examined
Distance between girders	Fact	Smaller distance increases C_D	No
Incomplete jet contraction due to the approach channel	Fact	Incomplete contraction increases C_D	No
Size / scale effects	Verification needed	A smaller scale is assumed to increase C_D	Yes, to some degree
Flow velocity	Verification needed	Contradictory reports in literature	Yes, to some degree
Downstream water level, when partly submerged, $h_D < h_O$	Verification needed	Higher downstream water level is assumed to decrease C_D	Yes
Downstream water level, when fully submerged, $h_D > h_O$	Verification needed	A higher h_D/h_O ratio is assumed to decrease C_D	Yes
Inclination	Verification needed	Increase in inclination is assumed to decrease C_D	Yes
Number of openings on the girder	Verification needed	A girder with two manholes is assumed to have a higher C_D	Yes

3 Methods

3.1 Laboratory studies

3.1.1 Flume and water circulation system

Experiments were carried out in a 50 m long, 1.09 m wide and 1.40 m deep flume. The flume has a horizontal bed, and a steel frame supports the glass walls. Pumps are used to pump water from a storage tank into a head tank, in which the water level is maintained at a constant level. Discharges up to 360 l/s were released into the flume through a stilling basin and a flow straightener.

A dam plate with attachments for the test object divided the flume into an upstream side and a downstream side. The upstream flow depth depends on the released discharge and the downstream flow depth, which was adjusted with a tailgate (an overflow weir). A pipe with a valve connects the downstream to the storage tank. The test flume and the water circulation system are shown schematically in Figure 8.

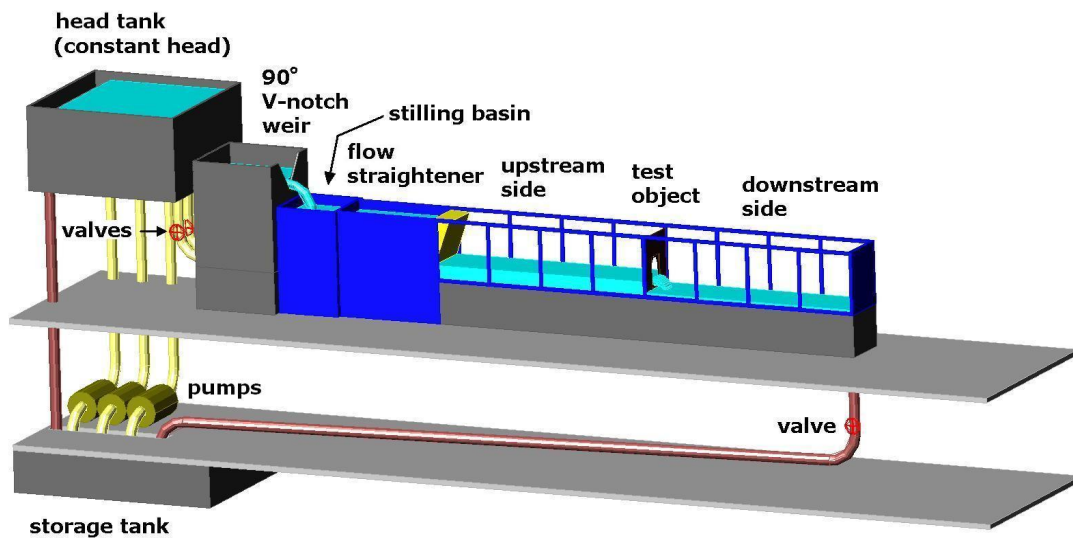


Figure 8. A schematic overview of the flume and water circulation system.

The water levels in the flume and the measurement weir basin were monitored with pressure transducers connected to a data-logging system. The actual discharge Q_A over the 90° V-notch measurement weir is

$$Q_A = 6.8 \cdot 10^{-8} h_V^{2.428677} , \quad (10)$$

where h_V is the elevation head in [mm] above the weir. Equation (10) is based on earlier measurements at the Aalto University.

Flow velocities were recorded with a Prandtl tube and a 3D ADV device.

3.1.2 Measurement considerations and arrangements

The dam plate was located 12 m from the upstream end of the flume (Figure 9). The front wall of the test object was attached to the dam plate. The adjustable tailgate was at a distance of 13 m downstream from the dam plate. The dam plate and tailgate were kept in the same place in all test cases.

In order to avoid the flow obstacle to influence the water depth, it is recommended that the distance from the head measurement location to the obstacle should be at least 2 to 4 times the total head H_U (Blevins 1984, p. 202). In this study, the distance from the dam plate to the upstream measurement location was 5.5 m. The downstream measurement location was located 3.5 m in front of the tailgate. The largest up- and downstream heads were 0.95 m and 0.85 m, respectively.

It is recommended that the Froude number F_R at the measurement locations should not exceed 0.5, and preferably it should be below 0.2 (Bos et al. 2001, p. 54). In this study F_R was well below 0.2 both at the upstream and downstream measurement locations.

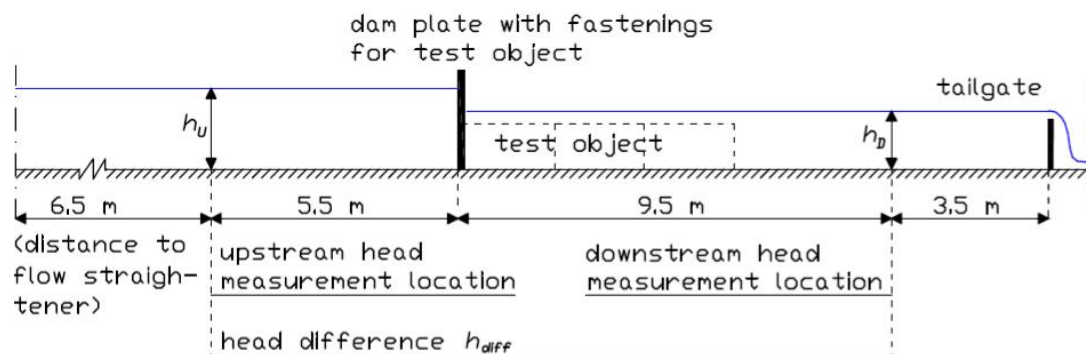


Figure 9. Schematic overview of measurement arrangements.

The absolute values of the upstream and downstream elevation (piezometric) heads were measured with two separate pressure transducers. A differential pressure transducer was used to measure the head difference. The values measured with the differential pressure transducer were used in computations instead of the calculated difference between the two absolute meters. The downstream water level at the opening was estimated visually in a few test cases (see section 3.2.3).

The pressure transducers give a voltage output, which is directly proportional to the elevation head $U \sim h$. The elevation head h is simply

$$h = aU + b, \tag{11}$$

where a and b are calibration constants. Calibration of the pressure transducers was done in the following way:

- 1) The valve in the downstream end was closed and the water was set to a constant level h_1 , which was measured with a point gauge. The corresponding voltage U_1 was recorded.
- 2) The water surface was set to higher level by releasing some water into the flume. The new water level h_2 was measured and the corresponding voltage U_2 was recorded.
- 3) The calibration constants a and b are calculated as:

$$a = \frac{h_2 - h_1}{U_2 - U_1} \quad (12)$$

$$b = -(aU_1 - h_1) \quad (13)$$

The measurements were ½ and 1 minute long and values were recorded every 0.2 second. The head in the V-notch weir basin was also checked with a point gauge during each measurement.

The flow velocity measurement devices were attached to a rail. The rail was fastened across the top of the flume. A 3D ADV device was used to measure all velocity components (x-, y-, z-directions) on the upstream side of the girder. A Prandtl tube was used to measure the x-component of the flow velocity on the downstream side of the girder.

3.1.3 Description of the test objects

The basic test object in this study was a manhole. There is some variation in the size and shape of manholes, but their typical shape can be described as two half-circles connected by a straight (rectangular) portion. Three different manholes were used as test object:

- A full-scale manhole (height 600 mm, width 400 mm) provided by STX Turku shipyard. The opening was cut with a plasma-cutting machine into a 15 mm thick steel plate.
- A 1:2 scale model manhole (height 300 mm, width 200 mm) made of 8 mm thick plywood.
- A 1:3 scale model of a girder with two manholes (height 234 mm, width 134 mm). The scale model girder was made of 6.5 mm thick plywood. The full-scale height and width of these two manholes is 700 and 400 mm, respectively. Thus they are not equal to the previous test objects.

The dimensions and geometry of the three manholes in upright position are presented in Figure 10.

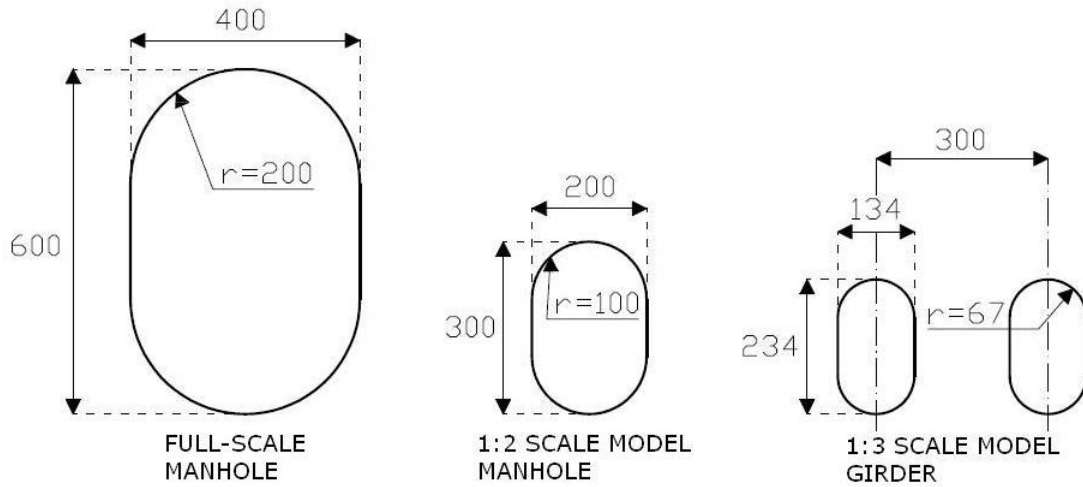


Figure 10. The geometry of the test object openings consisted of two half-circles (with the radius r) connected by a rectangle. The girder manholes were proportionally higher than the single manholes.

The variation of the width of the manholes in full-scale is described by:

$$b_M(z) = \begin{cases} 2\sqrt{0.4z - z^2} & , \quad 0 \leq z < 0.2 \\ 0.4 & , \quad 0.2 \leq z \leq 0.4, \\ 2\sqrt{0.8z - z^2 - 0.12} & , \quad 0.4 < z \leq 0.6 \end{cases} \quad (14)$$

$$b_{GM}(z) = \begin{cases} 2\sqrt{0.402z - z^2} & , \quad 0 \leq z < 0.201 \\ 0.402 & , \quad 0.201 \leq z \leq 0.502, \\ 2\sqrt{0.201^2 - (z - 0.501)^2} & , \quad 0.502 < z \leq 0.702 \end{cases} \quad (15)$$

where b_M is the width of the full-scale manhole and the 1:2 scale model manhole (in full-scale) at height z from the lower edge of the opening (see Figure 14 on p. 30). b_{GM} is the corresponding full-scale width of the girder manholes. The width of the full-scale manhole and the 1:2 scale model manhole in horizontal position is described by

$$b_M(z) = 0.2 + 2\sqrt{0.4z - z^2} \quad , \quad 0 \leq z \leq 0.4 \quad (16)$$

Eventual inaccuracies in the cutting of the steel and plywood plates were assumed to be negligible.

The cross-duct model consisted of three separate modules. The cross-duct modules were 2 meter long, 0.6 meter high and 0.6 meter wide. Each module had 2 or 3 girders, with 2 manholes in upright position on each. The modules

could be connected to each other. Consequently, the cross-duct model could be made 2, 4 or 6 meter long. The dimensions of one model cross-duct module are shown in Figure 11. The scale model cross-ducts were designed and built by the wood & metal workshop of Marine technology of the Department of Applied Mechanics at the Aalto University.

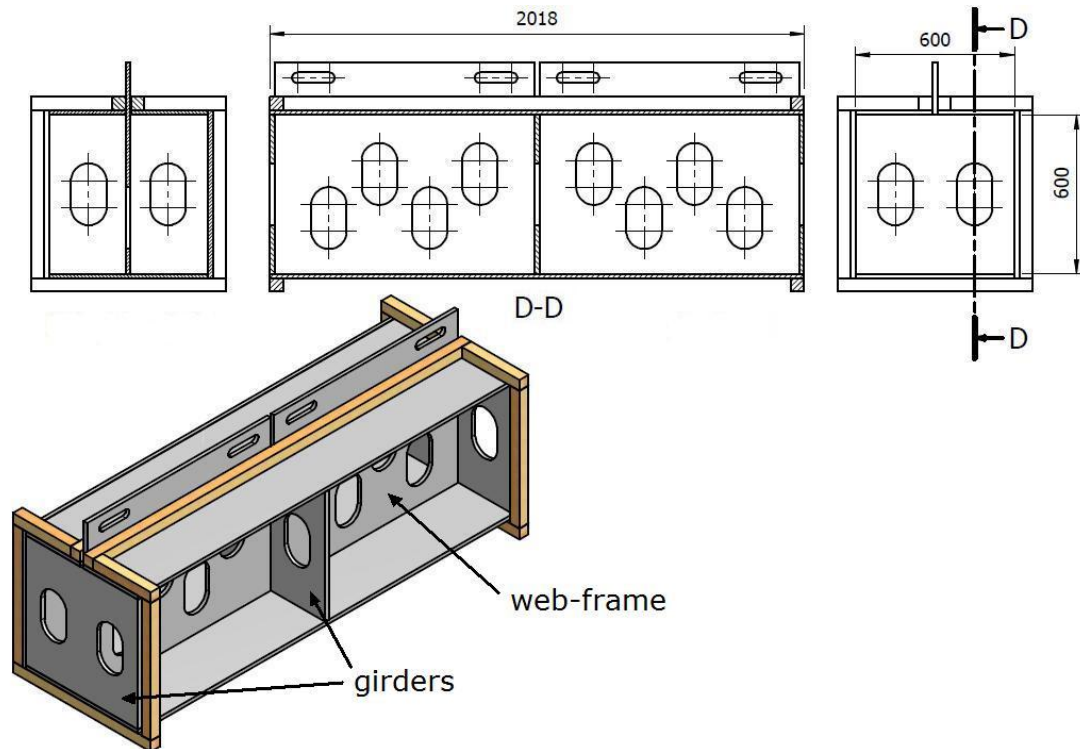


Figure 11. The dimensions of one 1:3 scale model cross-duct module with a web frame in the middle of the cross-duct. The web-frame was not present in the model during most tests.

The 1:3 scale model cross-duct was constructed of plywood. The front wall was made of plexus. Real cross-ducts are made of steel, but the dimensions of the model were geometrically similar to those of a full-scale cross-duct. More detailed descriptions of the test object specifications in different test cases are presented in section 4.

3.2 Discharge equations for different flow conditions

In order to determine the discharge coefficient, the actual discharge must be determined and the corresponding ideal discharge computed. The governing equations for the computation of ideal flow depend on the flow conditions, which therefore have to be defined.

Flow conditions are typically categorized as weir or orifice flow. Weirs can be described as overflow structures, whereas orifices are located entirely below the upstream water level (Bos 1989, pp. 28, 267). Flow can further be categorized

into free flow and submerged flow, depending on the downstream (tail water) level and whether the flow is modular or not. A distinction between the following types of flow was made in this study:

- 1) Free flow. The downstream water level is below the opening and does not affect the flow, i.e. the flow depends on the upstream head and the test object properties only. Free discharge is further divided into:
 - 1.a) Free weir flow. The upstream water level is below the top of the opening ($h_D < 0, h_U < h_O$)
 - 1.b) Free orifice flow. The upstream water level is above the top of the opening ($h_D < 0, h_O < h_U$)
- 2) Submerged orifice flow. Both the up- and downstream water levels are above the top of the opening ($h_O < h_D < h_U$)
- 3) Partly submerged flow. The downstream water level is between the lower edge and the top of the opening. Depending on the upstream water level, partly submerged discharge is further divided into:
 - 3.a) Submerged weir flow. The up- and downstream water levels are between the bottom and the top of the opening ($0 < h_D < h_U < h_O$)
 - 3.b) Partly submerged orifice flow. The upstream water level is above the top of the opening and the downstream water levels is between the lower edge and the top of the opening ($0 < h_D < h_O < h_U$)

The characteristics of each flow condition and computation principles for the theoretical flow Q_T are presented in sections 3.2.1-3.2.3.

3.2.1 Free flow

In free flow the flow is supercritical, which means that downstream influences cannot propagate up through the nappe and influence the flow. Therefore the flow is a function of the upstream head and opening properties only (Blevins 1984, p. 202). Depending on the upstream head, free flow is divided into free weir flow (Figure 12) and free orifice flow (Figure 13).

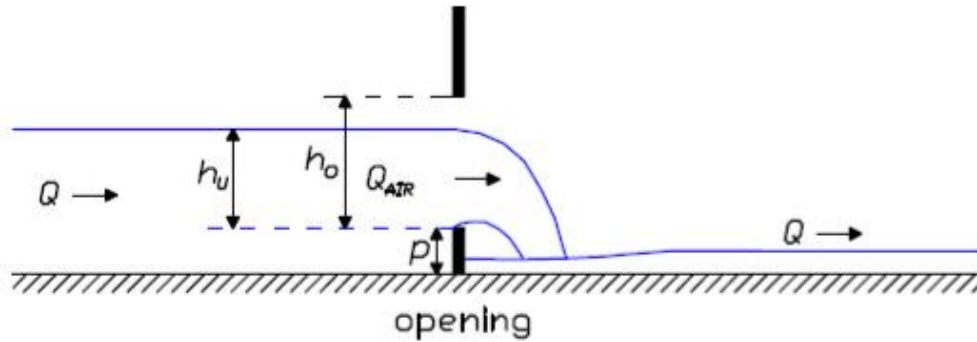


Figure 12. A definition sketch of free weir flow ($h_u < h_o$).

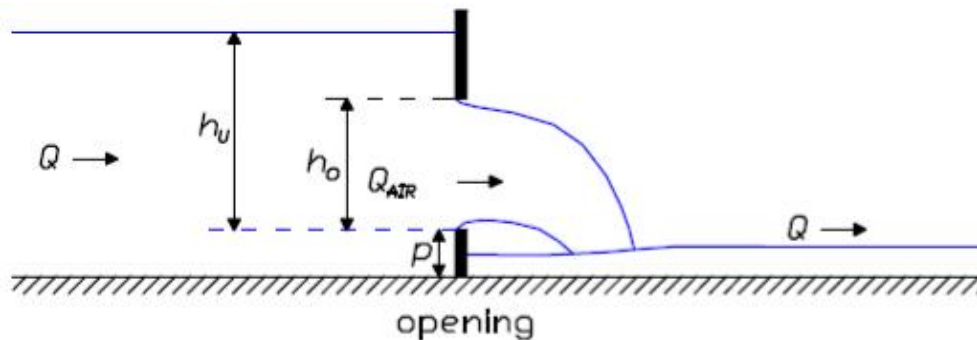


Figure 13. A definition sketch of free orifice flow ($h_u > h_o$).

The manhole is a large opening compared to the total head, which means that the flow velocity in free discharge cases varies at different heights from the reference level. An expression for the theoretical ideal discharge δQ_T through a small section δA of the manhole is derived from equations (1) and (2):

$$\delta Q_T(z) = u_o(z)\delta A(z) = \sqrt{2g(h_u - z) + u_U^2} b(z)\delta z, \quad (17)$$

where h_u is the upstream elevation head above the lower edge of the opening and $b(z)$ is the width of the opening at height z from the lower edge of the opening (Figure 14). The terms in the square root describe the theoretical flow velocity through the opening, u_o , at height z according to Torricellis theorem (e.g. Chanson et al. 2002). The average upstream velocity head can be included as u_U^2 , because the discharge and flume dimensions are known (Bos 1989, pp. 23-24).

The velocity head was at most 0.9% of the total head in the tests with the full-scale manhole, and caused a maximum decrease of 1% in the value of the discharge coefficient. The velocity head was so small in the tests with the scale model manholes that it was not taken into account in respective computations.

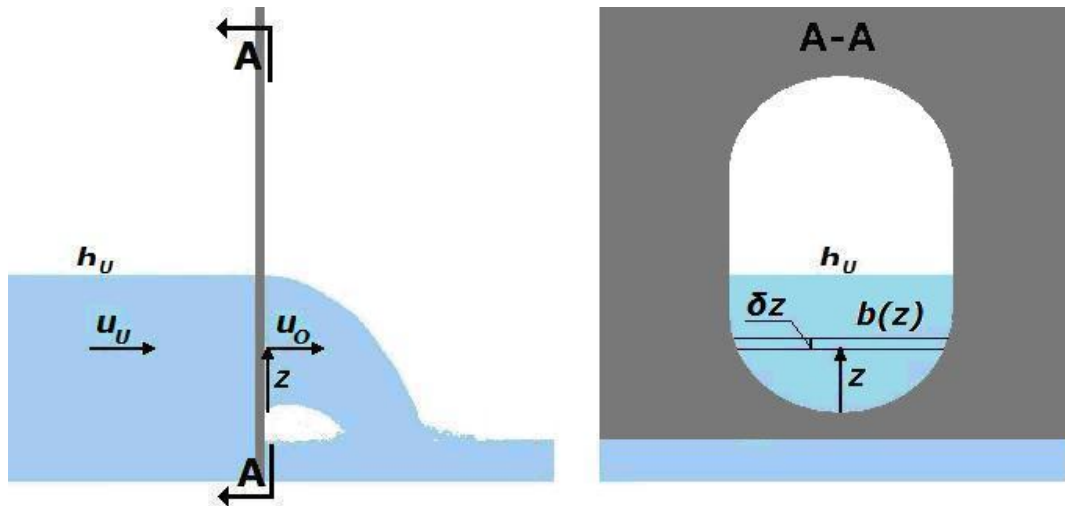


Figure 14. A definition sketch for the variables used in equation (17). Free weir flow is depicted, but the same computational principles apply for free orifice flow.

To obtain the entire ideal discharge Q_T through the opening equation (17) has to be integrated from the lower edge of the opening to the upstream water level or the top of the opening. The analytical integration described for instance by Bos (1989, pp. 50-52) is possible, but considered unpractical in this context. In this study the integration was therefore conducted numerically with the Simpson's method:

$$Q_T = \int_0^h \delta Q_T(z) = \frac{\Delta z}{3} \left[\delta Q_T(z_{ends}) + 4 \sum \delta Q_T(z_{odds}) + 2 \sum \delta Q_T(z_{evens}) \right], \quad (18)$$

where h is the integration limit ($h = h_u$ or $h = h_o$), Δz is the length of the integration interval, z_{ends} are the values of z at the first and last intervals, z_{odds} are the values of z at odd interval indexes and z_{evens} are the values of z at even interval indexes. In this research the length of the integration interval was $\Delta z = 1$ mm.

Free flow tests were carried out by releasing a discharge into the flume and measuring the corresponding upstream head. The downstream water level was kept below the opening. The discharge was then gradually increased and measurements were conducted in each stationary flow condition.

3.2.2 Submerged orifice flow

The flow is submerged when both the upstream and downstream water levels are above the top of the opening (Figure 15). The equation for submerged flow is quite simple, because the entire area of the opening is affected by the same upstream and downstream head difference, and therefore the flow velocity is in

theory constant across the opening area. The theoretical discharge is given by the submerged orifice equation (Hersch 1995):

$$Q_T = A_O \sqrt{2g(h_U - h_D)}, \quad (19)$$

where h_D is the downstream elevation head and A_O is the cross-sectional area of the opening. The velocity heads are neglected due to the lack of an appropriate method that would consider velocity head in submerged flow. Velocity is, however, a property that affects the results in the tests with the full-scale manhole. It is therefore desirable to include velocity when the discharge coefficients of the full-scale manhole and the scale model manholes are compared. The flow velocities on both the up- and downstream side of the full-scale manhole increase the discharge through the opening. By assuming that the up- and downstream velocity potentials have a direction, the velocity heads were included in the submerged orifice equation:

$$Q_T = A_O \sqrt{2g(h_U - h_D) + u_U^2 + u_D^2} \quad (20)$$

Equation (20) was only used in analysis of scale effects in order to correct for the velocity heads. All other submerged flow computations were conducted using equation (19).

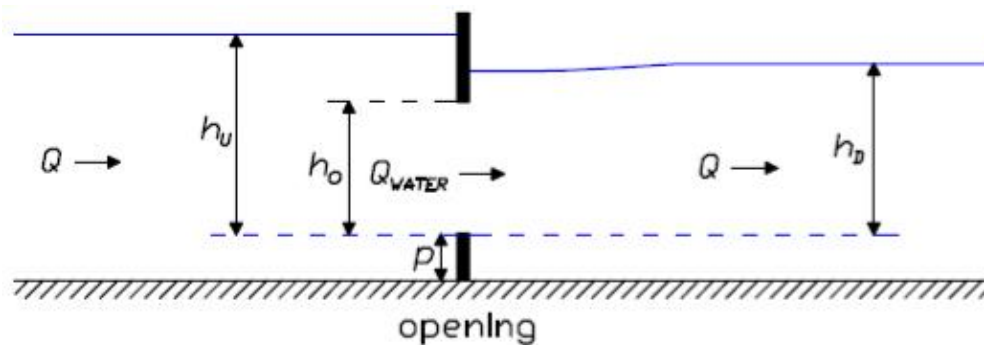


Figure 15. Definition sketch of submerged orifice flow. The opening is submerged on both sides.

Partly and completely submerged flow tests were in practice carried out in the following way:

1. The upstream head h_U was set to a predefined level above the lower edge of the opening by adjusting the discharge into the flume. The downstream water level was initially below the opening.
2. The downstream water level was raised with a tailgate. The discharge was kept constant. Consequently, the upstream water level raised and settled to a new level. Measurements were conducted when the flow was stationary. Step 2 was repeated several times.

The principle is depicted schematically in Figure 19 in section 4.1.

3.2.3 Submerged weir flow and partly submerged orifice flow

In this study, submerged weir flow and partly submerged orifice flow were defined as flow conditions, where the downstream (tail water) level at the opening is between the lower edge and top of the opening. The upstream head is between the lower edge and top of the opening in submerged weir flow (Figure 16) and above the opening top in partly submerged orifice flow (Figure 17).

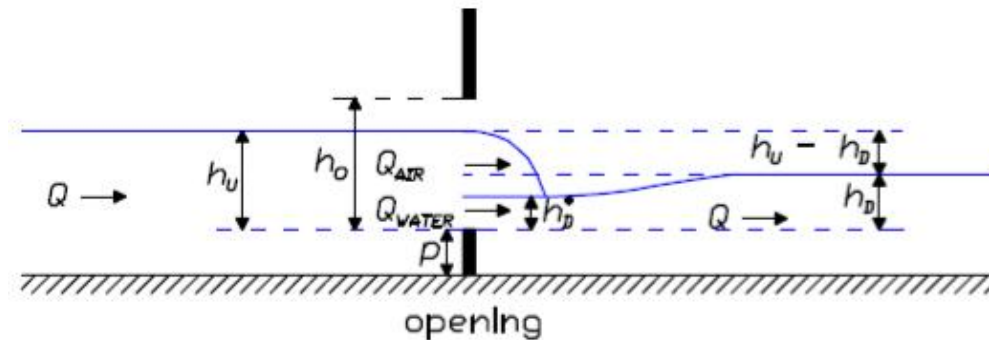


Figure 16. A definition sketch of submerged weir flow. Both the up- and downstream water levels are between the lower edge and top of the opening.

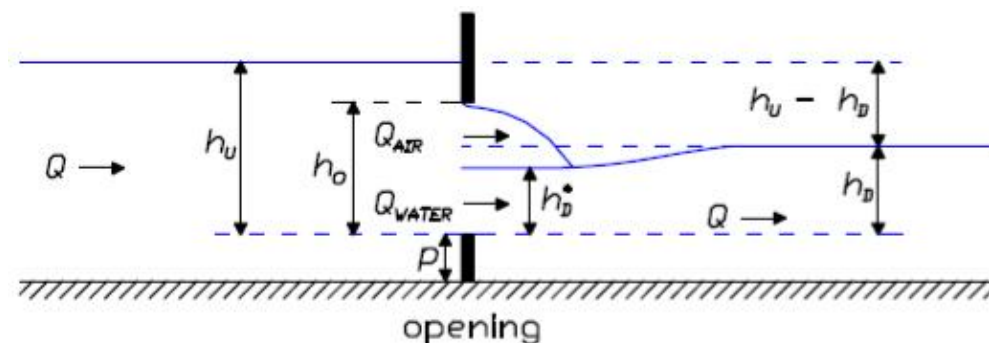


Figure 17. A definition sketch of partly submerged orifice flow. The upstream water level is above the top of the opening and the downstream water level is between the lower edge and top of the opening.

Because of the flow from the opening, the downstream water level at the opening, h_D^* , is lower than in the rest of the downstream compartment. The raise in the downstream water level is caused by the slow-down of subcritical flow and a hydraulic jump caused by supercritical flow turning into subcritical flow. The height of this water level raise depends on the discharge and the downstream water volume.

Sometimes flow simulations use a model with two discharge coefficients, one coefficient for discharge into air C_{Dair} and one for discharge into water C_{Dwater} (e.g. Katayama and Ikeda 2005). This approach was not applied in this study, because the actual discharge cannot be separated into a free and submerged

discharge. The discharge coefficient is therefore presented as a single coefficient for different degrees of downstream submergence. Three different methods were used to compute the theoretical discharge in partly submerged flow cases. Each method is based on simplifying assumptions.

The first two methods are based on the assumption that the discharge consists of two parts: (1) a free flow above the downstream water level (Q_{AIR} in Figure 16 and Figure 17) and (2) a submerged orifice flow below the downstream water level (Q_{WATER} in Figure 16 and Figure 17). This assumption is also made in flooding simulation computations (e.g. Ruponen 2007, pp. 58-59). The third method is based on Villemonte's (1947) superposition principle of two free flows in opposite directions. The velocity heads are not taken into account in the methods.

Method (1). The part of the flow, which is above the downstream water level at the opening, h_D^* , is computed as free flow by integrating equation (17) from h_D^* to h_U or h_O . The submerged part of the jet is computed as submerged orifice flow with equation (19) using the head difference h_U and h_D and the cross-sectional area of the opening below h_D^* , $A(h_D^*)$. The equations, which need to be solved, are:

$$Q_{WATER} = \sqrt{2g(h_U - h_D)}A(h_D^*) \quad (21)$$

for the submerged part of the flow and

$$Q_{AIR} = \int_{h_D^*}^{h_U} \delta Q_T(z) = \int_{h_D^*}^{h_U} \sqrt{2g(h_U - z)}b(z)\delta z \quad (22)$$

for the free part of the flow in submerged weir flow or

$$Q_{AIR} = \int_{h_D^*}^{h_O} \delta Q_T(z) = \int_{h_D^*}^{h_O} \sqrt{2g(h_U - z)}b(z)\delta z \quad (23)$$

for the free part of the flow in partly submerged orifice flow. Equations (22)-(23) were solved numerically with equation (18).

Method (2). The downstream water level is assumed constant (dashed line in Figure 16 and Figure 17). The part of the flow, which is above the downstream water level, h_D , is computed as free flow by integrating equation (17) from h_D to h_U or h_O . The submerged part of the jet is computed as submerged orifice flow with equation (19) using the head difference h_U and h_D and the cross-sectional

area of the opening below h_D , $A(h_D)$. Same equations as in method (1) are used with different integration limits:

$$Q_{WATER} = \sqrt{2g(h_U - h_D)}A(h_D)$$

for the submerged part of the flow and

$$Q_{AIR} = \int_{h_D}^{h_U} \delta Q_T(z) = \int_{h_D}^{h_U} \sqrt{2g(h_U - z)}b(z)\delta z$$

for the free part of the flow in submerged weir flow or

$$Q_{AIR} = \int_{h_D}^{h_o} \delta Q_T(z) = \int_{h_D}^{h_o} \sqrt{2g(h_U - z)}b(z)\delta z$$

for the free part of the flow in partly submerged orifice flow. Results computed with method (1) are slightly smaller than corresponding results with method (2). The difference between the methods is negligible in tests with the scale models because h_D^* approaches h_D as the downstream compartment is large compared to the discharge.

Method (3). Villemonte (1947) questioned the principles of method (1) and (2) because it had not been satisfactorily verified with experimental data. Instead, Villemonte suggested an exponential formula based on the idea of two imaginary oppositely directed free flows, one driven by the upstream head in the flow direction and another in the opposite direction driven by the downstream head (Figure 18).

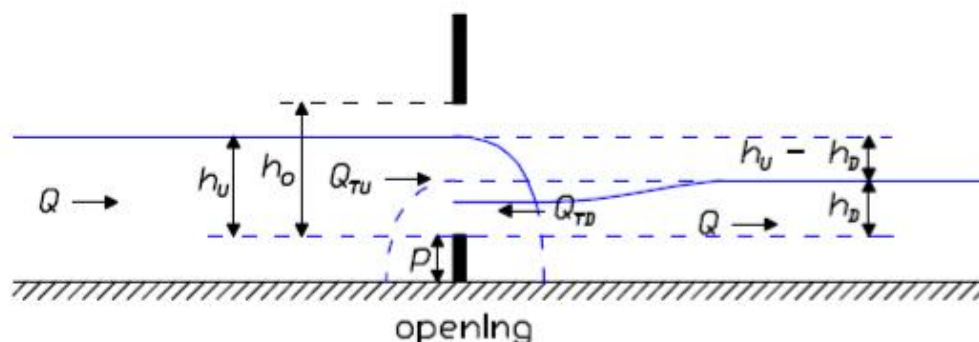


Figure 18. The general superposition principle and variables of the Villemonte equation.

The Villemonte equation has been widely accepted in engineering practice (e.g. Tullis et. al. 2007). A general form of the Villemonte (1947) formula for sharp crested weirs is

$$Q_T = Q_{TU} \left(1 - \frac{Q_{TD}}{Q_{TU}} \right)^{0.385}, \quad (24)$$

where Q_{TU} and Q_{TD} are the computed ideal free discharges corresponding to the upstream and downstream heads h_U and h_D , respectively. Equation (24) does not consider the raise in downstream water level, and it is designed for sharp-crested thin-plate weirs. In this study, the Villemonte equation was used only in submerged weir flow test cases and for submergence degrees less than 0.9, because this is the range for which it is verified (Villemonte 1947).

3.3 Other computational aspects

3.3.1 Scale similarity formula

The theoretical (ideal) discharge Q_T was computed using full-scale values. A similarity equation was defined in order to translate the measured discharge in tests with scale models, Q_{AM} , into a corresponding full-scale discharge Q_{AF} .

The length scales of the scale models in this study were 1:2 and 1:3. The discharge, however, is not linearly related to the length scale. According to Froudian (gravity) model theory, the relationship between the discharge and the length scale is (e.g. Walshaw and Jobson 1979, pp. 251-256)

$$\frac{Q_{AM}}{Q_{AF}} = \frac{1}{X^{5/2}}, \quad (25)$$

where X is the length scale factor. The relationship between the scale model velocity u_{AM} and the full-scale velocity u_{AF} is

$$\frac{u_{AM}}{u_{AF}} = \frac{1}{X^{1/2}} \quad (26)$$

3.3.2 Inclination

Inclination has no effect on computations in submerged flow cases, in which equation (19) is used to compute the theoretical discharge. The free flow discharge equations need some modifications to account for inclination. If the manhole is inclined at an angle α against the flow direction, the equations (14) and (16) are modified into:

$$b_M(z) = \begin{cases} 2\sqrt{\frac{0.4z - z^2}{\cos \alpha}} & , \quad 0 \leq z < 0.2 \cos \alpha \\ 0.4 & , \quad 0.2 \cos \alpha \leq z \leq 0.4 \cos \alpha \\ 2\sqrt{\frac{0.8z}{\cos \alpha} - \frac{z^2}{\cos^2 \alpha} - 0.12} & , \quad 0.4 \cos \alpha < z \leq 0.6 \cos \alpha \end{cases} \quad (27)$$

$$Q_T = \int_0^{h \cos \alpha} \delta Q_T(z) = \frac{\Delta Z}{3 \cos \alpha} \left[\delta Q_T(z_{ends}) + 4 \sum \delta Q_T(z_{odds}) + 2 \sum \delta Q_T(z_{evens}) \right] \quad (28)$$

The error due to numerical integration increases slightly but can still be neglected for small angles.

3.3.3 Discharge coefficient of a duct

The discharge coefficient was determined in the same way for the entire cross-duct as for a single opening (sections 3.2.1 and 3.2.2). The discharge coefficient of a cross-duct was also estimated by using equation (5) and experimentally determined discharge coefficients of single girders, $C_{D,G}$. The pressure loss coefficients for the girders, k_G , were determined by rearranging equation (5):

$$k_G = \frac{1}{C_{D,G}^2} - 1$$

The discharge coefficients of the cross-duct, $C_{D,C}$, were estimated with the following expression (IMO A.266(VIII)):

$$C_{D,C} = \frac{1}{\sqrt{1 + k_C}} = \frac{1}{\sqrt{1 + \sum k_G}} = \frac{1}{\sqrt{1 + n \left(\frac{1}{C_{D,G}^2} - 1 \right)}}, \quad (29)$$

where k_C is the pressure loss coefficient of the cross-duct and n is the number of girders in the cross-duct. The girders were in most test cases equipped with stiffeners pointing either in the up- or downstream direction. The direction of the stiffeners was found to influence the discharge coefficient of the girder. In order to take the direction of the stiffeners into account, equation (29) was rearranged into:

$$C_{D,C} = \frac{1}{\sqrt{1 + i \left(\frac{1}{C_{D,G1}^2} - 1 \right) + j \left(\frac{1}{C_{D,G2}^2} - 1 \right)}}, \quad (30)$$

where i is the number of girders with the discharge coefficient $C_{D,G1}$ and j is the number of girders with the discharge coefficient $C_{D,G2}$.

3.3.4 Scale effect correction factor

Scale effects were estimated by comparing discharge coefficients determined with the full-scale manhole to those determined with the scale model manhole and girder. As the cross-duct model consists of several girders, the scale effects of a cross-duct depend on the number of girders. The scale effects for a cross-duct were estimated as

$$S_c = \frac{\sqrt{1 + n \left(\frac{1}{S_G C_{D,G}^2} - 1 \right)}}{\sqrt{1 + n \left(\frac{1}{C_{D,G}^2} - 1 \right)}}, \quad (31)$$

where S_c is the computed scale correction factor for the cross-duct and S_G is the estimated scale correction factor of a single girder.

4 Test cases

In this section the set-up of each test case is described. The test cases were categorized depending on the test object and flow conditions, i.e. free, submerged and partly submerged flow (see section 3.2). Each measurement was done in stationary flow conditions, which means that the up- and downstream water levels were nearby constant.

The material, dimensions and the geometry of the test objects were presented in section 3.1.3. Manholes are installed both in upright and horizontal position on ships, although the upright position is more common. Both positions were examined in tests. Partly submerged flow was examined with the full-scale manhole and the 1:2 scale model manhole. The focus of the girder and cross-duct tests was on the submerged flow conditions. Following abbreviations were used for the different test cases:

- V1-V6 Full-scale manhole in upright position (Figure 10)
- H1 Full-scale manhole in horizontal position
- VM1-VM2 1:2 scale model manhole in upright position (Figure 10)
- HM1 1:2 scale model manhole in horizontal position
- G1-G7 1:3 scale model girder with manhole(s)
- C1-C6 1:3 scale model cross-duct

4.1 Full-scale manhole

The lower edge of the manhole was located 0.21 m above the flume bed. Following flow conditions were examined:

- V1. Free flow through the full-scale manhole in upright position. The discharge was gradually increased.
- V2. (The results from test case V2 could not be used due to measurement errors in the recorded elevation heads.)
- V3. Submerged weir flow through a full-scale upright manhole. The upstream water head was initially set to 0.30 m or 50% of the opening height. The downstream water level was then gradually raised.
- V4. Submerged weir flow, partly and completely submerged orifice flow through a full-scale upright manhole. The upstream water head was initially set to value of 0.45 m or 75% of the opening height. The downstream water level was gradually raised. As the upstream water level reached the opening top, submerged weir flow became partly submerged orifice flow. The flow became completely submerged when the downstream water level was raised above the opening.
- V5. Partly and completely submerged orifice flow through a full-scale upright manhole. The upstream water head was initially set to a value of 0.60 m or 100% of the opening height. The downstream water level was gradually raised. The flow became completely submerged when the downstream water level was raised above the opening.
- V6. Partly submerged orifice flow through a full-scale upright manhole. The maximum possible discharge was used. The flume was not high enough to enable completely submerged flow.
- H1. Free flow through the manhole in horizontal position.

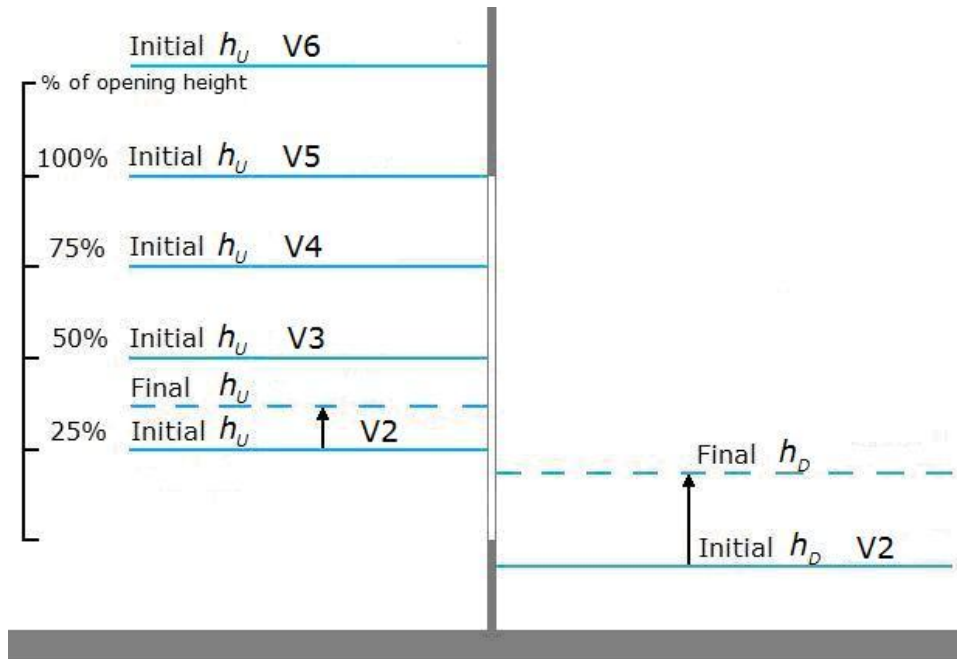


Figure 19. A definition sketch of the initial water levels and test procedures in test cases V2-V6. The discharge was kept constant and the downstream water level was raised gradually with a tailgate.

4.2 Scale model manhole

The lower edge of the 1:2 scale model manhole in upright and horizontal positions was 0.16 m and 0.21 m above the flume bed, respectively. Following flow conditions were examined:

- VM1. Free flow through the 1:2 scale model manhole in upright position. The discharge was gradually increased.
- VM2. Partly and completely submerged orifice flow through an upright 1:2 scale model manhole. The upstream water head was initially set to a value of 0.30 m or 100% of the opening height (the test was similar as test case V5). The downstream water level was gradually raised. The flow became completely submerged when the downstream water level was raised above the opening.
- HM1. Free flow through the 1:2 scale model manhole in horizontal position. The discharge was gradually increased.

4.3 Scale model girders

The 1:3 scale model girder was taken from the cross-duct model. It is made of plywood and has two manholes in upright position. The girder was also examined with one of the openings covered with a plate. The dimensions of the girder are shown in Figure 20.

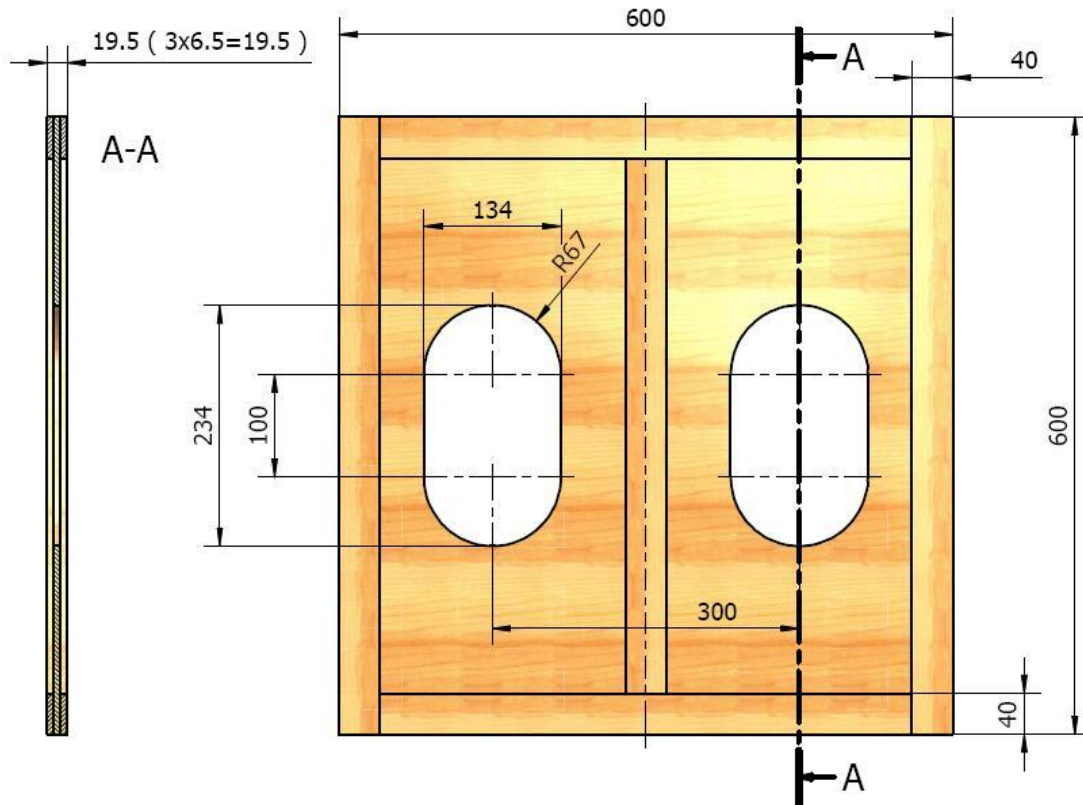


Figure 20. The dimensions of the 1:3 scale model girder.

Real cross-duct girders are usually equipped with stiffeners. The influence of stiffeners on the flow was examined with the use of aluminium scale model stiffeners shown in Figure 21. These were applied symmetrically above and below the opening at a distance of 270 mm from each other and with the 80 mm wide part pointing in the direction of the normal to the opening (see Figure 25). The edges of the scale model stiffeners were sharper than the corresponding real stiffeners. The effect of the sharpness is assumed to be small.

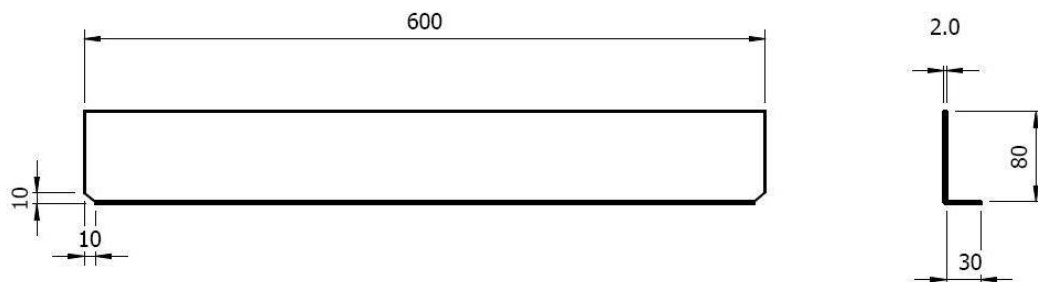


Figure 21. Dimensions of the scale model stiffeners. Girder stiffeners are fastened above and below the opening with the 80 mm wide part in the direction of the normal to the opening.

Following tests with girders were conducted:

- G1. Free flow through a 1:3 scale model girder with *two* manholes in upright position. The girder was not equipped with stiffeners. The discharge was gradually increased.

- G2. (The results from test case G2 could not be used due to measurement errors in the recorded elevation heads.)
- G3. Submerged flow through a 1:3 scale model girder with *two manholes* in upright position. The girder was equipped with *stiffeners* above and below the openings. The stiffeners were pointing *upstream*. The flow conditions were submerged and several discharges and tailgate heights were used.
- G4. Submerged flow through a 1:3 scale model girder with *two manholes* in upright position. The girder was equipped with *stiffeners* above and below the openings. The stiffeners were pointing *downstream*. The flow conditions were submerged and several discharges and tailgate heights were used.
- G5. Submerged flow through a 1:3 scale model girder with *two manholes* in upright position. The girder was not equipped with stiffeners. The flow conditions were submerged and several discharges and tailgate heights were used.
- G6. Free flow through a 1:3 scale model girder with one manhole in upright position. The girder is not equipped with stiffeners. The discharge was gradually increased.
- G7. Submerged flow through a 1:3 scale model girder with *one manhole* in upright position. The girder was not equipped with stiffeners. The flow conditions were submerged and several discharges and tailgate heights were used.

4.3.1 Velocity measurements

The flow velocities in the vicinity of the girder with two manholes were recorded in one flow condition, which was considered typical for the experiments with the girders and the cross-duct. The upstream and downstream water levels were set to about 855 mm and 650 mm, respectively. The discharge was approximately 70 l/s, which corresponds to 1.1 m³/s through a full-scale girder.

The flow velocity measurements were conducted on both the upstream (Figure 22) and the downstream side (Figure 23) of the girder. The flow velocity measurements on the upstream side were conducted with a 3D ADV (Acoustic Doppler Velocimetre) (Figure 24A). The velocities on the downstream side were measured with a Prandtl's tube (Figure 24B).

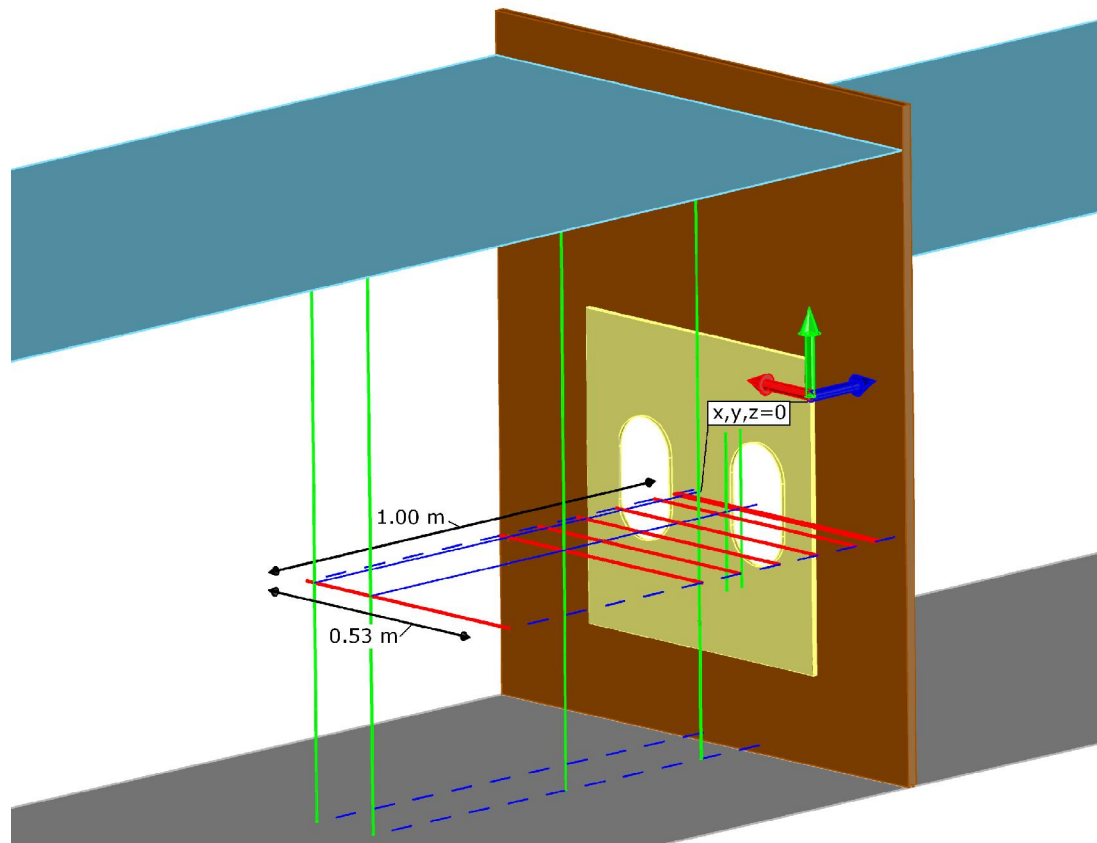


Figure 22. Red bars: horizontal flow velocity measurement lines at distances 0.04 m, 0.05 m, 0.01 m, 0.02 m, 0.03 m, 0.04 m, 0.05 m and 1.00 m upstream from the girder.
Green bars: vertical flow velocity measurement lines at distances 0.04 m, 0.08 m, 0.15 m, 0.50 m and 1.00 m upstream from the girder.

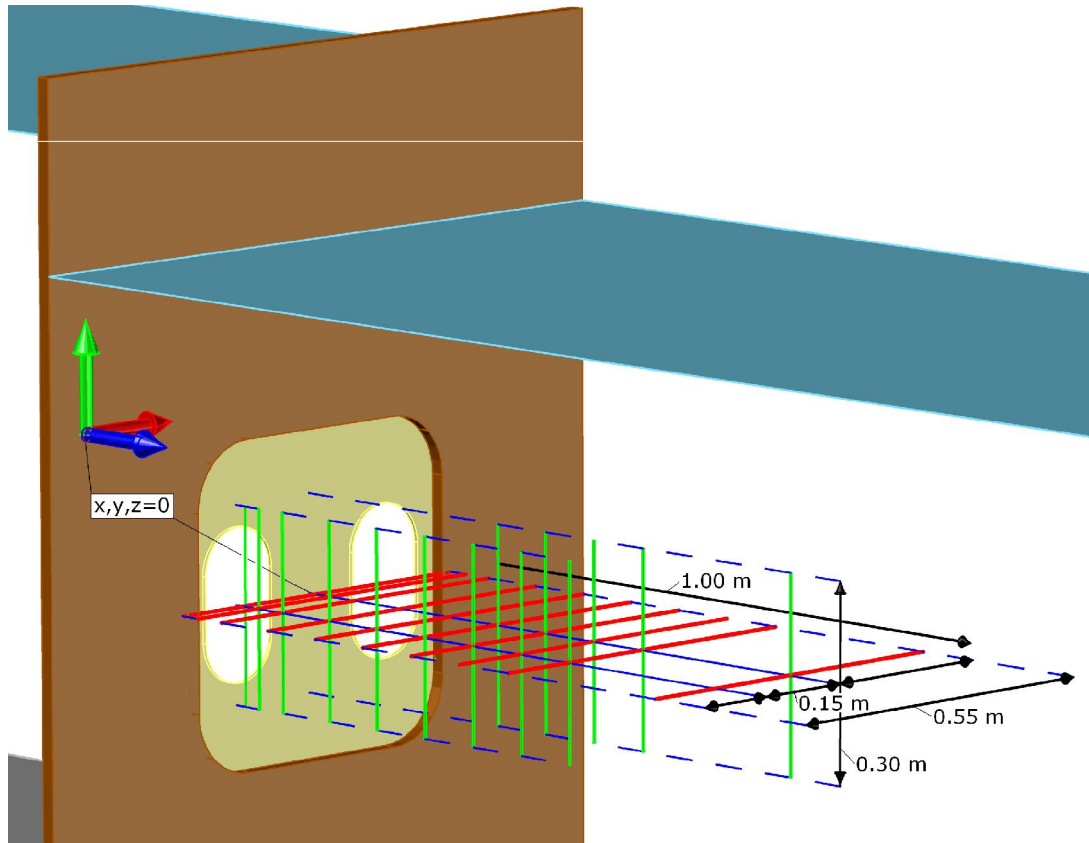
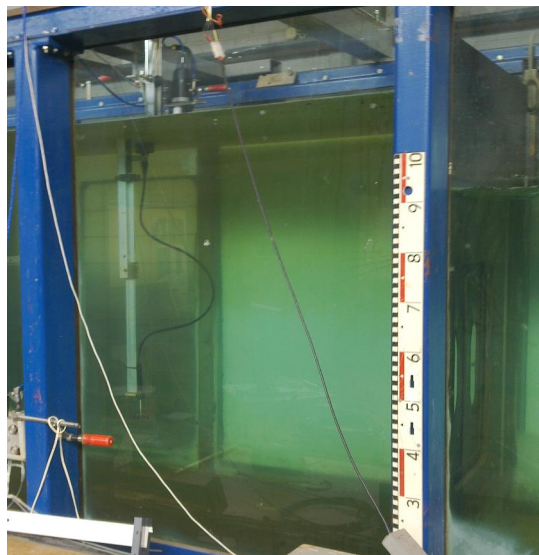


Figure 23. Red bars: horizontal flow velocity measurement lines at distances 0.04 m, 0.05 m, 0.01 m, 0.02 m, 0.03 m, 0.04 m, 0.05 m, 0.06 m, 0.07 m and 1.00 m downstream from the girder. Green bars: vertical flow velocity measurement lines at distances 0.05 m, 0.10 m, 0.20 m, 0.30 m, 0.40 m, 0.50 m, 0.06 m and 0.70 m downstream from the origin and 0.40 m, 0.50 m, 0.06 m, 0.70 m and 1.00 m downstream from the centre of the manhole.



A)



B)

Figure 24. A) The flow velocity measurements on the upstream side of the girder were conducted with a 3D ADV device. B) A Prandtl tube was used on the downstream side.

4.4 Scale model cross-duct

The 1:3 scale model cross-duct module was presented in section 3.1.3. Stiffeners were added into the cross-duct in most test cases. In one test case a web-frame was also present in the duct (Figure 25).

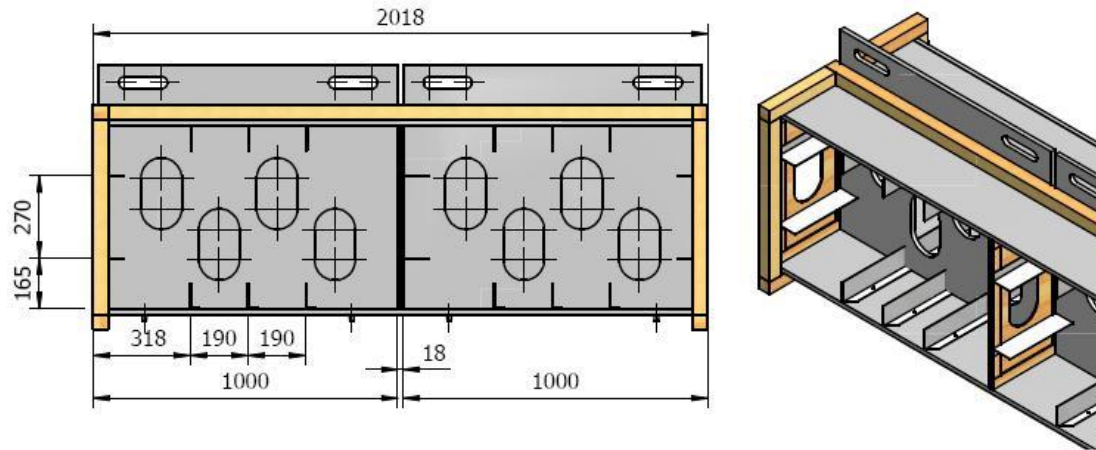


Figure 25. The location of the stiffeners and the web-frame inside a cross-duct module. The stiffeners were located on the girders and the bed and roof of the cross-duct.

The wing tank at the end of a cross-duct is in the case of an accident filled up quickly (Figure 6). The interest in cross-duct tests was therefore primarily on submerged flow conditions. The cross-duct was examined in following test cases:

- C1. The cross-duct consisted of *two modules* and 5 *girders*. There were no stiffeners and no web-frame in the cross-duct.
- C2. The cross-duct consisted of *two modules* and 5 *girders*. *Stiffeners* have been added. *Two girders* have stiffeners pointing *upstream* (against the flow). The other *three girders* have stiffeners pointing *downstream*.
- C3. Cross-duct specification was otherwise the same as in test case C2, but the *web-frame* was added into the cross-duct.
- C4. Cross-duct specification was the same as in test case C2, but the cross-duct was inclined at an angle of 7° towards the flow (downstream end was lifted up).
- C5. The cross-duct consisted of *one module* and 3 *girders*. *Stiffeners* were in place. *Two girders* had stiffeners pointing *upstream* and *one girder* had stiffeners pointing *downstream*. No web-frame.
- C6. The cross-duct consisted of *three modules* and 7 *girders*. *Stiffeners* were in place. *Four girders* had stiffeners pointing *upstream*. The other *three girders* had stiffeners pointing *downstream*. No web-frame.

5 Errors and uncertainty of measurements and computations

Uncertainties or potential errors are classified as either random or systematic. Random and systematic errors should be treated separately and both should be included in the estimate of overall uncertainty (Ackers et. al. 1980, p. 275). The main reasons for the discharge coefficient error ΔC_D were assumed to be:

- 1) The error due to the measurement equipment and calibration, $\Delta C_{D,M}$
- 2) The error due to the inaccuracy of the formula for actual discharge determination, $\Delta C_{D,E}$
- 3) Uncertainty related to the statistical variation of the recorded values, $\Delta C_{D,S}$

Other sources of errors are discussed briefly, but they were assumed negligible. The total uncertainty estimate, ΔC_D , which is shown as the 95% confidence limits in the result figures, was expressed as:

$$\pm \Delta C_D = \pm (|\Delta C_{D,M}| + |\Delta C_{D,E}| + |\Delta C_{D,S}|) \quad (32)$$

The 95 % confidence limits of the determined discharge coefficients were in the order of $\pm \Delta C_D = 3-10\%$ of C_D . The contribution of $|\Delta C_{D,M}|$ was around 50-70 %, $|\Delta C_{D,E}|$ around 20-40 % and $|\Delta C_{D,S}|$ around 10 %. The main reason for uncertainty was thus the inaccuracy of measuring equipment, calibration and the determination of the actual discharge. The statistical variation of the measured values was small. The error bars are explained visually in Figure 26.

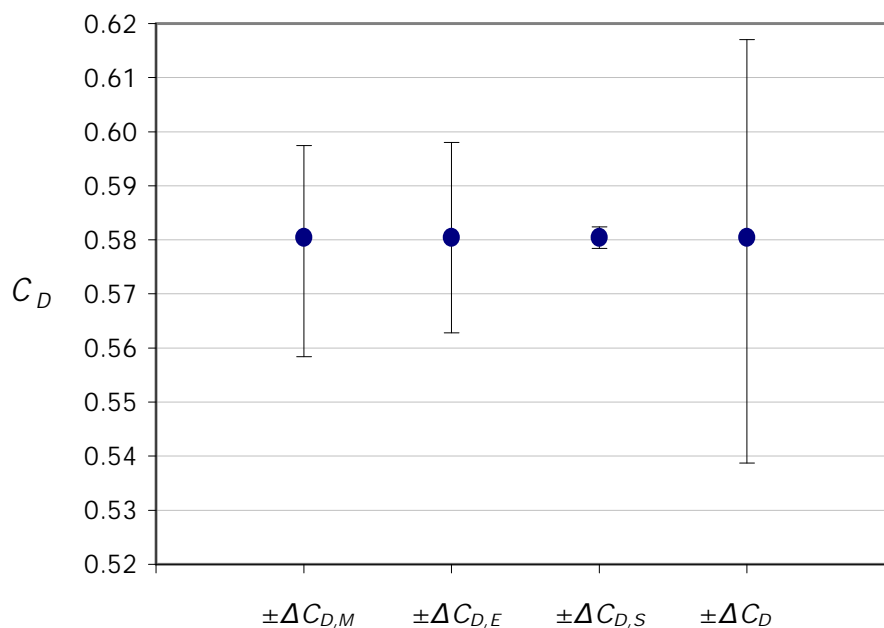


Figure 26. The 95% confidence limits $\pm \Delta C_D$, which are displayed for each computed average C_D value in the results section, are the sum of random and systematic uncertainties. The statistical variation is small compared to the potential systematic errors (example from test case V1).

5.1 Calibration and measurement accuracy

The calibration procedure was described in section 3.1.2. The measurement accuracy of the calibration water levels h_1 and h_2 was estimated to be ± 0.25 mm, which means a maximum error of $\Delta h = 0.5$ mm for the difference h_2-h_1 . The accuracy of the voltage output of the pressure transducer is according to the manufacturer $\Delta U = 0.25\%$ (Valmet 1985). The water temperature (approximately 15°C) does not affect the measuring equipment. By taking the natural logarithm of equation (3) and differentiating with respect to each variable, an expression for the total relative error for the calibration constant a in equation (12) is obtained:

$$\frac{\Delta a}{a} = \frac{\Delta h}{h_2 - h_1} + \frac{(U_1 + U_2)}{U_2 - U_1} \Delta U, \quad (33)$$

where $\Delta a/a$ is the relative error of the constant a . The error is a function of the differences in calibration water levels and respective voltages.

The difference between calibration water levels h_2-h_1 was approximately 350 mm and the corresponding voltages U_1 and U_2 measured with the upstream pressure transducer were typically in the order of 2.2 V and 4.9 V, respectively. The downstream values for U_1 and U_2 were 4.3 V and 6.9 V, respectively. The voltages measured with the differential pressure transducer were 1.9 V and 5.4 V for water level differences of 0 mm and 350 mm, respectively. The error budget for the calibration constant a is summarized in Table 2. Subscripts U , D , $diff$ and V are used for the different measurement devices.

Table 2. Error budget for calibration constant a (equation (12)) in up- and downstream head and head difference measurement devices.

Variable	Differential	Relative error, upstream head	Relative error, downstream head	Relative error, head difference
h_2-h_1	$\frac{\Delta h}{h_2 - h_1}$	$0.0014a_U$	$0.0014a_D$	$0.0014a_{diff}$
U_2-U_1	$\frac{(U_1 + U_2)}{U_2 - U_1} \Delta U$	$0.0066a_U$	$0.0108a_D$	$0.0052a_{diff}$
a	$\frac{\Delta a}{a}$	$\pm 0.0080a_U$	$\pm 0.0122a_D$	$\pm 0.0066a_{diff}$

Typical values for a_U , a_D and a_{diff} were 130, 134 and 100, respectively. Consequently, the total error due to the calibration constant a is 1.0 mm/V for a_U , 1.6 mm/V for a_D and 0.7 mm/V for a_{diff} . The error of the calibration constant b in equation (12) is derived from the error of constant a . The error of b is

$$\Delta b = a\Delta U + U_1\Delta a + 0.5\Delta h \quad (34)$$

The error budget for the constant b in equation (13) is given in Table 3.

Table 3. Error budget for calibration constant b (equation (13)) in up- and downstream head and head difference measurements devices.

Variable	Differential	Error, up-stream head	Error, down-stream head	Error, head difference
a	$U_1\Delta a$	2.20 mm	6.88 mm	1.33 mm
U_1	$a\Delta U$	0.33 mm	0.34 mm	0.25 mm
h_1	$\Delta h/2$	0.25 mm	0.25 mm	0.25 mm
b	Δb	2.8 mm	7.5 mm	2.3 mm

A conservative estimate of the maximum inaccuracy of calibration and measurement is

$$h = (a \pm \Delta a)(1 \pm \Delta U)U + b \pm \Delta b \quad (35)$$

The head in the V-notch weir was also checked with a point gauge during each measurement. The error in the V-notch head value is therefore assumed to be less than a 1 mm. Values of the estimated error constants are:

- V-notch weir head: $\Delta a_V = 0$ mm/V, $\Delta b_V = 1$ mm and $\Delta U = 0\%$
- Upstream head: $\Delta a_U = 1.0$ mm/V, $\Delta b_U = 2.8$ mm and $\Delta U = 0.25\%$
- Downstream head: $\Delta a_D = 1.6$ mm/V, $\Delta b_D = 7.5$ mm and $\Delta U = 0.25\%$
- Head difference: $\Delta a_{diff} = 0.7$ mm/V, $\Delta b_{diff} = 2.3$ mm and $\Delta U = 0.25\%$

The error of the visual estimate of the water level at the opening, Δh_D^* , is estimated to be ± 10 mm.

The general form of the maximum error caused by measurement inaccuracy is:

$$\Delta C_{D,M+} = \frac{Q_{A,MAX}}{Q_{T,MIN}} - \frac{Q_{A,AVG}}{Q_{T,AVG}} \quad (36)$$

$$\Delta C_{D,M-} = \frac{Q_{A,AVG}}{Q_{T,AVG}} - \frac{Q_{A,MIN}}{Q_{T,MAX}} \quad (37)$$

For submerged flow the equations (36) and (37) are evaluated into:

$$\Delta C_{D,M+} = \frac{6.8 \cdot 10^{-8} (h_V + \Delta b_V)^{2.428677}}{A_0 \sqrt{2g(a_{diff} - \Delta a_{diff})(1 - \Delta U)U + b_{diff} - \Delta b_{diff},)}} - \frac{6.8 \cdot 10^{-8} h_V^{2.428677}}{A_0 \sqrt{2gh_{diff}}}$$

$$\Delta C_{D,M-} = \frac{6.8 \cdot 10^{-8} h_V^{2.428677}}{A_0 \sqrt{2gh_{diff}}} - \frac{6.8 \cdot 10^{-8} (h_V - \Delta b_V)^{2.428677}}{A_0 \sqrt{2g(a_{diff} + \Delta a_{diff})(1 + \Delta U)U + b_{diff} + \Delta b_{diff}}}$$

Error equations for other flow conditions are expressed in a similar way.

The inaccuracy of the actual discharge equation is estimated as $\Delta Q_{A,E} = \pm 2\%$ for discharges up to 200 l/s and $\Delta Q_{A,E} = \pm 3\%$ for $Q_A > 200$ l/s. These errors agree with common accuracy estimates for thin-plate triangular weirs (Ackers et al. 1980, p. 275). The relationship between error terms $\Delta Q_{A,E}$ and $\Delta C_{D,E}$ is:

$$\Delta C_{D,E} = \frac{\Delta Q_{A,E} Q_A}{Q_T} \quad (38)$$

5.2 Statistical distribution of measured values

The presented discharge coefficients were computed from the average measured elevation head values (see section 3.1.2). A Gaussian normal distribution of the measured values was assumed.

The equation for the discharge coefficient involves two or three variables, h_V , h_U and h_{diff} , depending on the flow condition. The statistical uncertainty equations for each flow condition are derived by differentiating equation (3) with respect to each of its variables:

$$\Delta C_{D,S} = \frac{\partial \frac{Q_A}{Q_T}}{\partial h_V} \Delta h_{V,S} + \frac{\partial \frac{Q_A}{Q_T}}{\partial h_U} \Delta h_{U,S} \quad (39)$$

for free flow,

$$\Delta C_{D,S} = \frac{\partial \frac{Q_A}{Q_T}}{\partial h_V} \Delta h_{V,S} + \frac{\partial \frac{Q_A}{Q_T}}{\partial h_{diff}} \Delta h_{diff,S} \quad (40)$$

for submerged flow and

$$\Delta C_{D,S} = \frac{\partial \frac{Q_A}{Q_T}}{\partial h_V} \Delta h_{V,S} + \frac{\partial \frac{Q_A}{Q_T}}{\partial h_U} \Delta h_{U,S} + \frac{\partial \frac{Q_A}{Q_T}}{\partial h_{diff}} \Delta h_{diff,S} \quad (41)$$

for partly submerged flow. The variables $\Delta C_{D,S}$, $\Delta h_{V,S}$, $\Delta h_{U,S}$ and $\Delta h_{diff,S}$ are the statistical errors of the discharge coefficient, head above the V-notch weir, upstream head and the difference in elevation head between the upstream and downstream, respectively. The statistical errors $\Delta h_{V,S}$, $\Delta h_{U,S}$ and $\Delta h_{diff,S}$ are computed from

$$\Delta h_{X,S} = 2 \sqrt{\frac{\sum_{i=1}^N (h_{X,i} - h_{X,AVG})^2}{N(N-1)}}, \quad (42)$$

where N is the number of observations. The function is the mean error of the mean value multiplied with two and it corresponds to a certainty of approximately 95% (e.g. Ackers et al. 1980, p. 276).

5.3 Statistical comparison of results

The purpose of statistical analyses was to examine whether two averages differed significantly from each other. The flow conditions in the compared measurements must be similar and the potential systematic errors have to be assumed small to allow any statistical comparison. The head values in each single measurement were assumed to be normally distributed, but the variances and sample sizes varied to some degree. The Student's t-test for unequal sample sizes and unequal variances was therefore applied. The t statistic is given by (e.g. Spiegel 1972, p. 190):

$$t = \frac{\bar{X}_1 - \bar{X}_2}{\sqrt{\frac{s_1^2}{n_1} + \frac{s_2^2}{n_2}}}, \quad (43)$$

where \bar{X}_X are the averages, s_x^2 are the variances and n_x the sample sizes of the two compared measurements X . The Welch-Satterthwaite equation was used in order to estimate the degrees of freedom (e.g. Brownlee 1960, p. 236):

$$d.f. = \frac{(s_1^2 / n_1 + s_2^2 / n_2)^2}{(s_1^2 / n_1)^2 / (n_1 - 1) + (s_2^2 / n_2)^2 / (n_2 - 1)}, \quad (44)$$

The length scale was taken into account in the statistical analyses. The threshold for statistical significance was chosen as 0.01 (1%).

5.4 Pressure losses due to the flume

Measurements were conducted to determine the energy losses caused by the flume bed and wall friction. Two different discharges were released into the flume and the depth of the flow was varied with a tailgate. The elevation head differences between the up- and downstream measurement locations were recorded (Figure 27).

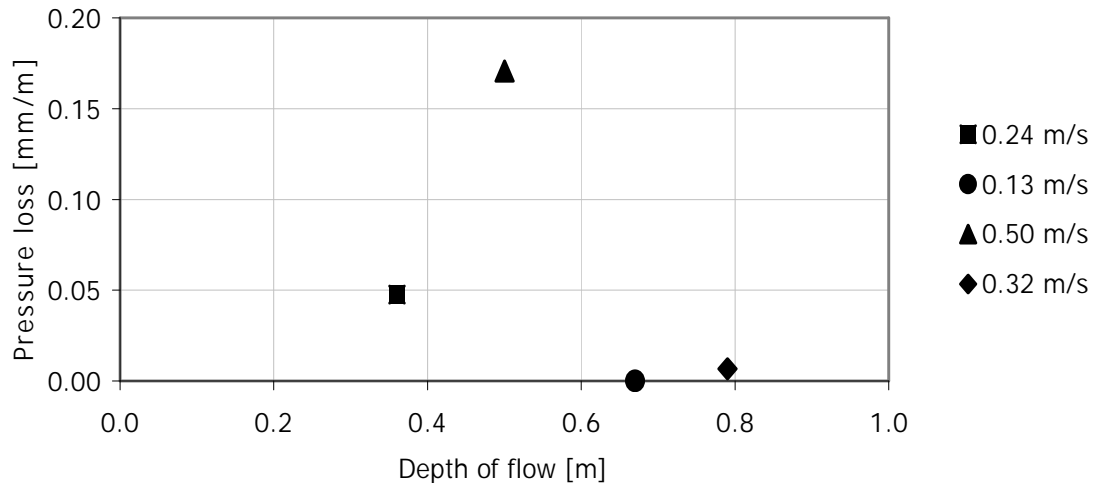


Figure 27. The pressure losses due to the flume were so small, that they were neglected in the uncertainty analysis.

The measurements indicated that pressure losses due to the flume are very small compared to the measurement accuracy. The pressure losses need to be taken into account only with a large discharge at small flow depths. Such flow conditions did not occur in the tests of this study, and therefore pressure losses due to the flume were neglected.

5.5 Other sources of error

Numerical integration with the Simpson's method (section 3.2.1) causes a small error, which is negligible due to the small integration interval.

In the test cases with free discharge from the cross-duct, there is a potential error related to the position of the test object. Measurements of the location of both the upstream and downstream girder openings were performed in order to ensure that the cross-duct was in a horizontal position. Consequently, the error source was neglected.

The cross-duct was intended to be waterproof, but some leakage was observed during the tests. Leakage could be observed especially in the seams or joints between modules, between the plexus glass and plywood and from the opening for the web frame on the top of the model. The leakages were estimated to be in the order $10^{-4} \text{ m}^3/\text{s}$. The observed leakage had no significance for the results.

The head in the V-notch tank and the elevation heads in the flume were recorded simultaneously. In reality, it takes some time for the water to flow from the V-notch tank to the test object. In this study, the discharge over the V-notch weir was assumed to correspond to the discharge through the test object.

6 Results and discussion

All figures in the results section are shown with 95% confidence intervals based on the uncertainty analysis in section 5. The displayed confidence limits are the sum of uncertainties related to the variation of measured head values and the maximum error due to the accuracy of measurements and computations.

6.1 Single manholes and girders

6.1.1 Free flow

Free flow test cases involved the full-scale manhole, the 1:2 scale model manhole and the 1:3 scale model girder with two manholes or one of the manholes covered with a plate. The manholes were tested in both upright and horizontal positions. The girder was tested with the manholes in upright position only. For more detailed descriptions of test cases V1, I1, VM1, G1, G6, H1 and HM1, see section 4.

The jet separated from the opening edges at the upstream face in all free flow tests. This means that the manhole acts like a sharp edged weir or orifice in free flow conditions (Figure 28). Consequently, the thickness of the opening plate is irrelevant for the discharge coefficient in free flow.

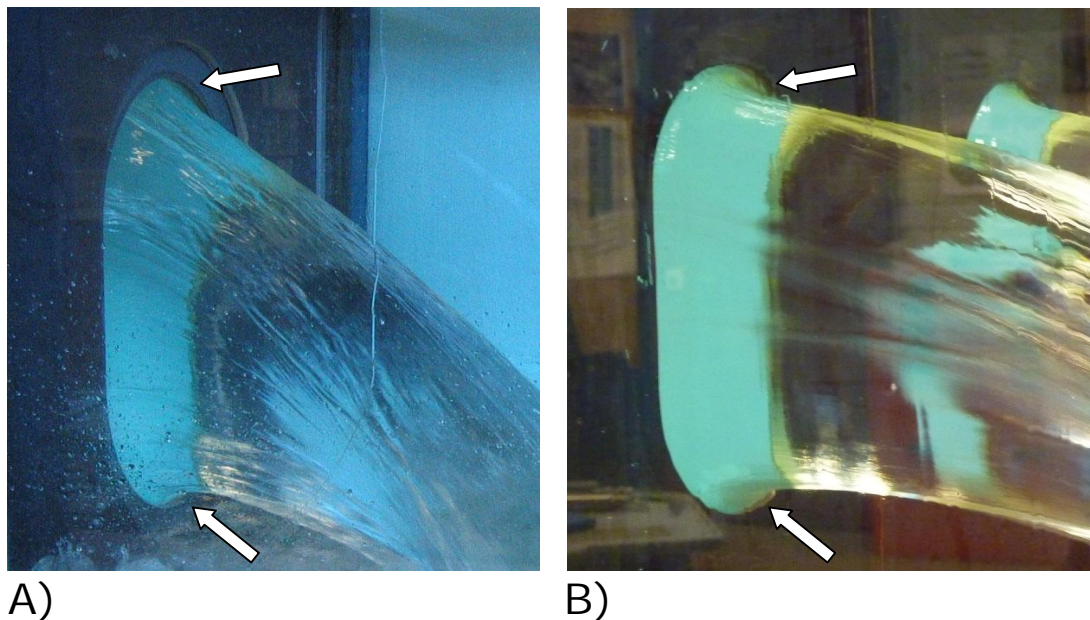


Figure 28. The jet separated from the opening edge at the upstream face, which means that the thickness of the opening plate does not affect the discharge coefficient in free flow. A) Orifice flow through a full-scale manhole and B) free orifice flow through a scale model girder.

The influence of the average upstream velocity head was clearly observed in the test case with free flow through the full-scale manhole in upright position (Figure

29). The velocity head caused a decrease of approximately 1% in the discharge coefficient. The actual discharges in test case V1 were $Q_A = 3-314$ l/s.

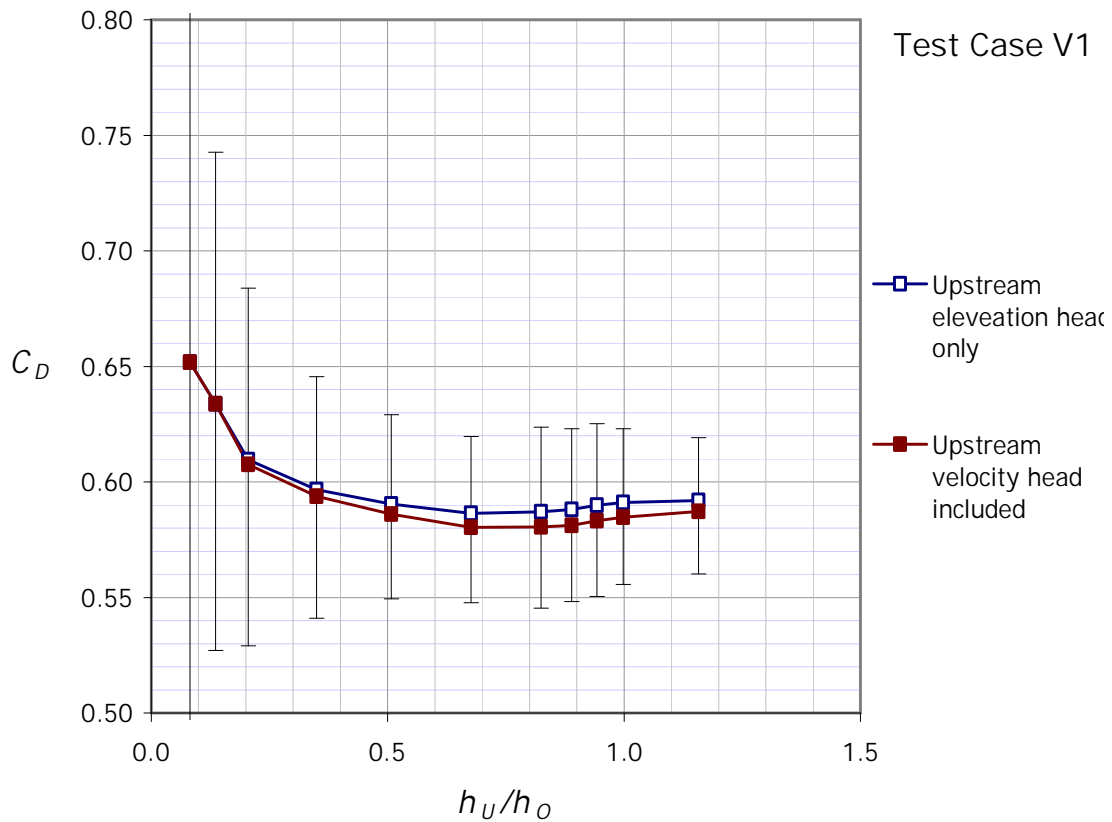


Figure 29. The discharge coefficients from test case V1 plotted against the upstream head to opening height ratio. The 95% confidence intervals are the sum of uncertainties related to the variation of measured head values and the maximum error due to the accuracy of measurements and computations. The statistical variation of the values is actually quite small (see Figure 26).

The discharge coefficient was typically in the order of 0.58-0.59 for the full-scale manhole when the velocity head was taken into account. It is possible that the discharge coefficient in test case V1 was slightly affected by the vicinity of the flume walls and bed (see Figure 6A and Figure 7A in section 2.4). This would mean that the presented C_D values are slightly higher than corresponding values for a fully contracted flow.

The influence of the manhole geometry (the half circles) was clearly visible in the form of the C_D curves in all free flow cases. The discharge coefficient first sharply decreases to its minimum value and then slightly rises in the transition between weir and orifice flow (compare Figure 29 and Figure 30 to Figure 7B). Tests with the scale model manholes showed that the discharge coefficient decreases against a constant value in orifice flow with high upstream heads (Figure 30). This value was approximately 0.60, 0.61 and 0.62 for the 1:2 scale model manhole (test case VM1), 1:3 scale model girder with two manholes (test case G1) and the same girder with one opening covered (test case G6), respectively.

A smaller cross-sectional area of the opening seems to yield higher discharge coefficients in free flow. The discharges in test cases G6, G1 and VM1 were 14–57 l/s, 3–113 l/s and 1–119, respectively.

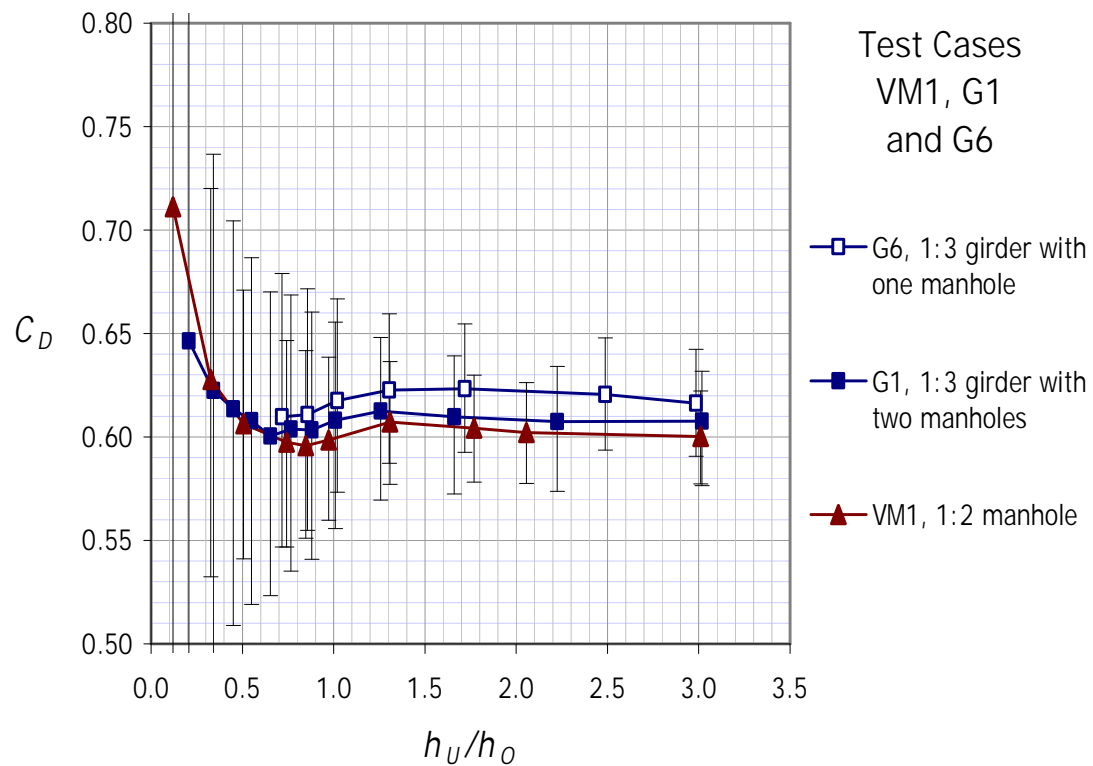


Figure 30. The discharge coefficients from test cases VM1, G1 and G6 plotted against the upstream head to opening height ratio. The form of the C_D curves were similar as in the full-scale test, but the value of the discharge coefficient increased as the scale decreased (compare to Figure 29).

The form of the C_D value curve was similar in free flow through the manhole in horizontal position (Figure 31). The discharge coefficients from the test with the full-scale manhole in horizontal position (test case H1) are clearly higher than corresponding values with the full-scale manhole in vertical position (test case V1, Figure 29). The increase is caused by the wideness of the manhole compared to the flume width. In horizontal position the maximum width of the manhole is 0.60 m or 55% of the flume width (see Figure 7A).

In fully contracted flow the discharge coefficient of the full-scale manhole would be lower than corresponding values determined with the scale model (test case HM1). The curve from test case H1 decreases slightly as the upstream head increases. The reason for this is that the relative influence of the side walls decreases in orifice flow with high upstream heads as a larger proportion of the total streamlines are unaffected by the flume walls. The discharges in test cases H1 and HM1 were 19–363 l/s and 4–124 l/s, respectively.

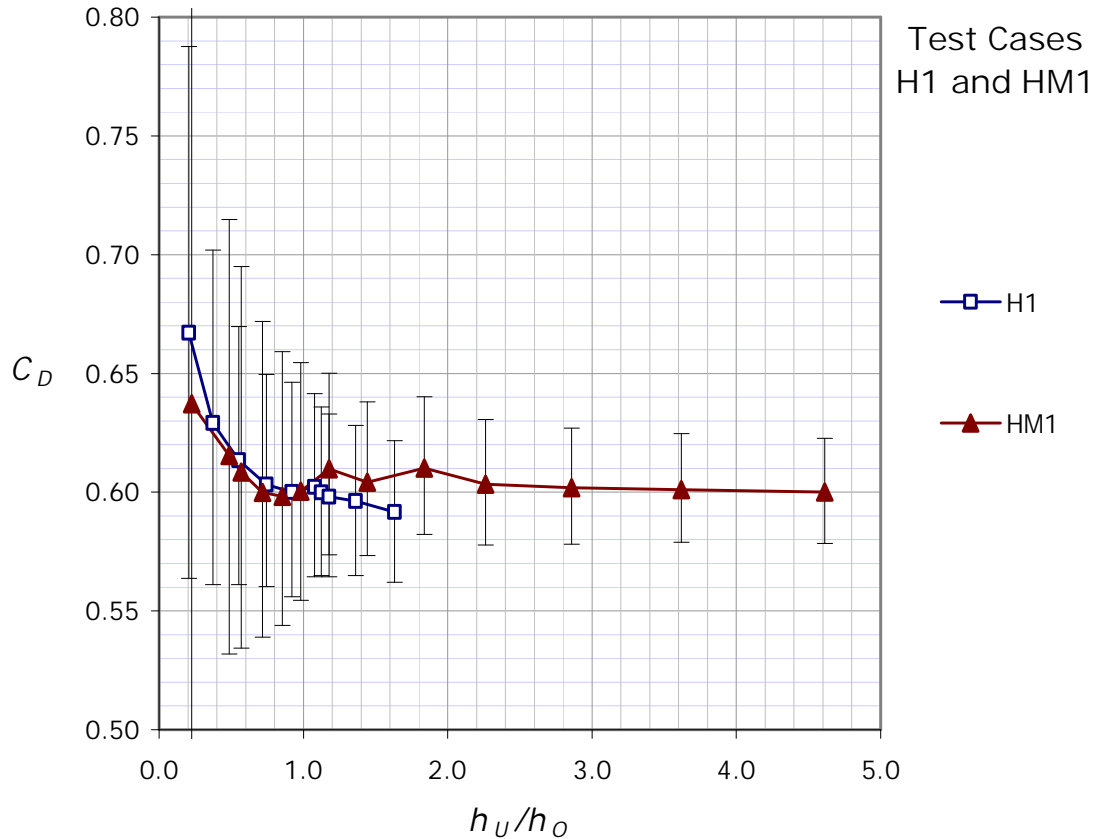


Figure 31. The discharge coefficients from test cases H1 and HM1 plotted against the upstream head to opening height ratio. Velocity was included in test case H1 results only. The side walls affected the flow through the full-scale manhole resulting in higher discharge coefficients for test case H1. Note that in horizontal position the opening height is $h_o = 0.4$ m.

With high upstream heads, the discharge coefficient in test case HM1 approaches the same value, approximately 0.6, as in the test with the 1:2 scale model manhole in vertical position (VM1, Figure 30). The discharge coefficients for the manhole in horizontal and vertical position are overall very similar. The same conclusion probably applies for submerged flow, but the manhole in horizontal position was not tested in submerged flow conditions in this study.

The discharge coefficients of a full-scale manhole inclined at an angle of 20° (test case I1, Figure 33) were lower than the corresponding values for an upright manhole (compare Figure 32 to Figure 29). The decrease was up to 5% and is likely caused by the weight of the jet water mass, which was not taken into account in the computations of the theoretical discharge Q_T . The drop and rise in the C_D curve becomes steeper as a result of inclination. The influence of inclination on the discharge coefficient was observed clearly only in free flow, whereas the influence seems negligible in submerged flow (compare to Figure 38 in section 6.1.2 and Figure 57 and Figure 58 in section 0). The discharges in the test case I1 were 19–366 l/s.

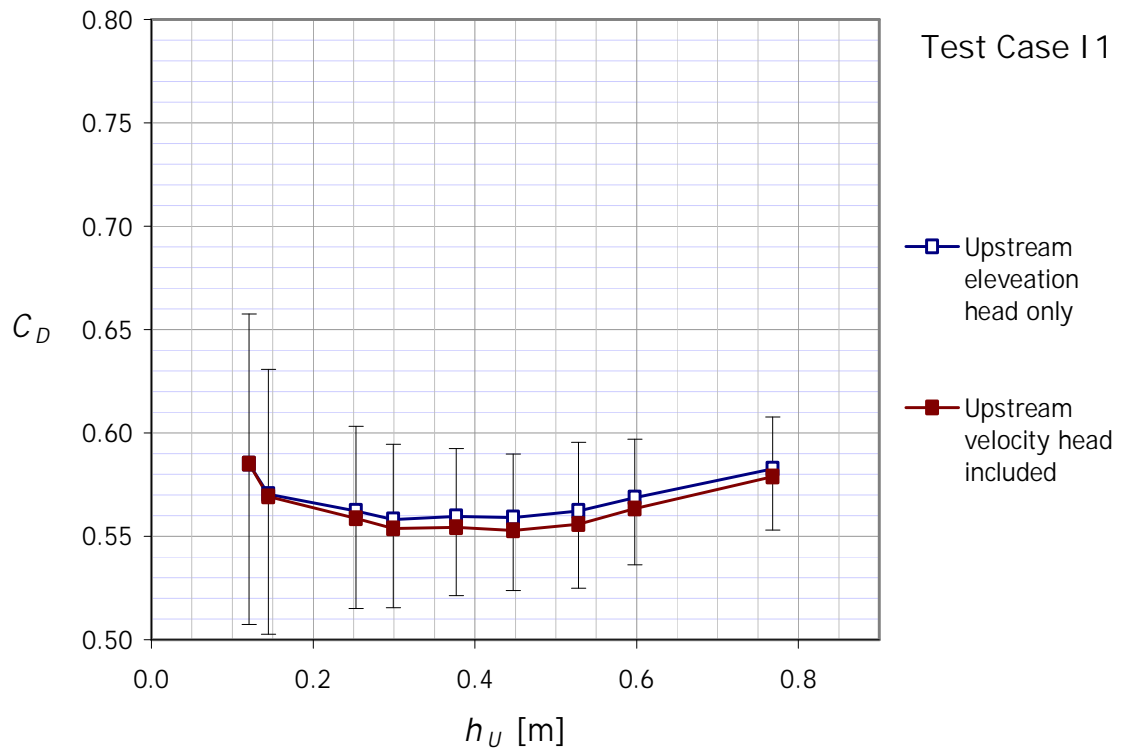


Figure 32. The discharge coefficients from test case I1 plotted against the upstream head. The test was generally the same as test case V1, but the manhole was inclined 20° towards the upstream (see Figure 33 below).



Figure 33. In test case I1 the full-scale manhole was inclined at an angle of 20° towards the flow. Orifice flow is shown with the maximum discharge of $Q_A = 366$ l/s.

6.1.2 Partly and completely submerged flow

The computed discharge coefficients from submerged weir flow cases (e.g. Figure 34) were depicted against the submergence degree, h_D/h_U . In partly and completely submerged orifice flow cases (e.g. Figure 35) the ratio between the downstream head and the opening height, h_D/h_O , was considered more appropriate for describing the results.

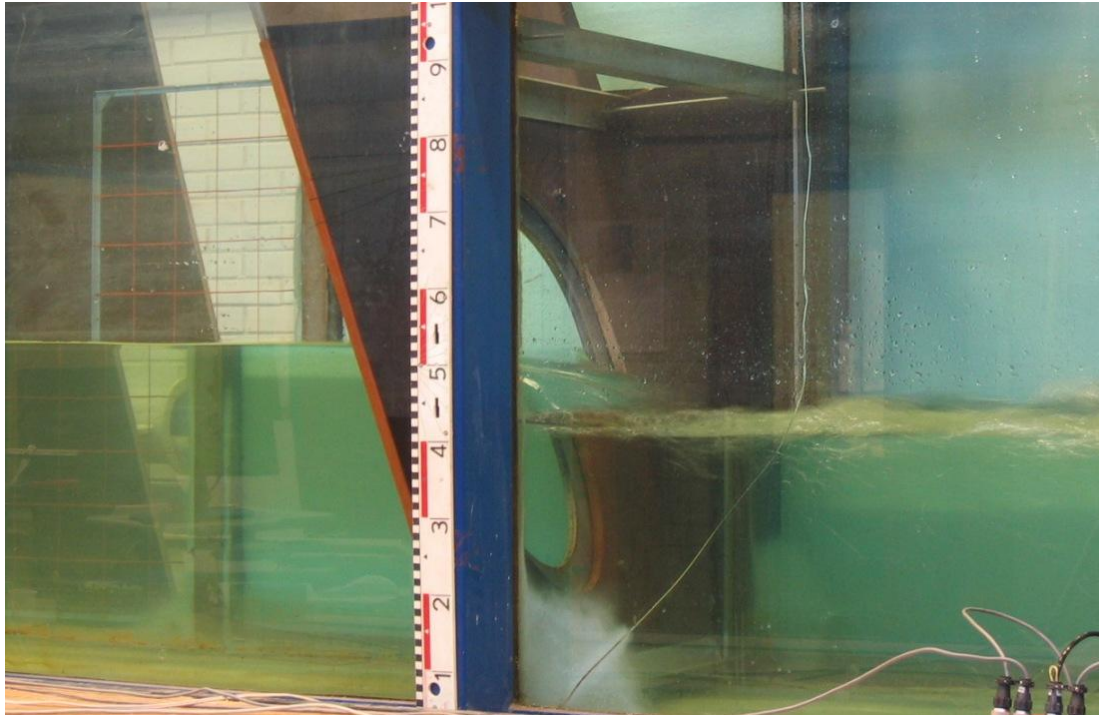
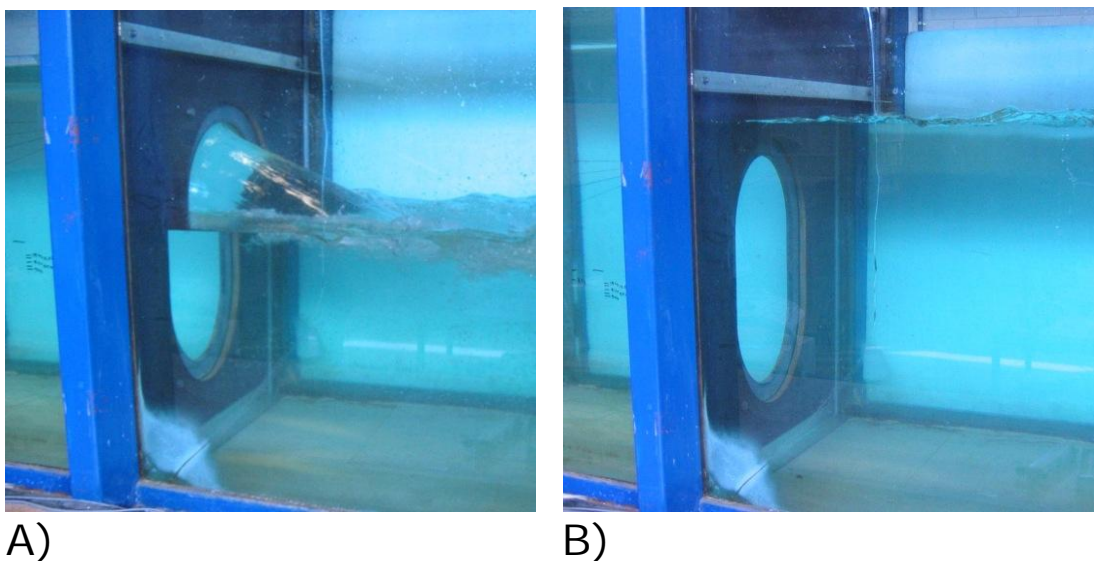


Figure 34. Submerged weir flow through an inclined full-scale manhole.



A)

B)

Figure 35. A) Partly submerged orifice flow and B) submerged orifice flow through a full-scale manhole.

Submerged flow tests do not produce unique relationships between the head and the discharge, because there is an infinite amount of discharge and up- and downstream combinations. The submergence degree $h_D/h_U = 0.5$, for instance, is the quotient of water levels $h_D = 0.25$ m and $h_U = 0.5$ m, but it is also the quotient of $h_D = 0.1$ m and $h_U = 0.2$ m. The discharge coefficient for these two variations of the same submergence level is not exactly the same.

Submerged weir flow was examined in three test cases: V3, V4 and I2. In test case V3 (Figure 36) the discharge was set to 92 l/s and in test case V4 (Figure 37) the discharge was 182 l/s. The discharge was 93 l/s in test case I2 (Figure 38), in which the manhole was inclined at an angle of 20° (see Figure 34). The velocity head was not included in the results. The confidence intervals are shown for method 1 only.

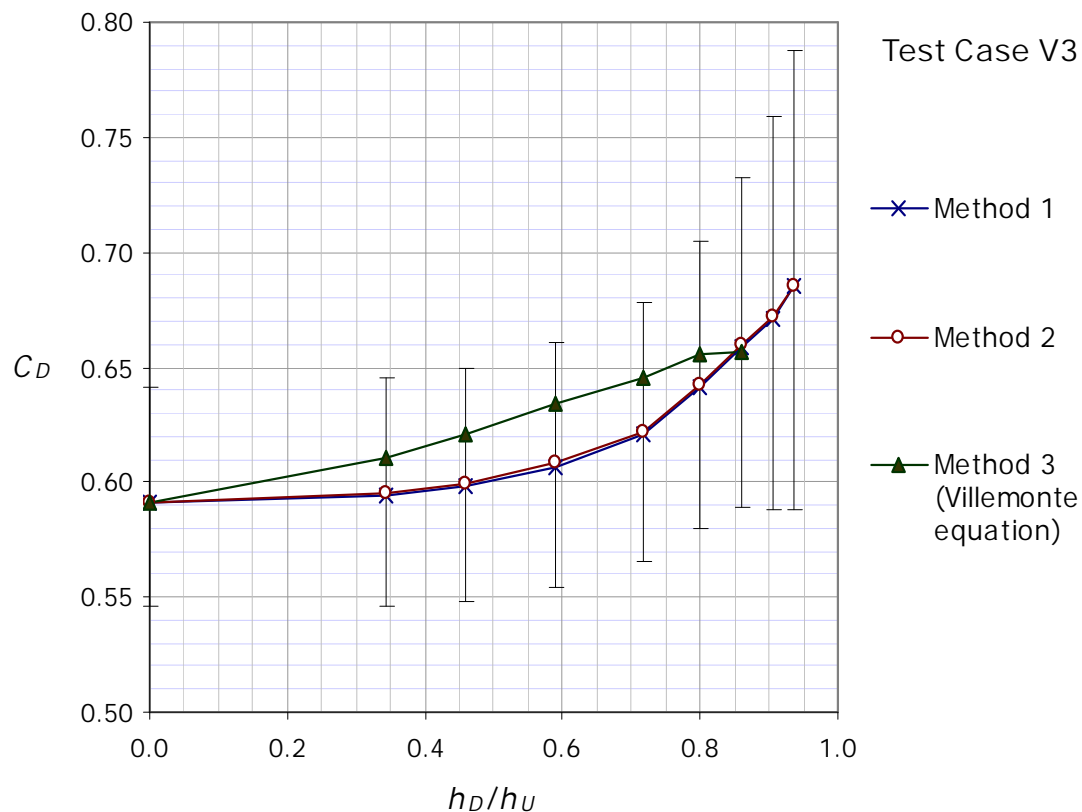


Figure 36. The discharge coefficients of a full-scale manhole in submerged weir flow plotted against the submergence ratio. The actual discharge was $Q_A = 92$ l/s, the initial upstream head (when $h_D/h_U = 0$) was 0.300 m and the final upstream head was 0.397 m.

The difference between results computed with method 1 and 2 (see section 3.2.3) was small, but increased slightly when the discharge was increased (compare Figure 36 to Figure 37). Method 3, or the Villemonte equation, gave a more gradual increase of C_D and typically slightly higher C_D values.

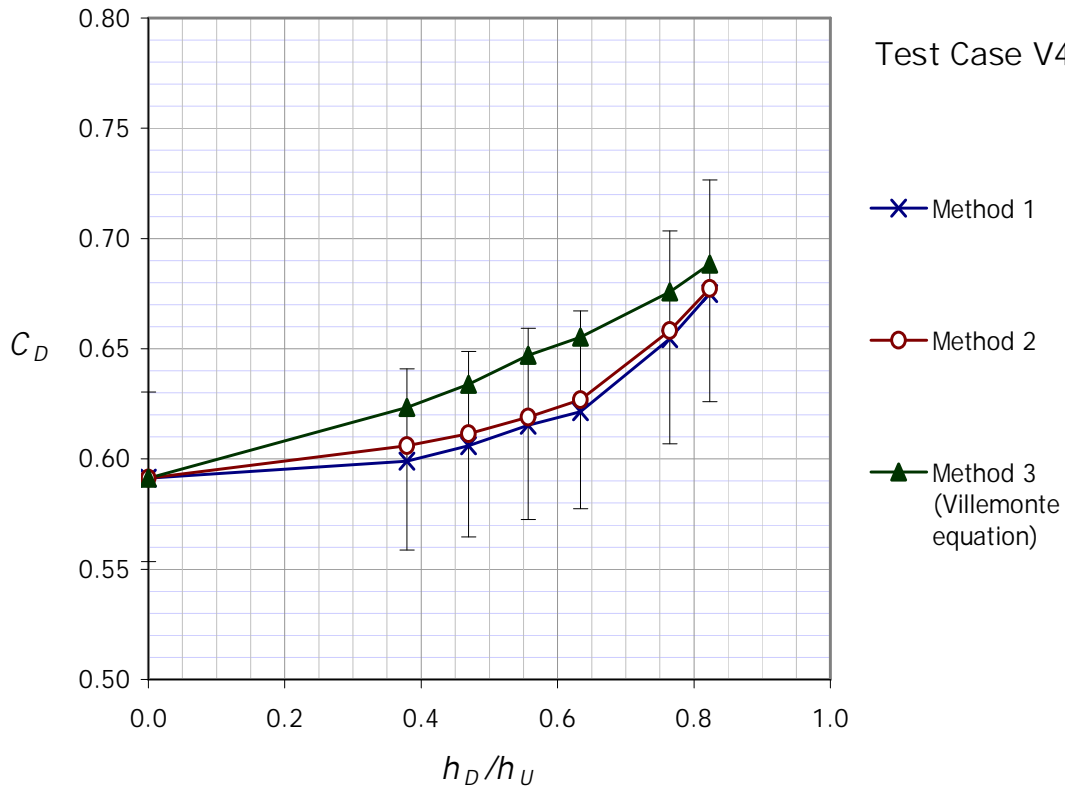


Figure 37. The relationship between the discharge coefficient of a full-scale manhole and the submergence ratio in submerged weir flow with the actual discharge $Q_A = 182$ l/s. Initial upstream head (when $h_D/h_U = 0$) was 0.450 m and the final upstream head was 0.567 m.

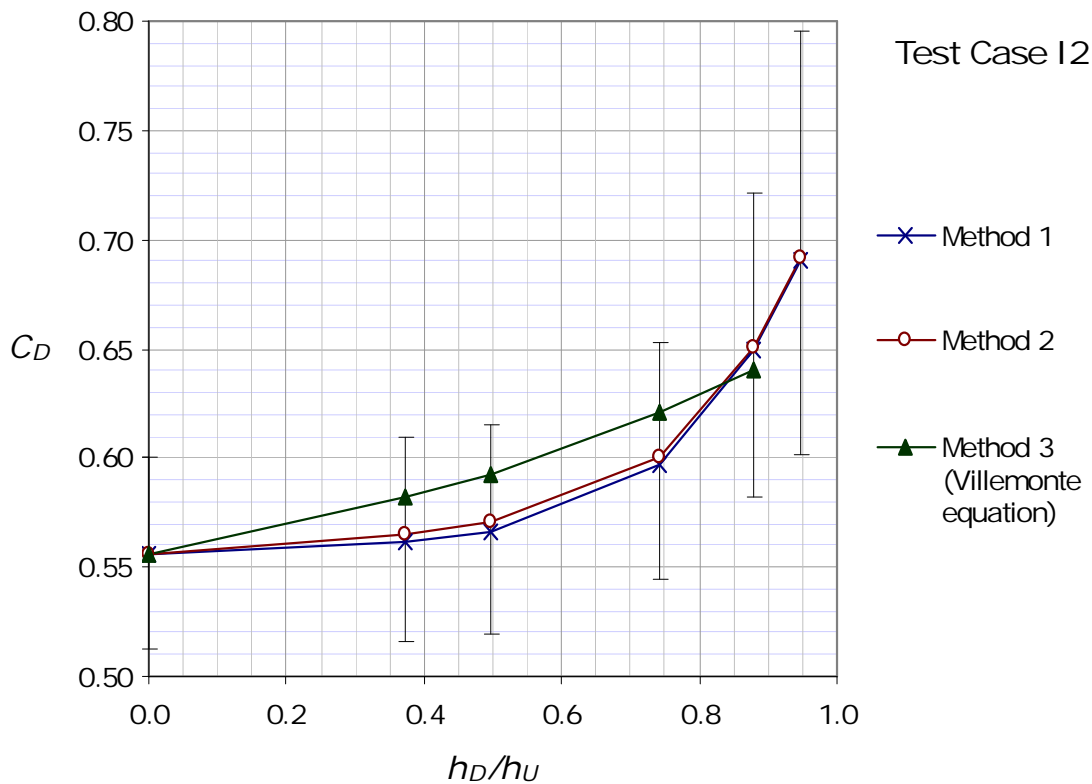


Figure 38. The relationship between the discharge coefficient and the submergence ratio in submerged weir flow through a 20° inclined full-scale manhole with the actual discharge $Q_A = 93$ l/s. Initial and final upstream heads were 0.299 m and 0.493 m, respectively.

By comparing Figure 38 to Figure 36 it can be seen that inclination does not affect the discharge coefficient for high submergence degrees. The difference between the discharge coefficient values in test cases V3 and V4 implies that the submergence level alone is not a parameter that sufficiently describes the flow conditions of a manhole. The ratio between discharge and size of the downstream compartment also influences C_D .

The velocity head was not included in the computations for test cases with downstream submergence. If there was an appropriate method to account for the velocity heads, the obtained discharge coefficients for the full-scale manhole would be slightly smaller.

Partly submerged orifice flow through a full-scale manhole was examined in test cases V4, V5 and V6. The behaviour of the discharge coefficient was found to be similar as in submerged weir flow. The greatest discharge coefficients were obtained when the opening was just fully submerged, but the value dropped slightly as the downstream to opening height was further increased (Figure 39). Because of the dimensional limitations of the laboratory flume, it was not possible to use higher downstream water heads than 0.8 m in the tests with the full-scale manhole.

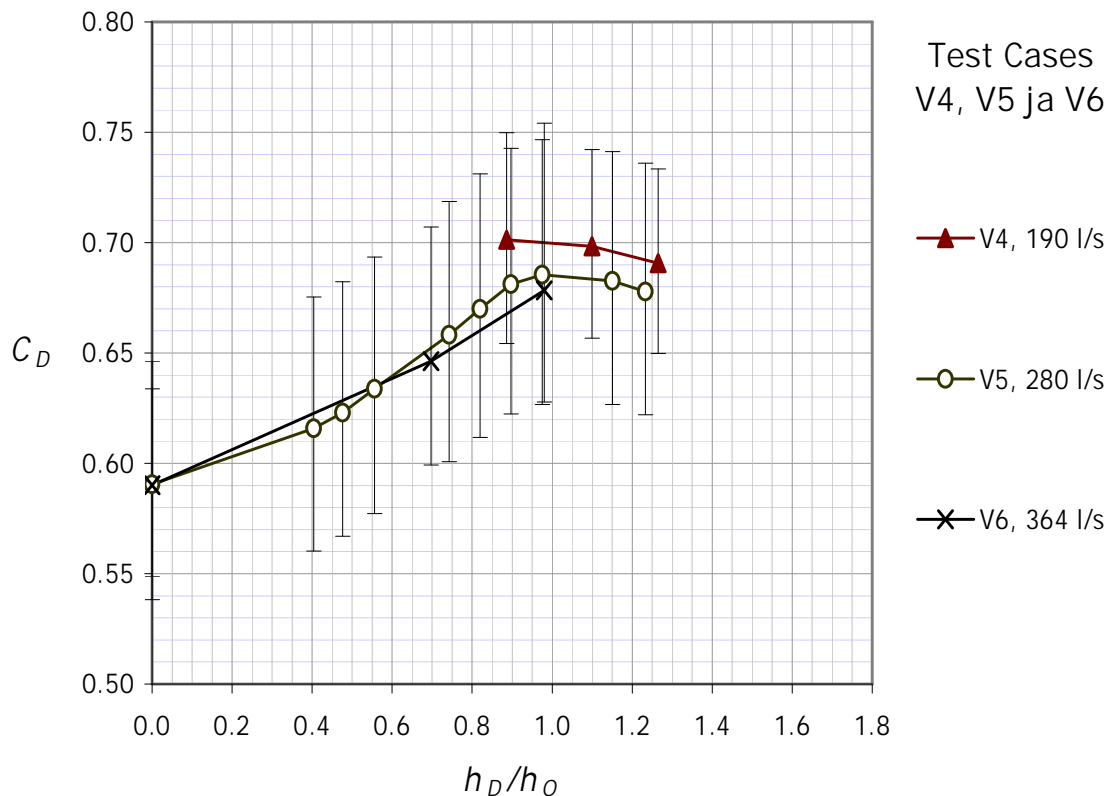


Figure 39. Relationship between the discharge coefficient and the downstream head to opening height ratio in partly and completely submerged orifice flow through the full-scale model manhole. The displayed values were computed with method 2 (see section 3.2.3).

In completely submerged conditions, the C_D values for $Q_A = 190$ l/s were higher than the C_D values with corresponding downstream submergence and $Q_A = 280$ l/s (Figure 39). This could indicate that an increase in the flow velocity decreases the value of C_D . A similar observation was made in the test cases with girders in submerged flow conditions, G3-G7. In those test cases the decrease of the discharge coefficient was smaller. More tests with a greater range of heads would be needed to make definite conclusions about the influence of flow velocity.

Partly and completely submerged orifice flow was examined also with the 1:2 scale model manhole (test case VM2, Figure 40). The actual discharge was $Q_A = 51$ l/s, which corresponds to 290 l/s through a full scale manhole. The obtained C_D values were much lower than in the corresponding test with the full-scale manhole (compare Figure 40 to test case V5 in Figure 39).

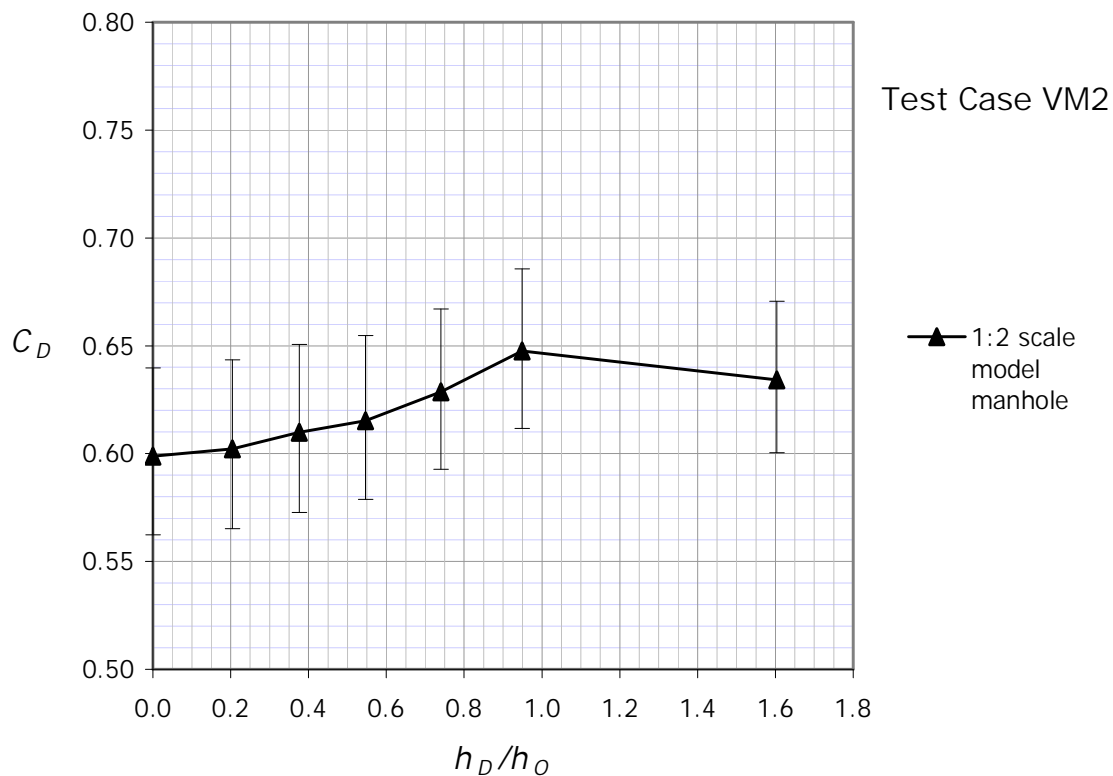


Figure 40. Relationship between the discharge coefficient and the downstream head to opening height ratio in partly and completely submerged orifice flow through the 1:2 scale model manhole. The discharge was 51 l/s. The displayed values were computed with method 2 (see section 3.2.3).

The scale model manhole and the full-scale manhole were not hydraulically similar. The flow through the scale model was fully contracted (Figure 6) and not as strongly affected by the turbulent eddies on the downstream side of the dam plate (Figure 4). However, a considerable part of the difference is probably

explained by the scale effects. This would indicate that the scale effects in submerged flow are different than in free flow. The magnitude of scale effects is estimated in section 6.2.1.

The 1:3 scale model girders (see section 4.3) were examined in submerged flow conditions in test cases G3-G5 and G7. One of the main aims of the girder tests was to examine the influence of stiffeners on the girders. The girder stiffeners were attached either to the downstream side (G3, Figure 43) or the upstream side of the girder (G4, Figure 44). Another objective was to examine whether the discharge coefficient of a girder with two manholes was different from the discharge coefficient of a girder with one manhole. This was done by covering the other girder manhole with a plate. The average values from test cases G3-G5 and G7 are presented in Table 4.

Table 4. Average results from test cases with girders in submerged flow.

Test case	Girder specification	Average C_D	$k_G = \frac{1}{C_D^2} - 1$
G3	stiffeners downstream, two manholes	0.644	1.411
G4	stiffeners upstream, two manholes	0.666	1.255
G5	no stiffeners, two manholes	0.638	1.457
G7	no stiffeners, one manhole	0.633	1.499

The tests with girders showed that girder stiffeners significantly affect the flow through the manholes. Their influence was most visible when the stiffeners were attached to the upstream side of the girder (Figure 41). Stiffeners pointing upstream caused a 4% increase in the C_D value of the girder (G4, Figure 44). The increase in the discharge coefficient value was less than 2% when the stiffeners were pointing downstream (Figure 43).

The influence on the flow by stiffeners on the upstream side of the girder can be observed visually by comparing Figure 41 and Figure 42, which are taken in free flow conditions. The streamlines are straightened due to the vicinity of the stiffeners and the contraction is incomplete on the bottom and the top of the jet (compare to Figure 6A and Figure 6B).

The model stiffeners were not exactly similar to real full-scale structural stiffeners. Real stiffeners with a rounded edge would possibly cause a slightly higher increase in the value of the discharge coefficient. Consequently, the

results suggest that stiffeners need to be taken into account in the CFD analysis of cross-ducts.



Figure 41. Free flow through a girder with the stiffeners pointing in the upstream direction (test case G4). The jet is smooth on the sides, but incompletely contracted on the bottom and the top.



Figure 42. Free flow through a girder without stiffeners (test case G5). The jet is smooth all around. The free flow case with stiffeners pointing downstream is similar.

By comparing the discharge coefficients in test cases G5 (Figure 45) and G7 (Figure 46), it can be seen that the discharge coefficient in submerged flow was slightly smaller for a girder with just one manhole than for a girder with two manholes. The difference was approximately 1%. In the CFD analysis by Pittaluga and Giannini (2006), the corresponding difference is approximately 4% when the distance between two girders is more than 4 m. The difference in the value of C_D depends on the geometry of the girders.

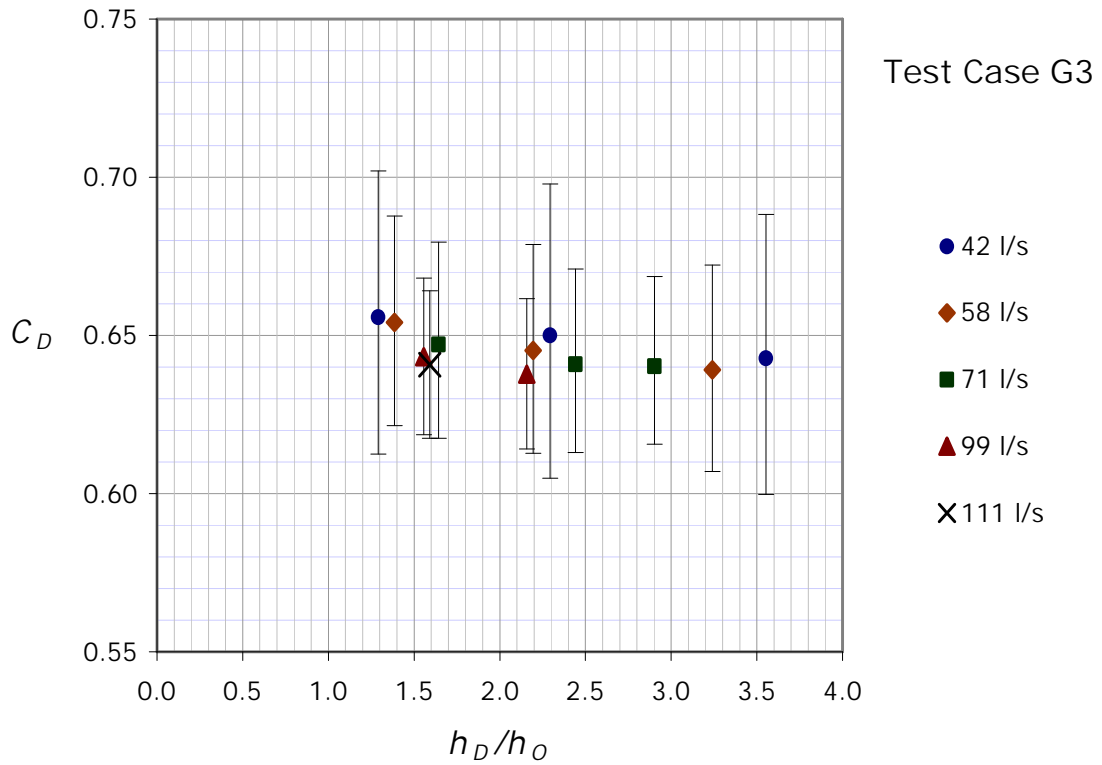


Figure 43. The relationship between the discharge coefficient and the downstream head to opening height ratio when the girder with two manholes was equipped with stiffeners pointing in the downstream direction.

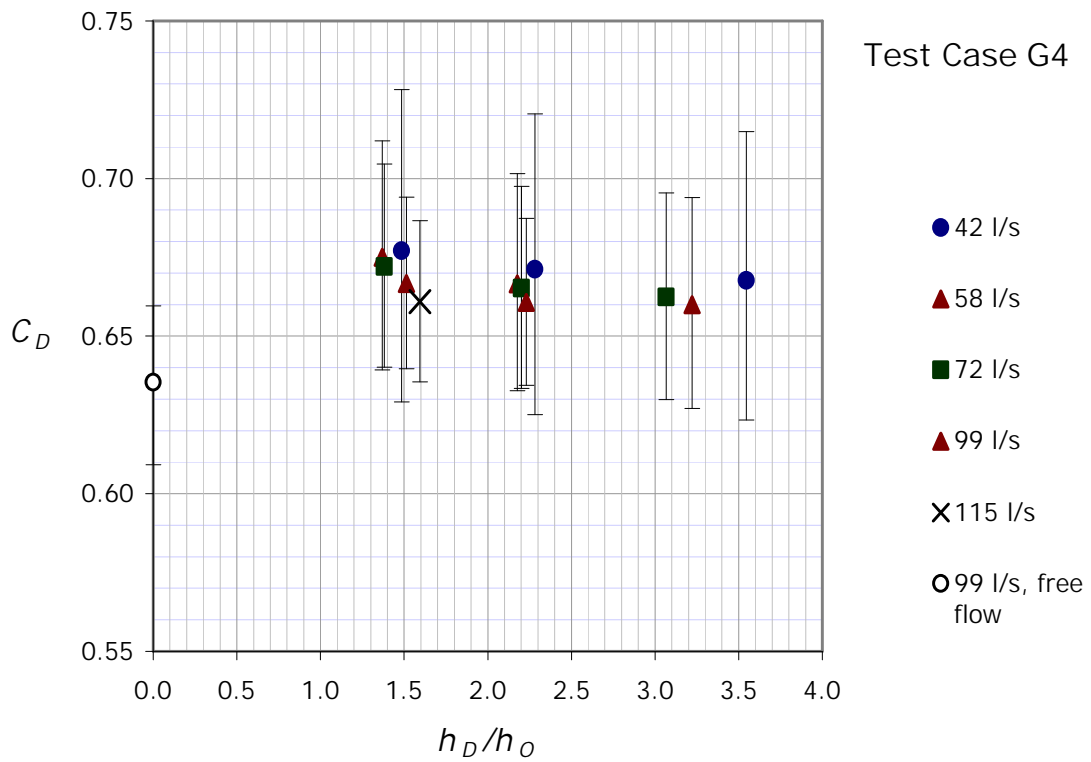


Figure 44. The relationship between the discharge coefficient and the downstream head to opening height ratio when the girder with two manholes was equipped with stiffeners pointing in the upstream direction (as in Figure 41).

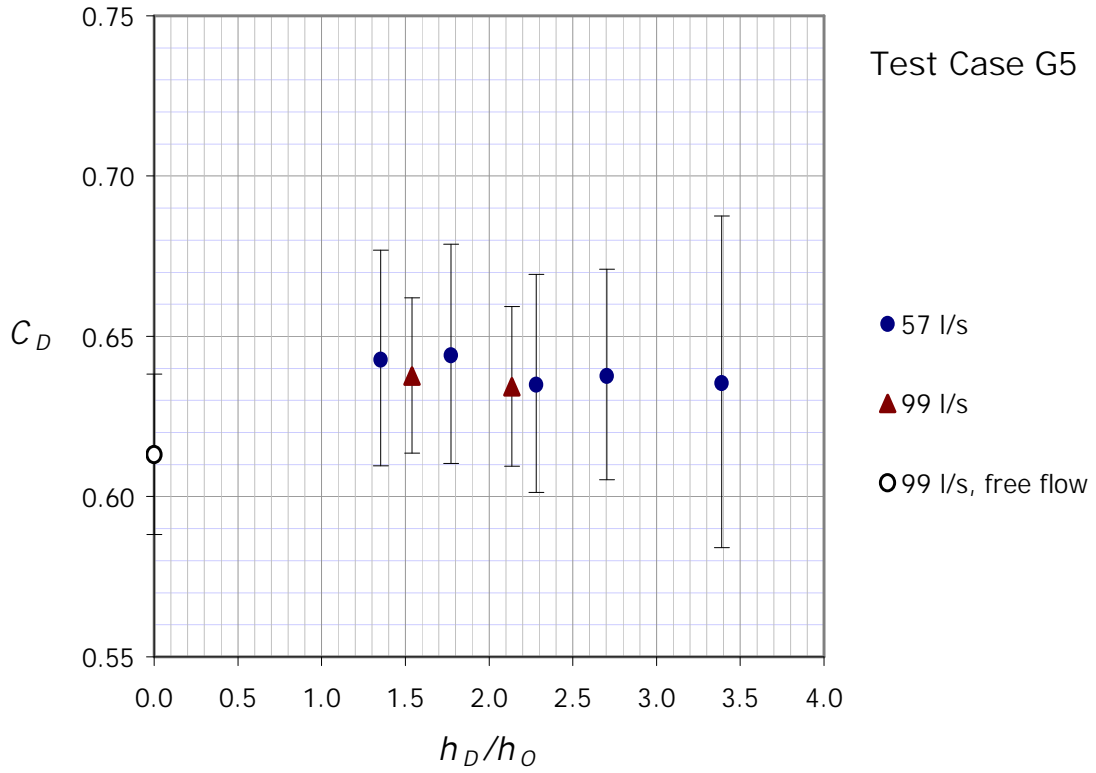


Figure 45. The relationship between the discharge coefficient and the downstream head to opening height ratio when the girder with two manholes had no stiffeners.

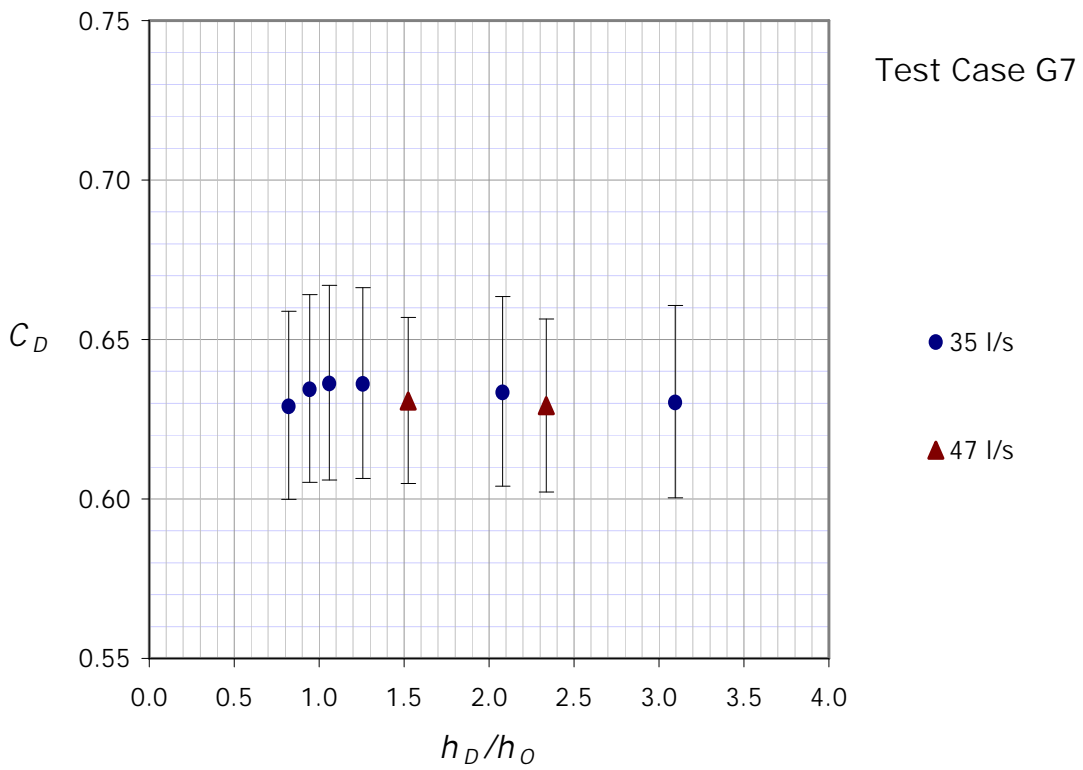


Figure 46. The relationship between the discharge coefficient and the downstream head to opening height ratio when one of the girder manholes was covered with a plate. The girder had no stiffeners.

Some systematic variation of the discharge coefficient could be observed in all girder tests with submerged flow. An increase in the downstream to opening height ratio (h_D/h_O) caused a small decrease in the value of C_D , although the decrease was much smaller than in the tests by Nielsen and Weber (2000) (see section 2.5).

An increase of the discharge caused a small decrease in the discharge coefficient. The same phenomenon was observed in the tests with the full-scale manhole (Figure 39). This result was surprising, since the influence of increased velocity on the C_D value was assumed to be the opposite on the basis of experiments by Vredeveldt and Journée (1991). The drop in the discharge coefficient due to increased discharge and h_D/h_O ratio was, however, very small compared to the uncertainty related to the measurements. Additional tests with greater heads would be needed to verify the observations.

An important discovery in all partly or completely submerged flow cases was that the C_D value increased as the jet discharged into water instead of air. Ruponen (2007) mentions that flooding simulations yield better estimates when a slightly smaller C_D is used for submerged flow conditions. Bos (1989, p. 271) and Katayama and Ikeda (2005) report smaller discharge coefficients in submerged flow than in free flow, but the difference between the submerged and free flow C_D values became smaller as the opening size increased. For a sharp crested circular orifice with a diameter larger than 7.5 cm, the discharge coefficient is the same in submerged and free orifice flow (Bos 1989, p. 271). The openings in the mentioned references were, however, much smaller than in this study.

It is possible that the relation between the submerged and free flow discharge coefficients generally depends on the size of the opening. The difference between the submerged and free flow discharge coefficients was greatest for the full-scale manhole and decreased as the scale decreased. For the 1:3 scale model girder with one of the openings covered, the submerged orifice flow C_D was around 0.63 and the free orifice flow C_D was around 0.62. The corresponding C_D values for the full-scale manhole in submerged and free orifice flow were 0.67-0.7 and 0.58-0.59, respectively.

The size or the cross-sectional area of the opening is, however, not the only possible explanation for the difference between the free and submerged discharge coefficients. In free flow the thickness of the plate did not affect C_D (see Figure 28), but a similar observation cannot be made in submerged flow. It is possible that the thickness of the opening plate affects the value of C_D in submerged flow.

6.1.3 Flow velocities in submerged flow through a girder

The 3D ADV velocity measurement device, which was used on the upstream side of the girder, recorded the directional velocities corresponding to the directions of the x-, y- and z-axis shown in Figure 22. All the directional components and the computed resultant of the velocity are plotted in Figure 47 and Figure 48.

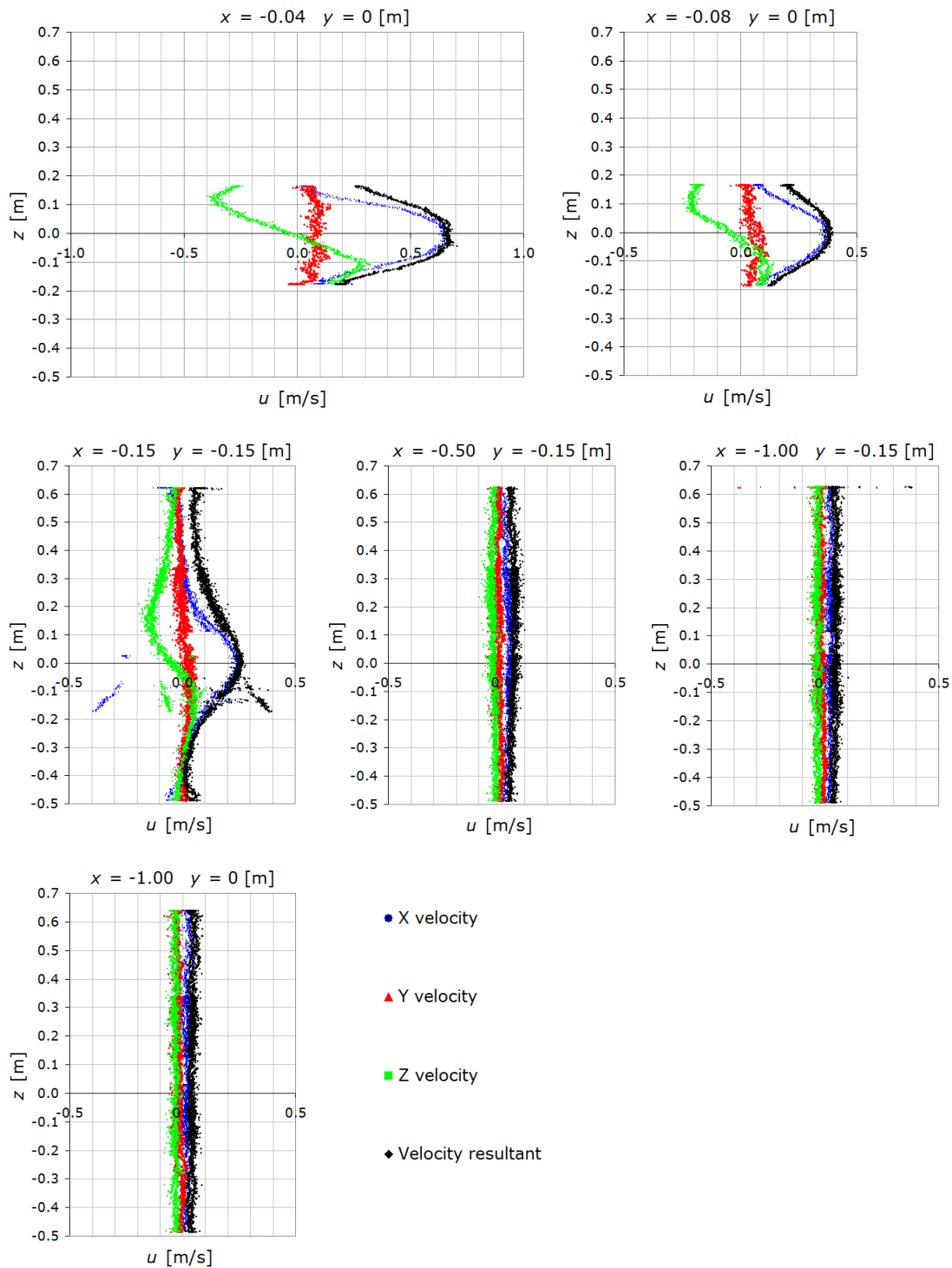


Figure 47. Flow velocities measured with the 3D ADV velocity measurement device along the vertical z-axis at distances x upstream from the girder (green bars in Figure 22).

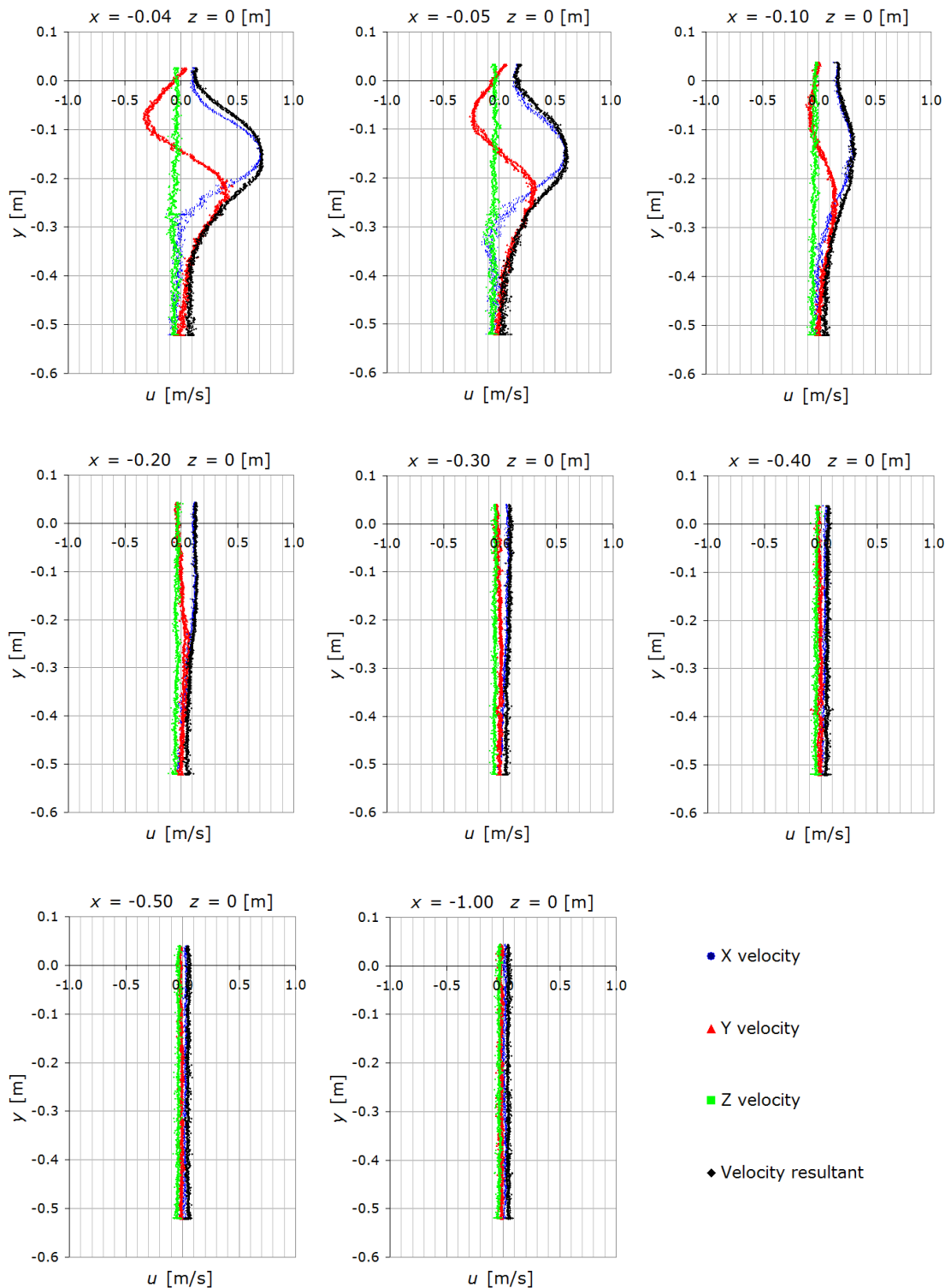


Figure 48. Flow velocities measured with the 3D ADV velocity measurement device along the horizontal y -axis at distances x upstream from the girder (red bars in Figure 22).

It can be seen from the measurements on the upstream side of the girder that the flow accelerates on a very short distance from the manholes on the girder. Due to practical limitations it was not possible to perform measurements closer than 4 cm from the upstream side of the girder.

The Prandtl tube was considered more suitable than the 3D ADV device for velocity measurements in the concentrated jet on the downstream side of the girder. The Prandtl tube recorded the velocity in the direction of the x-axis (in Figure 23). A few measurements on the downstream side of the girder were, however, also conducted with the 3D ADV device in order to compare the measured velocity values (compare Figure 49 to Figure 50).

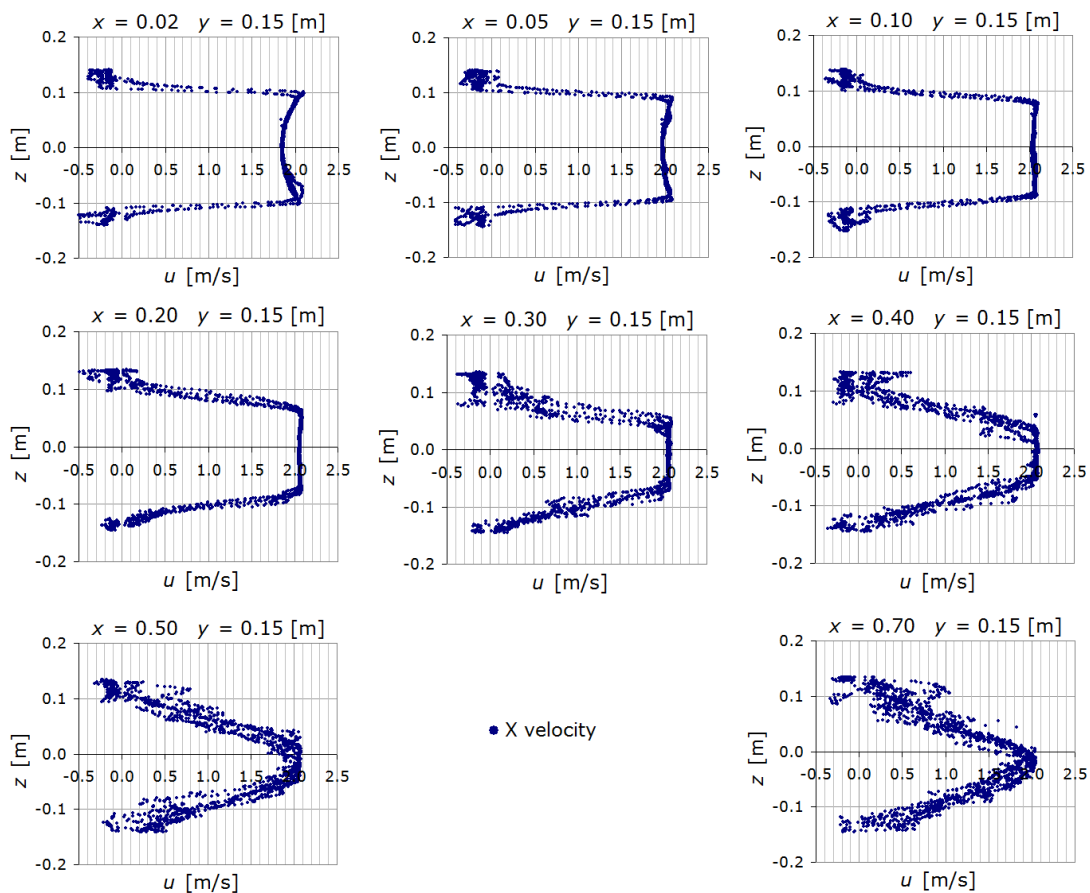


Figure 49. Velocities measured with the Prandtl tube along the vertical z-axis at distances x downstream from the middle of the manhole (see Figure 23)

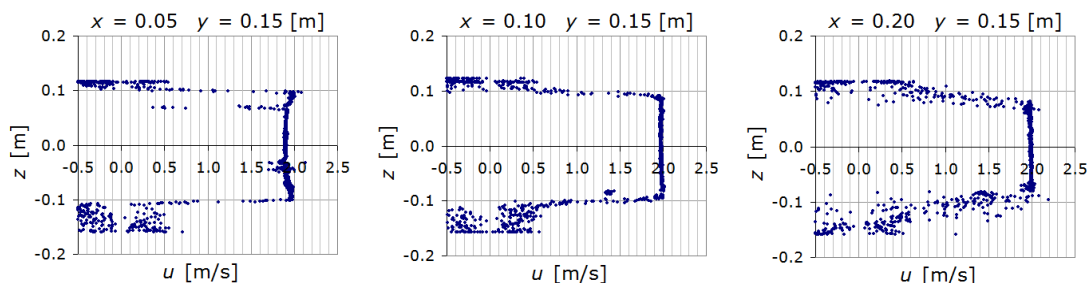


Figure 50. Velocities measured with the 3D ADV device along the vertical z-axis at distances x downstream from the middle of the manhole.

The water level elevation height difference between the upstream and the downstream side was about 205 mm. The elevation height difference corresponding to the velocity measured with the Prandtl tube was typically higher than 205 mm, which is not possible according to hydraulic theory. The velocity values measured with the 3D ADV device were slightly lower than the velocity values measured with the Prandtl tube. If the results obtained with the 3D ADV are assumed to be correct, the velocity coefficient C_V in equation (4) would obtain a value of approximately 0.98. Such a value for C_V is of the correct magnitude (see chapter 2.1), but the coefficient is very sensitive for eventual measurement errors. The results suggest that the Prandtl tube slightly overestimates the velocities whereas the measurements with the 3D ADV device yield values which are very close to the actual flow velocities.

The x-directional flow velocities between the manholes start growing at a distance of approximately 0.4-0.5 m downstream from the girder. This was observed in the measurements along the vertical z-axis between the manholes (Figure 51) and the measurements across both manholes along the horizontal y-axis (Figure 53).

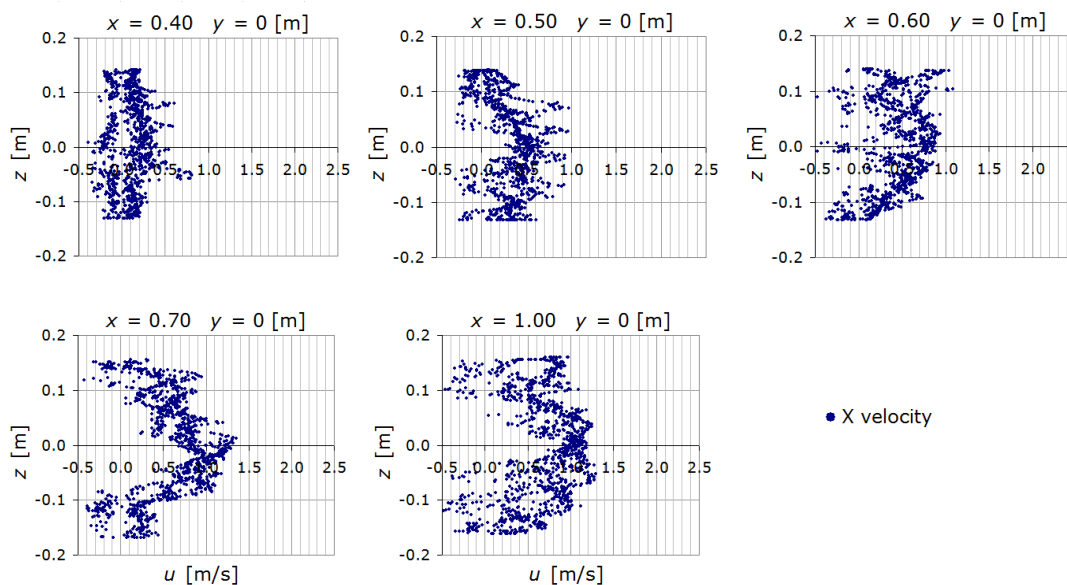


Figure 51. Velocities measured with the Prandtl tube along the vertical z-axis at distances x downstream from the middle of the girder (see Figure 23).

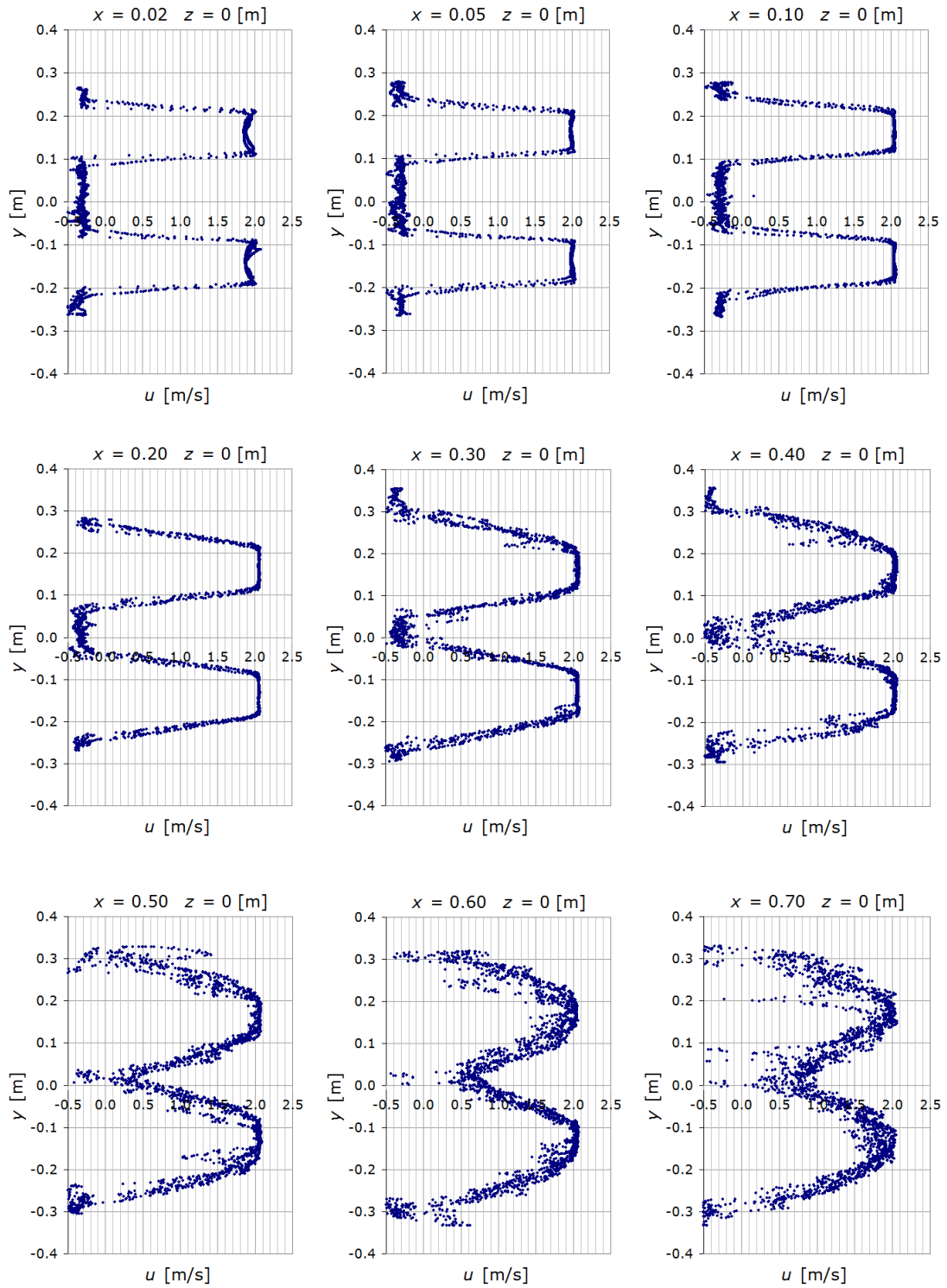


Figure 52. *x*-directional velocities measured with the Prandtl tube along the horizontal *y*-axis at distances *x* downstream from the middle of the girder (red bars in Figure 23). Last figure with *x* = 1.00 m is on next page.

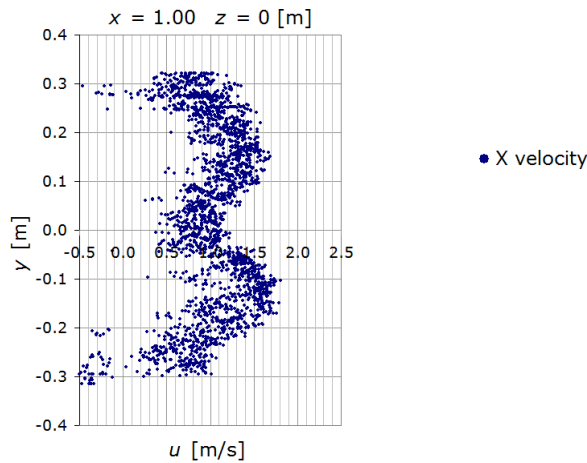


Figure 53. *x*-directional velocities measured with the Prandtl tube along the horizontal *y*-axis at distances *x* downstream from the middle of the girder (continues from previous page).

The velocity measurements were done on the up- and downstream side of a single girder. The determined velocity field therefore describes the inlet and the outlet of the cross-duct, but not the velocity field inside the cross-duct. The distance between the girders in the cross-duct model was 1 m. Consequently, the velocity field inside the cross-duct depends on the hydraulic interaction between at least two girders. It was not possible to conduct measurements inside the cross-duct due to practical limitations.

The flow measurements were conducted with a 1:3 scale model girder. Corresponding full-scale velocity values are obtained by multiplying the presented velocities with the velocity scale similarity factor presented in chapter 3.3.1.

6.2 Cross-duct

The internal variation of the discharge coefficient in the cross-duct test cases C1-C6 was found to be small. Average discharge coefficients and corresponding pressure loss coefficients were computed from the test cases (Table 5). A typical view of the cross-duct during a test measurement (C2) is shown in Figure 54.

Table 5. Average discharge coefficients for the cross-duct in submerged flow. Discharges were in the range of 24-91 l/s, which corresponds to 0.37-1.42 m³/s through a full-scale cross-duct. The h_D/h_0 ratio was 1.07-2.89. Pressure loss coefficients (k -values) were computed with equation (5).

Test case	Cross-duct specification	Average C_D	$k_C = \frac{1}{C_D^2} - 1$
C1	Two modules, 5 girders, no stiffeners	0.318	8.86
C2	Two modules, 5 girders, stiffeners	0.342	7.56
C3	Two modules, 5 girders, stiffeners, web-frame	0.340	7.64
C4	Two modules, 5 girders, stiffeners, 7° inclination	0.339	7.70
C5	One module, 3 girders, stiffeners	0.442	4.11
C6	Three modules, 7 girders, stiffeners	0.287	11.12



Figure 54. The cross-duct was completely under water during most measurements.

The variation of the C_D value in the test cases C1-C6 was less systematic than in the tests with single girders. In the tested flow range, the influence of flow velocity on the discharge coefficient was not as visible as in the tests with the girders. In the test with the short cross-duct with three girders (test case C3, Figure 59), an increase of the discharge caused a decrease in the C_D value in a similar way as in the girder test cases G3-G5 and G7. In all other test cases, the relationship was irregular and uncertain. The conclusion by Vredeveldt and Journée (1991), according to which the value of C_D increases with an increased flow velocity, was therefore not verified by the experiments in this study. Whenever the discharge was observed to influence the discharge coefficient, the effect on C_D was in fact the opposite compared to the effect in the experiments by Vredeveldt and Journée (1991). Experiments in this study were, however, conducted in stationary flow conditions and in a flow range limited by the flume dimensions and the durability of the model. It is possible that considerably greater heads would lead to different results and conclusions.

The difference between the discharge coefficients for the cross-duct consisting of two modules without stiffeners (C1, Figure 55) and for the same cross-duct with stiffeners (C2, Figure 56) was considerable. The stiffeners caused an increase of almost 8% in the value of the discharge coefficient.

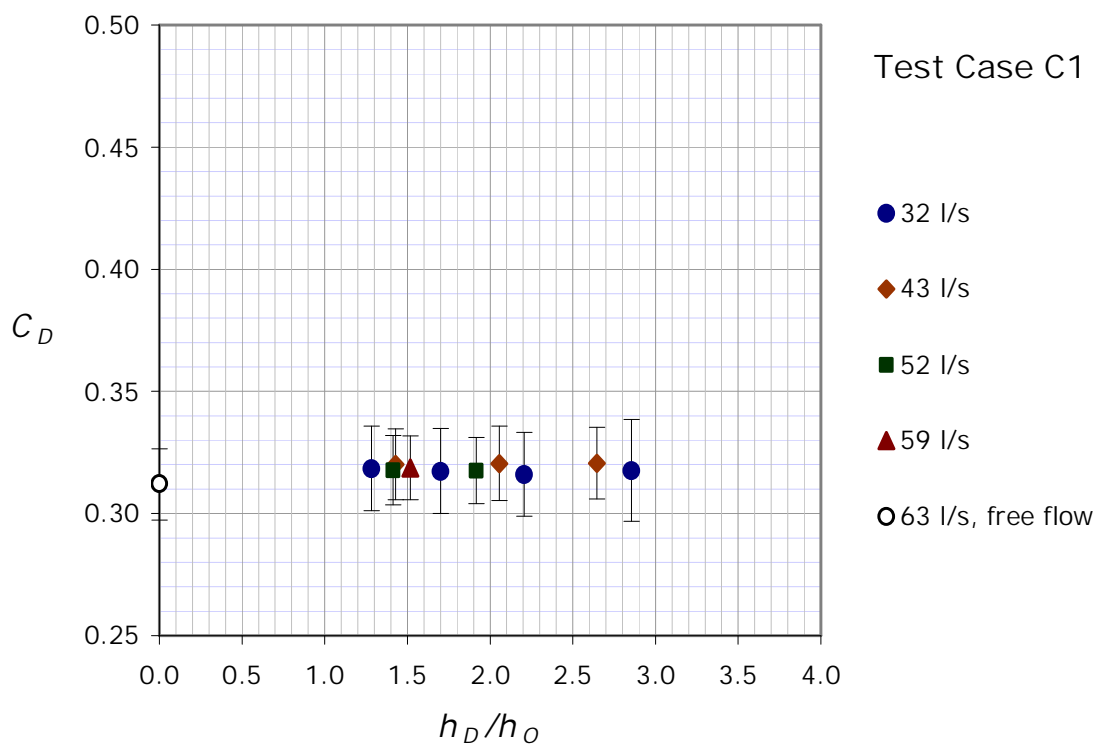


Figure 55. The relationship between the discharge coefficient and the downstream head to opening height ratio when the cross-duct consisted of two modules and 5 girders. The module compartments were not equipped with stiffeners or the web-frame.

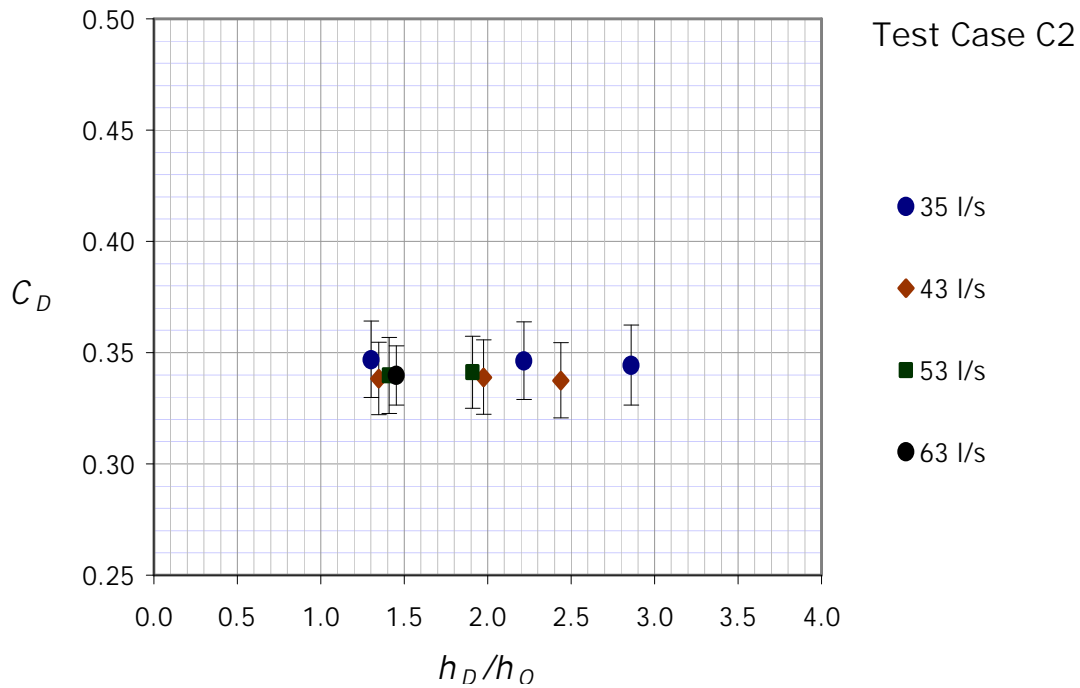


Figure 56. The relationship between the discharge coefficient and the downstream head to opening height ratio when the cross-duct consisting of two modules and 5 girders was equipped with stiffeners.

The downstream head to opening height ratio was varied in the range 1.2-2.8, but it had no visible effect on the C_D value of the cross-duct. It is possible that considerably higher h_D/h_O ratios would yield smaller C_D values, but the eventual effects would likely be visible in the tested flow range.

The discharge coefficient was found to be slightly lower when the last girder discharged into air instead of water. This free flow situation for a cross-duct occurs when the other wing tank is just starting to fill. The difference between the free flow and submerged flow discharge coefficient was smaller than in the test cases with the single manholes or girders. The reason for this is that all girders except the last girder were completely submerged. The results suggest that the downstream water level is not a factor that needs to be taken into account when the discharge coefficient for a cross-duct is selected.

The web-frame inside the cross-duct was insignificant for the value of C_D (compare Figure 56 to Figure 57). An inclination of the cross-duct at an angle of 7° towards the upstream side was unimportant for the average value of C_D (C2 and C4 in Table 5), but statistical analyses at similar flow conditions showed that the inclination caused a small but significant decrease in the discharge coefficient value (compare 35 and 32 l/s at $h_D/h_O \approx 1.3$ in Figure 56 and Figure 58, respectively).

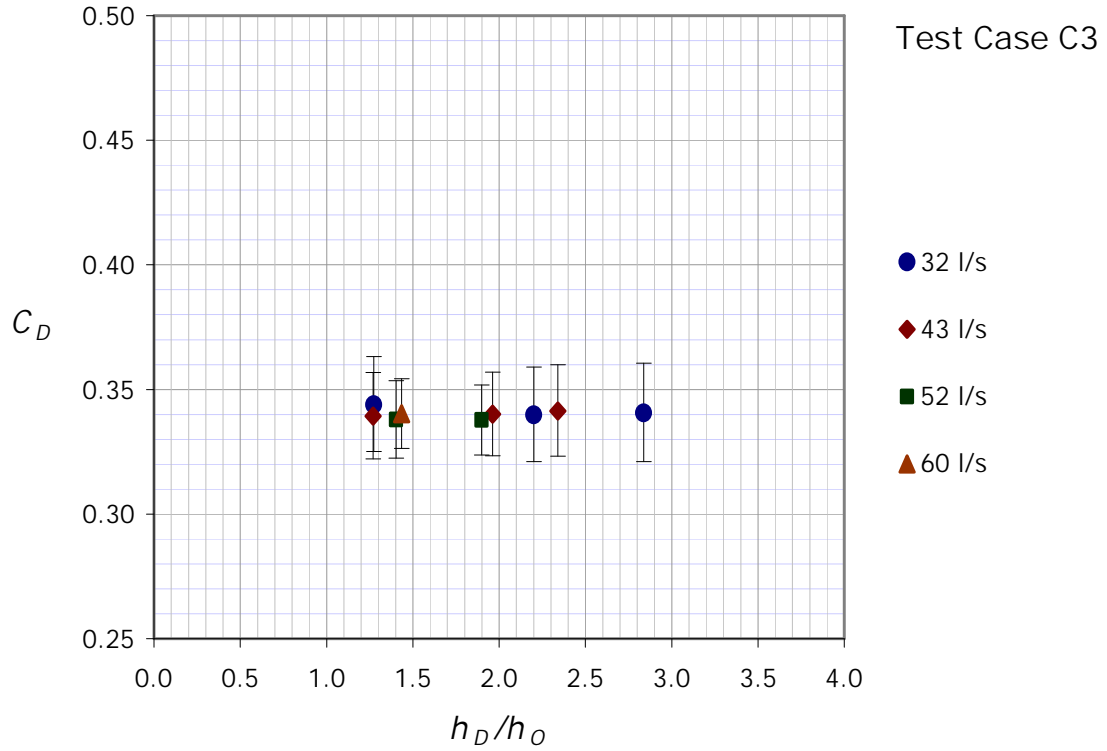


Figure 57. The relationship between the discharge coefficient and the downstream head to opening height ratio when the cross-duct consisting of two modules and 5 girders was equipped with stiffeners and the web-frame.

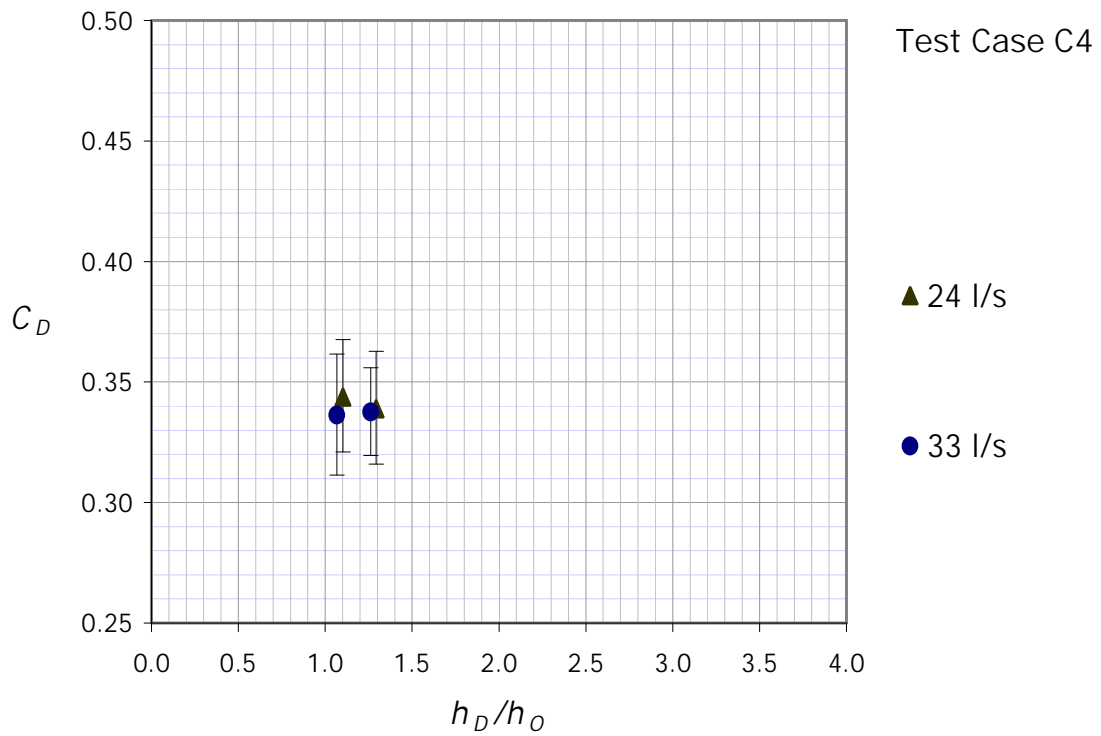


Figure 58. The relationship between the discharge coefficient and the downstream head to opening height ratio when the cross-duct consisting of two modules and 5 girders was equipped with stiffeners and inclined at an angle of 7° towards the flow (compare to Figure 38).

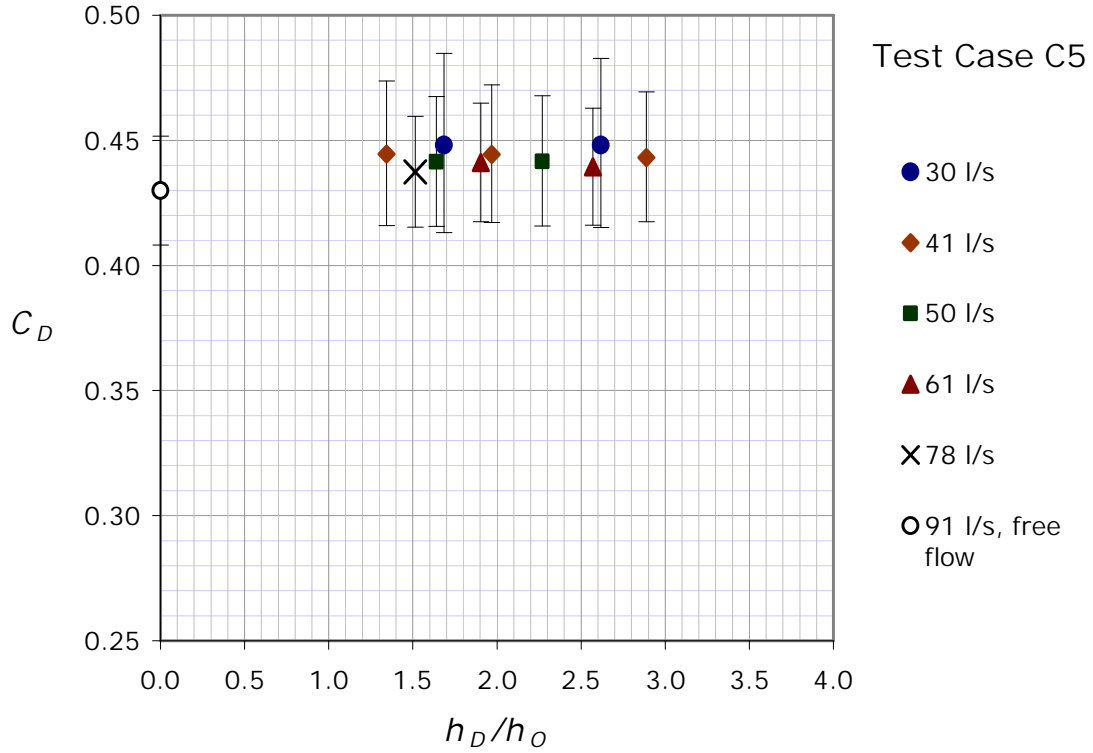


Figure 59. The relationship between the discharge coefficient and the downstream head to opening height ratio when the cross-duct consisted of one module and 3 girders. The cross-duct was equipped with stiffeners but not the web-frame.

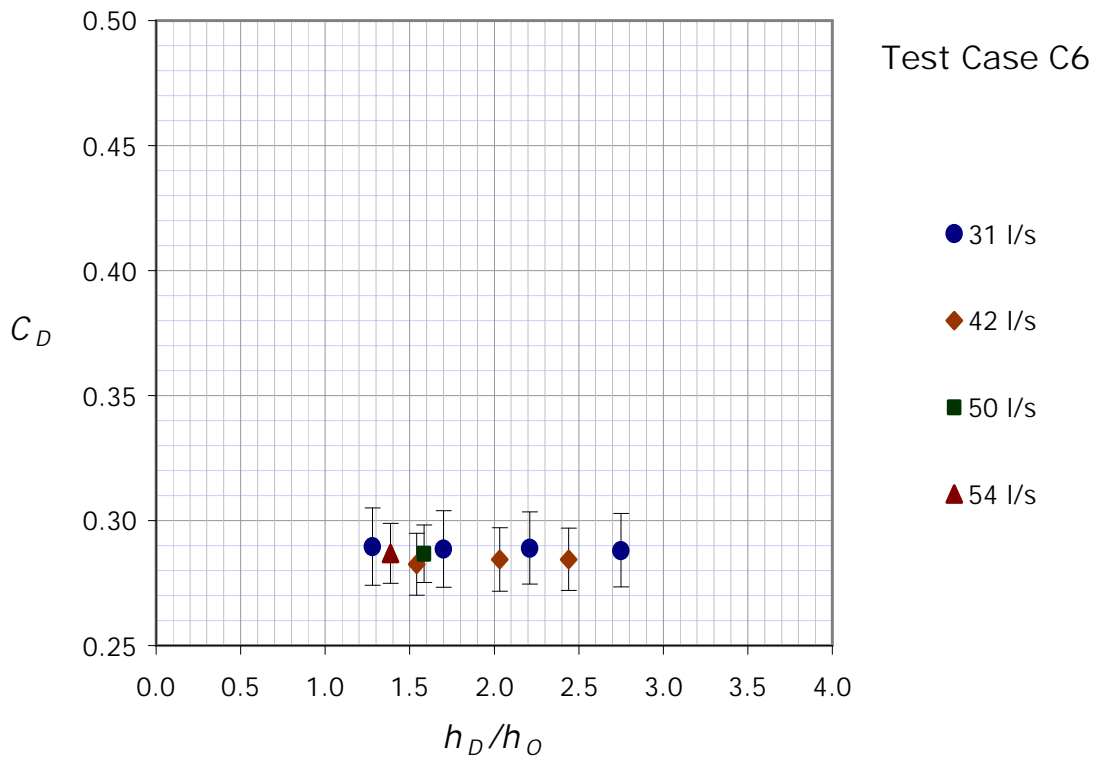


Figure 60. The relationship between the discharge coefficient and the downstream head to opening height ratio when the cross-duct consisted of three modules and 7 girders. The cross-duct was equipped with stiffeners but not the web-frame.

The difference between the discharge coefficients of the 6 m (18 m) long cross-duct and the 4 m (12 m) long cross-duct is much smaller than the difference between the C_D values of the 4 m and the 2 m long cross-ducts (compare Figure 60, Figure 59 and Figure 56). The influence of each added girder on the C_D value of the cross-duct becomes smaller.

6.2.1 Comparison of measured and computed discharge coefficients

The measured discharge coefficients from test cases C1-C6 (Table 5) were compared to the corresponding computed values. Two standard computational methods were used:

- (A) Equation (5) and the single girder C_D values presented in Table 5
- (B) MSC.245(83): equation (5) and the pressure loss coefficients related to each space between two adjacent girders obtained with equation (6)

The girder stiffeners and their direction (up- or downstream) were taken into account in the computations with method (A). Method (B), which is based on the CFD analyses by Pittaluga and Giannini (2006), did not take the stiffeners into account. Method (B) can be considered as the currently official method recommended by IMO.

An important consideration is that method (B) is based on CFD equations for a full-scale cross-duct, whereas the girder discharge coefficients used in method (A) and the measured C_D values for the cross-ducts from test cases C1-C6 are based on scale model experiments. The measured C_D values and the C_D values computed with method (A) need to be corrected for scale effects in order to compare them to the discharge coefficients computed with method (B). In this study the scale effects were estimated on the basis of the differences between the determined discharge coefficients for the full-scale and scale model manholes. In order not to overestimate the scale effects, the average C_D values were assumed to represent the correct values of the discharge coefficients for the different test objects.

In free flow, a smaller opening yielded a higher C_D value (Figure 61). There was not complete hydraulic similarity between the full-scale and scale model manholes because of the dimensions of the flume. The full-scale manhole was possibly slightly affected by the vicinity of the flume walls. The scale effects in free flow are therefore possibly slightly bigger than the presented difference between the full-scale and scale model discharge coefficients (see section 2.4 and p. 52).

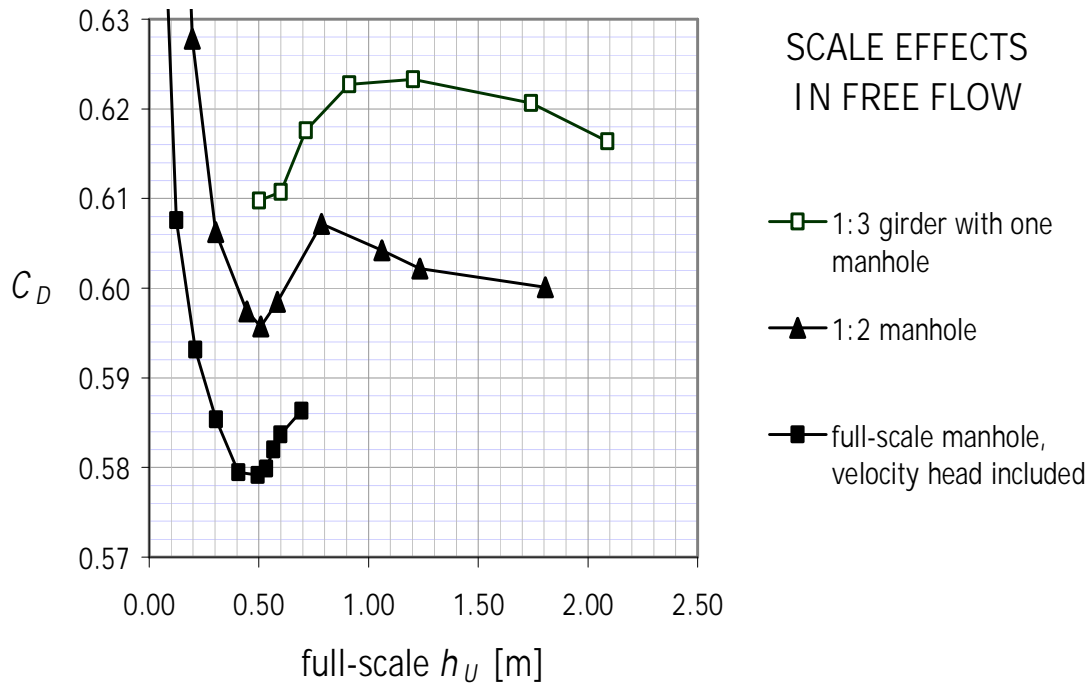


Figure 61. In free flow the discharge coefficients of the full-scale manhole were smaller than the corresponding scale model discharge coefficients.

Scale effects in free flow were estimated as the quotient between the scale model and the full-scale discharge coefficients at $h_U = 0.5$ m. The 1:2 scale model manhole had an approximately 3% higher discharge coefficient than the full-scale manhole. The corresponding increase was 5% for the 1:3 scale model manhole.

The estimated scale effects in free discharge were quite small compared to those reported by Takayama and Ikeda (2005), even though the difference in length scales in their tests was smaller than in this study (1:1-1:2.5 vs. 1:1-1:3). However, the narrowest opening dimension in their test was just 24 mm, whereas the narrowest test object dimension in this study was 134 mm. The scale effects of test objects with significantly smaller scales would be a highly important subject for further research, but the practical arrangements for such a research were not possible in this study because of the uncertainty related to the measurement of small discharges.

The scale effects were found to have the opposite influence on the discharge coefficient in submerged flow. In submerged flow, the value of C_D decreased as the opening size decreased (Figure 62). Because of the possible influence of the flume sidewalls and bed, the scale effects in submerged flow cannot be higher than the difference between the full-scale and scale model discharge coefficients when it is assumed that the average determined values for C_D are correct.

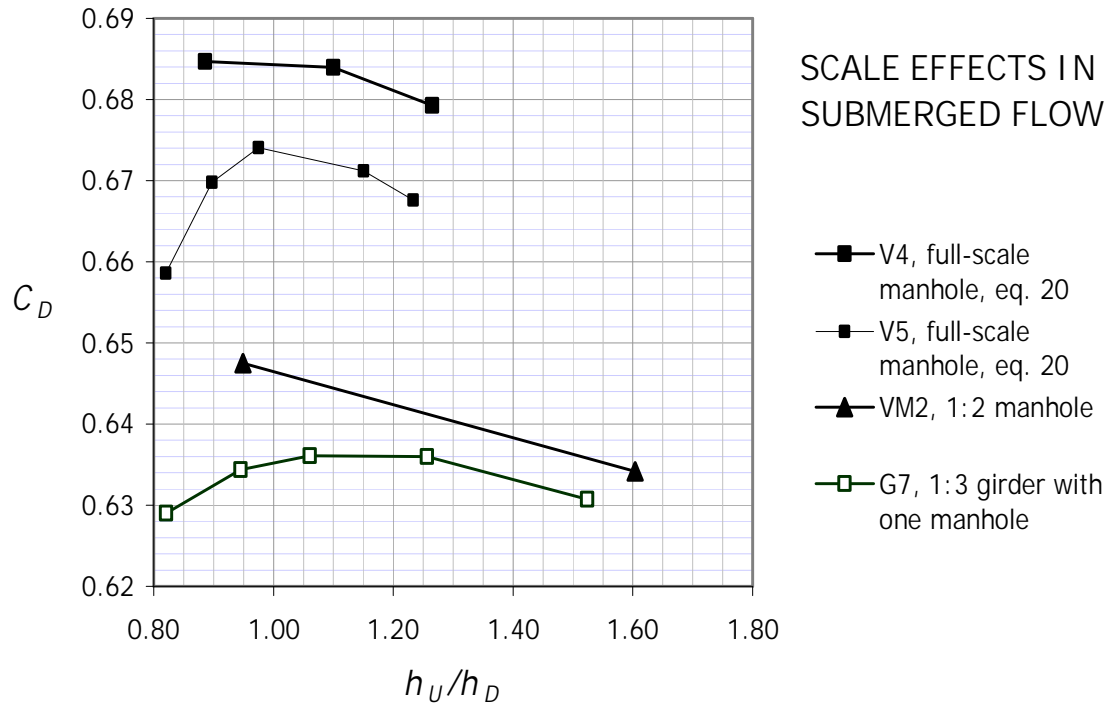


Figure 62. In submerged flow the discharge coefficients of the full-scale manhole were higher than the corresponding scale model discharge coefficients.

Scale effects in submerged flow were estimated as the quotient between the discharge coefficient in test case V4 and the corresponding scale model discharge coefficients at $h_D/h_O = 1.1$. The full-scale discharge coefficient was not more than 6% higher than the C_D value of the 1:2 scale model manhole and *not more than 8% higher than the C_D value of the 1:3 scale model manhole.*

The maximum scale effects of the 1:3 scale model cross-ducts were estimated on the basis of the scale effect estimate for a single 1:3 scale model manhole. The scale correction factor for the cross-duct depends on the number of girders and it was estimated with equation (31) (Table 6).

Table 6. Scale correction factors for the 1:3 scale model cross-ducts. The single girder coefficient was estimated from measurements and the cross-duct coefficients were computed with eq. (31)

Test object	Scale correction factor
Single girder	1.08 (8%)
Cross-duct with 3 girders	1.115
Cross-duct with 5 girders	1.126
Cross-duct with 7 girders	1.132

The measured cross-duct C_D values and the C_D values computed with method (A) (section 6.2.1) were multiplied with the corresponding scale correction factors in Table 6 in order to estimate their largest possible value (Figure 63).

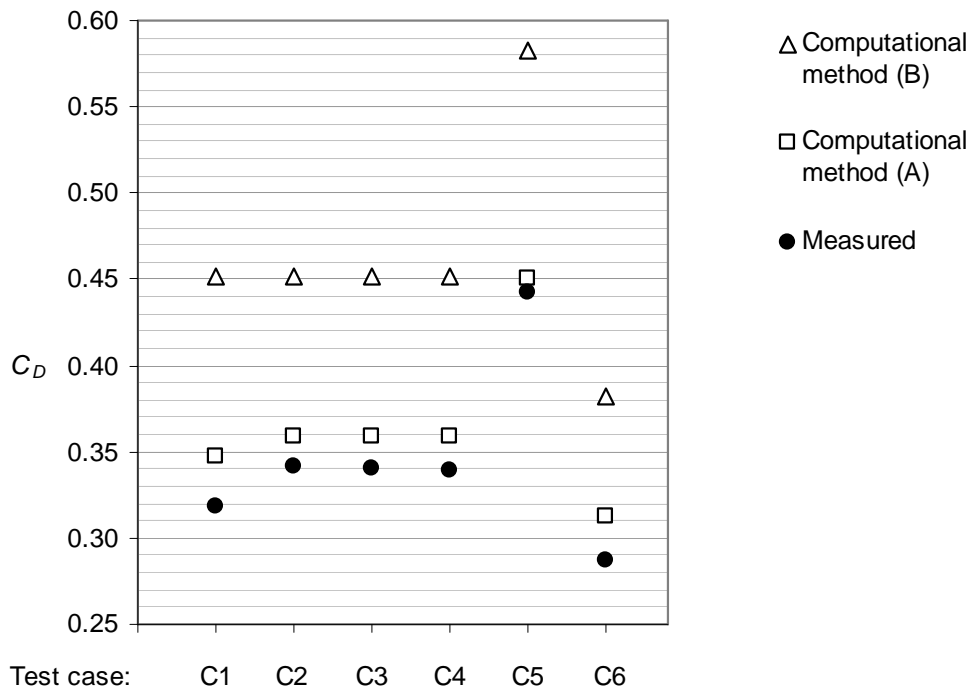


Figure 63. Comparison of the cross-duct discharge coefficient values obtained with measurements (Table 5) and computational methods (A) and (B). The results of the method (B) were computed with full-scale values, whereas the other results were derived from model-scale measurements without any corrections for eventual scale effects. The methods (A) and (B) are presented on page 77.

Both methods (A) and (B) overestimate the discharge coefficient of a cross-duct. The best estimate was obtained for the short cross-duct with three girders (C5). The estimates were most inaccurate for the long cross-duct (C6).

Method (A) took the influence of girder stiffeners into account, which considerably increased the C_D value estimates (compare the values in C1 and C2). Method (B) did not take the influence of stiffeners into account, but it yielded the highest C_D value estimates. There is, however, no reason to doubt the validity of the CFD based regression equation (equation (6)). The main reason for the higher C_D estimates with method (B) is that the dimensions of the manholes in the study by Pittaluga and Giannini (2006) were larger (500 mm wide and 800 mm high) and the cross-duct was 2 m high but only 1.42 m wide. This means, that the flow through the manholes in their study was probably less contracted due to the vicinity of the side walls (Figure 6A).

The regression equations in the resolution MSC.245(83) were determined in flow conditions with considerably higher heads than in this study. In this study, small

variations of the velocity did not affect the C_D value, but the maximum examined head in test cases C1-C6 was only about 1.75 m in full-scale. It is possible that an increase of the head from 1.75 m to 5 m would increase the value of the discharge coefficients. The influence of flow velocity should be examined properly either experimentally with a smaller scale model or with CFD computations.

The difference between the measured values in the test cases C1 and C2 was 0.024. The corresponding difference with method (A) was only 0.012. Girder stiffeners thus explain half of the increase in the discharge coefficient value, but the rest of the increase must be due to the stiffeners in the cross-duct roof and bottom. Instead of acting as flow obstacles, the bottom and roof stiffeners probably reduce the eddying motion around the jet, which leads to smaller energy losses and enhanced flow (Figure 4).

6.3 Remarks on the applicability of the results

Scale effects should be taken into account when results obtained from scale model experiments are applied in flooding simulations. These scale effects were found to be different in free and submerged flow. The errors related to scale effects were estimated on the basis of the test results and presented as percentage values. By applying the scale correction factors to the discharge coefficients determined in the scale model tests, more realistic values are obtained.

The velocity head was taken into account in the free discharge test cases with the full-scale manhole. In flooding simulations, which do not take the velocity head into account, it is suggested to use the C_D values which take the velocity head into account for manholes between large compartments. The discharge coefficients determined with the elevation head only is recommended for narrow compartments (similar to the flume).

The velocity head in submerged flow test cases was neglected because of the lack of an appropriate computational method. For submerged flow between large compartments, it is recommended to apply slightly smaller C_D values than those presented for the full-scale manhole in section 6.1.2 (compare to Figure 62).

7 Conclusions and recommendations

The often applied discharge coefficient 0.6 was found to be a good approximation for the manhole in free flow conditions. The discharge coefficient of a full-scale manhole was mostly in the range 0.58-0.59. The scale model manholes had 3-5% higher discharge coefficients than the full-scale manhole in free flow. An inclination of the manhole at an angle of 20° towards the flow caused an approximately 5% decrease in the C_D value in free flow, but did not have any considerable effect in submerged flow conditions.

In submerged flow, the discharge coefficient was found to be higher than in free flow. The difference between the C_D values in free and submerged flow conditions was greater for the full-scale manhole than for the scale models. In fully submerged flow, the discharge coefficients of the full-scale manhole were in the range of 0.67-0.7. The scale model manholes had up to 8% smaller C_D values than the full-scale manhole in submerged flow.

The influence of structural stiffeners was found to increase the discharge coefficients of single girders up to 4%. The influence of the stiffeners was strongest when the stiffeners were attached to the upstream side of the girder. Stiffeners pointing downstream caused a small, although statistically significant, increase in the value of C_D . The discharge coefficient of a cross-duct with 5 girders was increased 8% due to the structural stiffeners. The results suggest that structural stiffeners should be taken into account when the discharge coefficient of a cross-duct is determined.

The computational estimates for the discharge coefficients of the cross-ducts were higher than the measured values. The application of the CFD based equation in the MSC.245(83) (see section 2.3) yielded more than 30% overestimated C_D values for the cross-duct, even though it did not take the girder stiffeners into account. There is a risk that the discharge coefficients of cross-ducts are overestimated if the CFD based equations are applied and the geometrical properties of the girders are not taken into account.

The flow velocity and the downstream head to opening height ratio had a small decreasing influence on the discharge coefficient value of the manholes and the girders, but the effect on the C_D value of the cross-duct did not follow a similar clear pattern. It is recommendable to examine a larger range of discharge values in order to verify the observation. CFD analyses are probably the most convenient method for such a study.

8 References

Ackers, P., White, W. R, Perkins, A and Harrison, A. J. M. (1980). Weirs and Flumes for Flow Measurement, Great Britain, 327 pages

Blevins, Robert D. (1984). Applied Fluid Dynamics Handbook, New York, 558 pages

Bos, M. G. (1989). Discharge Measurement Structures, International Institute for Land Reclamation and Improvement/ILRI, the Netherlands, 402 pages

Bos, M. G (1985). Long-throated Flumes and Broad Crested Weirs, the Netherlands, 142 pages

Brownlee, K. A. (1960). Statistical Theory and Methodology in Science and Engineering, New York, 236 pages

Chanson, M., Aoki, S., Maruyama, M.: Unsteady Two-dimensional Orifice Flow (2002). a large-size experimental investigation, Journal of Hydraulic Research, 1/2002, pages 63-71

Clemmens, A.J, Wahl, T.L., Bos, M.G., Replogle, J.A. (2001). Water Measurement with Flumes and Weirs, International Institute for Land Reclamation and Improvement / ILRI, the Netherlands, 384 pages

Hamill, L. (2001). Understanding Hydraulics, Second Edition, Bristol, Great Britain, 608 pages

Hersch, R. (1995). General Purpose Flow Measurement Equations for Flumes and Thin Plate Weirs, Flow Measurements Instruments, 4/1995, Great Britain, pages 283-293

IMO: Resolution A.266 (VIII): Recommendation on a standard method for establishing compliance with the requirements for cross-flooding arrangements in passenger ships, 1973, 4 pages

Katayama, T. and Ikeda, Y. (2005). An Experimental Study of Fundamental Characteristics of Inflow Velocity from Damaged Opening, Proceedings of 8th

International Ship Stability Workshop –Istanbul Technical University, Istanbul, Turkey, 6-7 October 2005, 6 pages

MSC: Resolution MSC.245(83), Recommendation on a Standard Method for Evaluating Cross-Flooding Arrangements, 2007, 11 pages

Nielsen, Kevin D. and Weber, Larry J. (2000). Submergence Effects on Discharge Coefficients for Rectangular Orifices. Building Partnerships Proceedings of Joint Conference on Water Resource Engineering and Water Resources Planning and Management 2000, Minneapolis 30 July – 2 August 2000, 6 pages

Pittaluga, C., Giannini, M. (2006). Pressure Losses Estimation for Structural Double Bottom by CFD Technique, CETENA Technical Report, Italy, 49 pages

Reader-Harris, M. J., Sattary, J. A., Spearman, E. P. (1995). The Orifice Plate Discharge Coefficient Equation –Further Work, Flow Measurement Instruments, 2/1995, pages 101-114

Ruponen, P. (2006a). Model Tests for the Progressive Flooding of a Box-shape Barge, Helsinki University of Technology, Ship Laboratory, Espoo, 92 pages

Ruponen, P. (2007). Progressive Flooding of a Damaged Passenger Ship, Helsinki University of Technology, Ship Laboratory, Tkk dissertations 94, Espoo, 128 pages

Ruponen, P. (2006b). Time-Domain Simulation of Cross-Flooding, Tkk Ship Laboratory, 9 pages

Spiegel, M. R. (1972). Theory and Problems of Statistics, Great Britain, 360 p.

Söding, H. (2002). Flow Computations for Ship Safety Problems, Ocean Engineering 29, 2002, pages 721-738

Tillis, G. M., Swain, E. D. (1998). Determining Discharge-Coefficient Ratings for Selected Coastal Control Structures in Broward and Palm Beach Counties, Florida, U.S. Geological Survey, Water Resources Investigations Report 98-4007, USA, 41 pages

Tullis, B. P., Young, J. C., Chandler, M. A. (2007). Head-Discharge Relationships for Submerged Labyrinth Weirs, *Journal of Hydraulic Engineering*, March 2007, pages 248-254

Tullis, B. P., Neilson, J. (2008). Performance of Submerged Ogee-Crest Weir Head-Discharge Relationships, *Journal of Hydraulic Engineering*, ASCE, April 2008, pages 486-491

VALMET Automation (1985). DIFF-EL SD elektroninen paine-erolähetin, 1985-08-15b, Technical specification of the pressure transducer, 28 pages

Walshaw, A. C. and Jobson, D. A (1979). *Mechanics of Fluids*, Third Edition, Great Britain, 599 pages

Vredeveltdt, A. W. and Journée, J. M. J. (1991). Roll Motions due to Sudden Water Ingress, Calculations and Experiments, RINA'91, International Conference on Ro-Ro Safety and Vulnerability the Way Ahead, London 17-19 April 1991, 17 pages

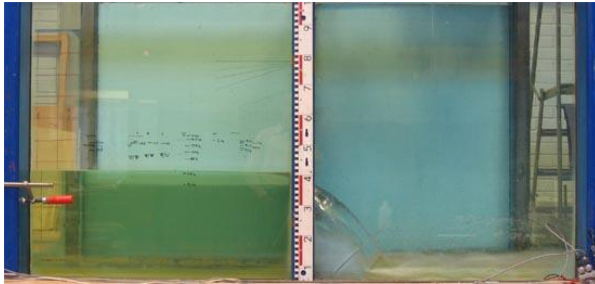
Villemonte, J. R. (1947). Submerged-Weir Discharge Studies, *Engineering News Record*, December 1947, pages 54-57

Appendix I: Photographs from the experiments

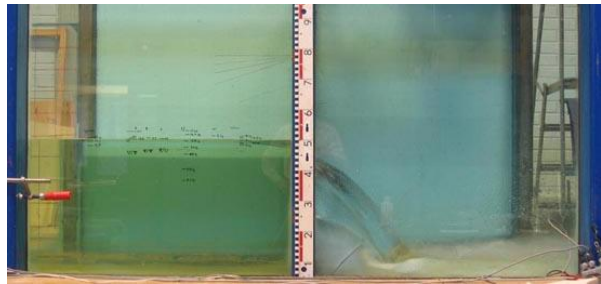
A. Full-scale manhole

A.1. Test case V1

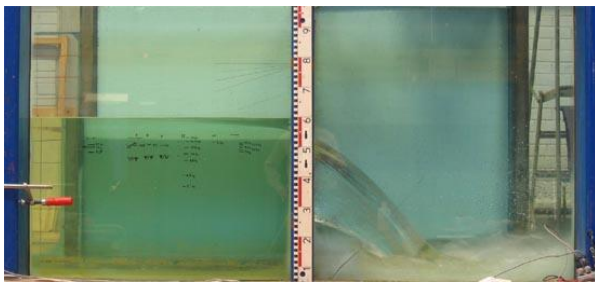
Free flow through a full-scale manhole in vertical position. The velocity head was included in the theoretical discharge computations.



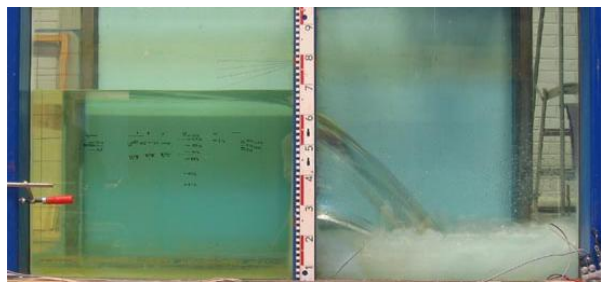
$h_U = 209.7 \text{ mm}$, $Q_A = 49.3 \text{ l/s}$, $Q_T = 83.1 \text{ l/s}$



$h_U = 304.7 \text{ mm}$, $Q_A = 94.4 \text{ l/s}$, $Q_T = 161.1 \text{ l/s}$



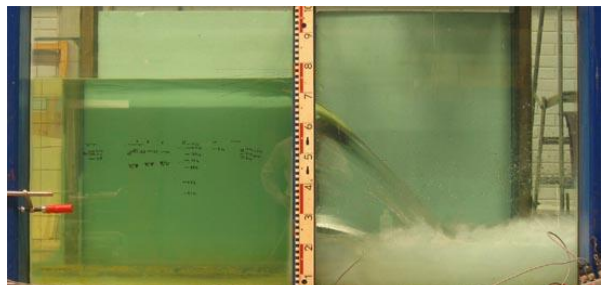
$h_U = 406.0 \text{ mm}$, $Q_A = 152.3 \text{ l/s}$, $Q_T = 262.5 \text{ l/s}$



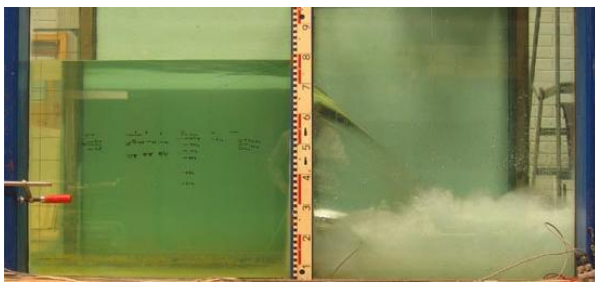
$h_U = 494.7 \text{ mm}$, $Q_A = 210.8 \text{ l/s}$, $Q_T = 363.1 \text{ l/s}$



$h_U = 533.5 \text{ mm}$, $Q_A = 237.5 \text{ l/s}$, $Q_T = 408.7 \text{ l/s}$



$h_U = 565.5 \text{ mm}$, $Q_A = 259.9 \text{ l/s}$, $Q_T = 445.6 \text{ l/s}$



$h_U = 598.9 \text{ mm}$, $Q_A = 281.7 \text{ l/s}$, $Q_T = 481.8 \text{ l/s}$



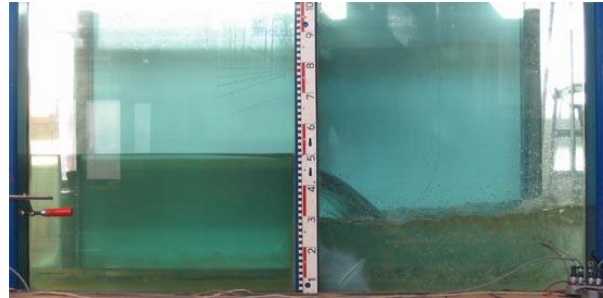
$h_U = 694.6 \text{ mm}$, $Q_A = 331.4 \text{ l/s}$, $Q_T = 564.3 \text{ l/s}$

A.2. Test case V3

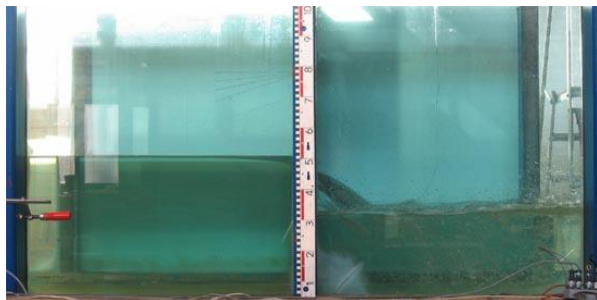
Submerged weir flow through a full-scale manhole with the actual discharge of approximately $Q_A = 92$ l/s. The velocity head was not included in the theoretical discharge computations. The displayed theoretical discharge Q_T values are computed with method 2.



$h_U = 300.0$ mm, $Q_A = 92.1$ l/s, $Q_T = 155.9$ l/s
 $h_D = < 0$ mm, $h_D^* = < 0$ mm



$h_U = 304.8$ mm, $Q_A = 92.2$ l/s, $Q_T = 154.8$ l/s
 $h_D = 104.4$ mm, $h_D^* = 85$ mm



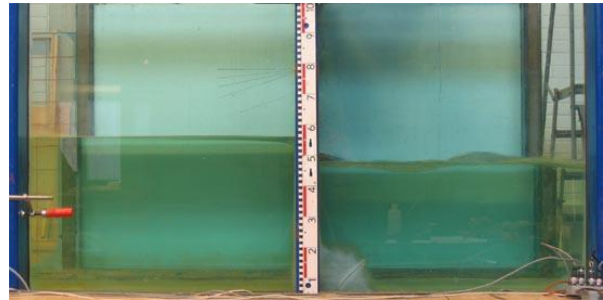
$h_U = 310.8$ mm, $Q_A = 92.1$ l/s, $Q_T = 153.7$ l/s
 $h_D = 143.1$ mm, $h_D^* = 125$ mm



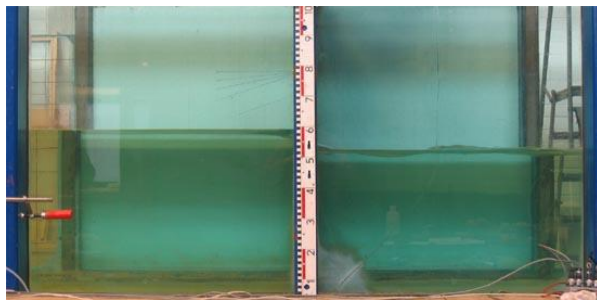
$h_U = 322.4$ mm, $Q_A = 92.2$ l/s, $Q_T = 151.5$ l/s
 $h_D = 190.5$ mm, $h_D^* = 170$ mm



$h_U = 342.5$ mm, $Q_A = 91.7$ l/s, $Q_T = 147.5$ l/s
 $h_D = 245.3$ mm, $h_D^* = 230$ mm



$h_U = 367.1$ mm, $Q_A = 92.2$ l/s, $Q_T = 143.6$ l/s
 $h_D = 294.0$ mm, $h_D^* = 280$ mm



$h_U = 397.1$ mm, $Q_A = 92.1$ l/s, $Q_T = 139.5$ l/s
 $h_D = 342.1$ mm, $h_D^* = 330$ mm



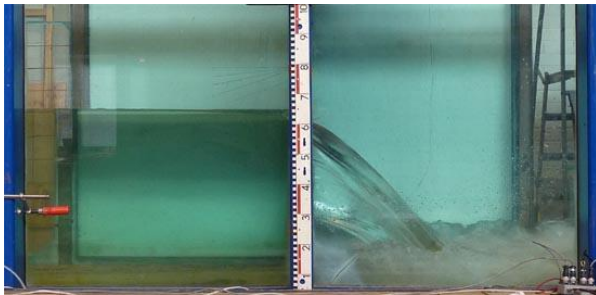
$h_U = 439.0$ mm, $Q_A = 92.1$ l/s, $Q_T = 137.1$ l/s
 $h_D = 398.0$ mm, $h_D^* = 390$ mm



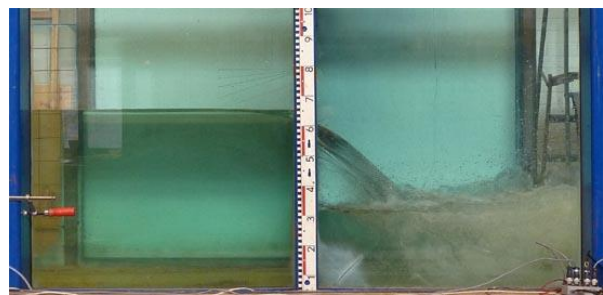
$h_U = 486.0$ mm, $Q_A = 92.1$ l/s, $Q_T = 134.4$ l/s
 $h_D = 455.0$ mm, $h_D^* = 450$ mm

A.3. Test case V4

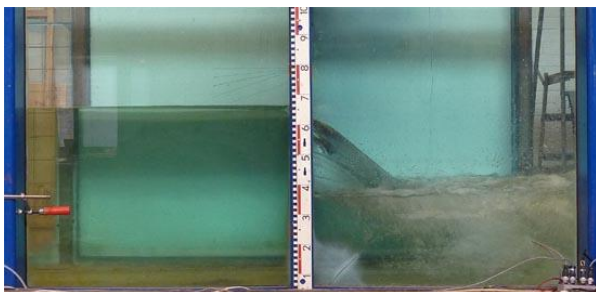
Submerged weir flow, partly submerged orifice flow and completely submerged orifice flow through a full-scale manhole with the actual discharge of approximately $Q_A = 182$ l/s. The velocity head was not included in the theoretical discharge computations. The displayed theoretical discharge Q_T values are computed with method 2.



$h_U = 450.0$ mm, $Q_A = 182.1$ l/s, $Q_T = 308.0$ l/s
 $h_D < 0$ mm, $h_D^* < 0$ mm



$h_U = 456.6$ mm, $Q_A = 182.3$ l/s, $Q_T = 300.8$ l/s
 $h_D = 173.2$ mm, $h_D^* = 105$ mm



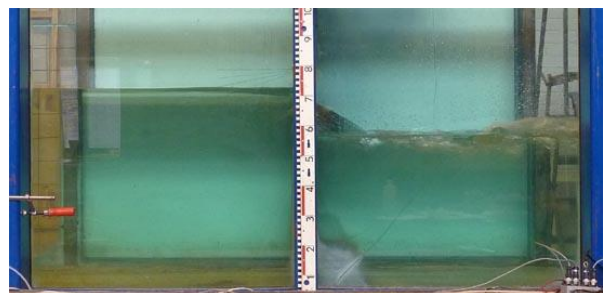
$h_U = 464.0$ mm, $Q_A = 182.1$ l/s, $Q_T = 297.8$ l/s
 $h_D = 217.7$ mm, $h_D^* = 160$ mm



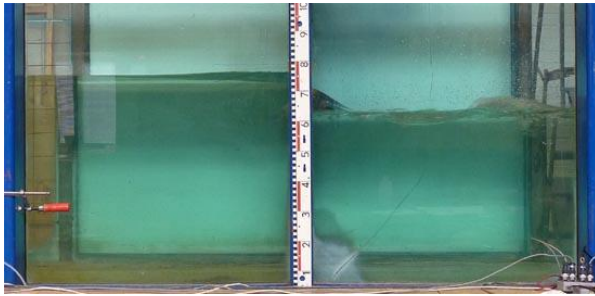
$h_U = 474.9$ mm, $Q_A = 181.7$ l/s, $Q_T = 293.6$ l/s
 $h_D = 264.4$ mm, $h_D^* = 220$ mm



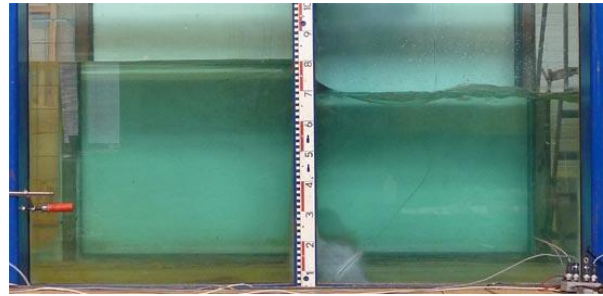
$h_U = 489.7$ mm, $Q_A = 181.5$ l/s, $Q_T = 289.6$ l/s
 $h_D = 310.2$ mm, $h_D^* = 260$ mm



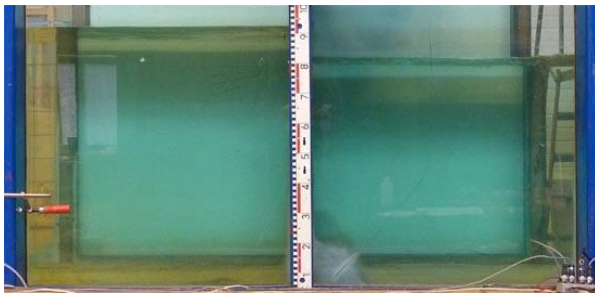
$h_U = 530.6$ mm, $Q_A = 181.9$ l/s, $Q_T = 276.3$ l/s
 $h_D = 405.7$ mm, $h_D^* = 370$ mm



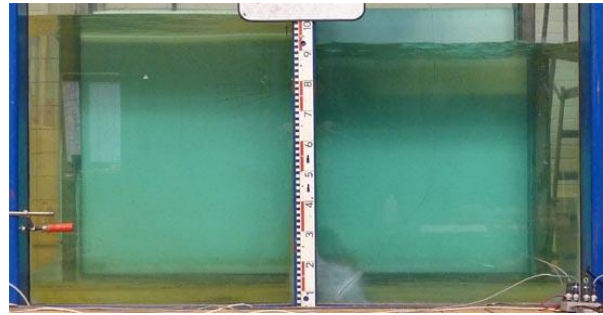
$h_U = 566.9 \text{ mm}$, $Q_A = 181.7 \text{ l/s}$, $Q_T = 268.2 \text{ l/s}$
 $h_D = 466.5 \text{ mm}$, $h_D^* = 440 \text{ mm}$



$h_U = 614.2 \text{ mm}$, $Q_A = 181.1 \text{ l/s}$, $Q_T = 258.3 \text{ l/s}$
 $h_D = 531.5 \text{ mm}$, $h_D^* = 505 \text{ mm}$



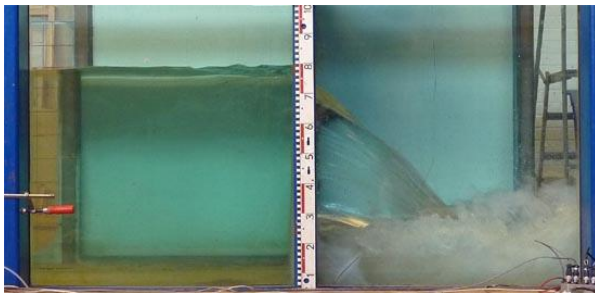
$h_U = 741.1 \text{ mm}$, $Q_A = 181.4 \text{ l/s}$, $Q_T = 259.8 \text{ l/s}$
 $h_D = 659.8 \text{ mm}$, $h_D^* = 640 \text{ mm}$



$h_U = 842.4 \text{ mm}$, $Q_A = 181.8 \text{ l/s}$, $Q_T = 263.2 \text{ l/s}$
 $h_D = 758.9 \text{ mm}$, $h_D^* = 740 \text{ mm}$

A.4. Test case V5

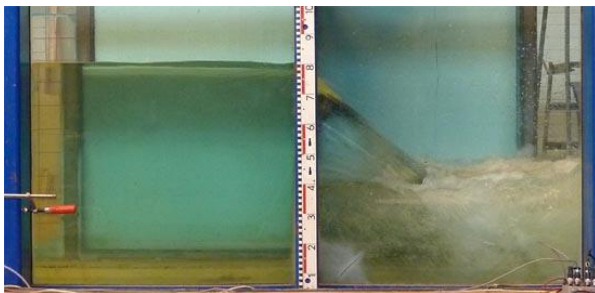
Partly and completely submerged orifice flow through a full-scale manhole with the actual discharge of approximately $Q_A = 281 \text{ l/s}$. The velocity head was not included in the theoretical discharge computations. The displayed theoretical discharge Q_T values are computed with method 2.



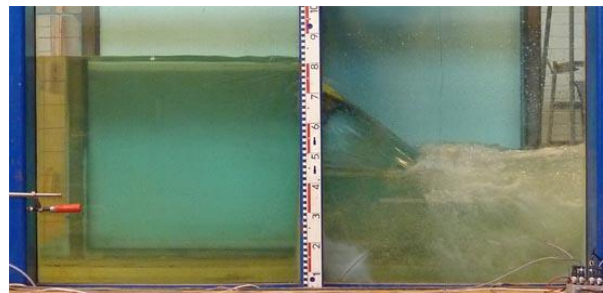
$h_U = 599.1 \text{ mm}$, $Q_A = 281.6 \text{ l/s}$, $Q_T = 476.8 \text{ l/s}$
 $h_D = < 0 \text{ mm}$, $h_D^* = < 0 \text{ mm}$



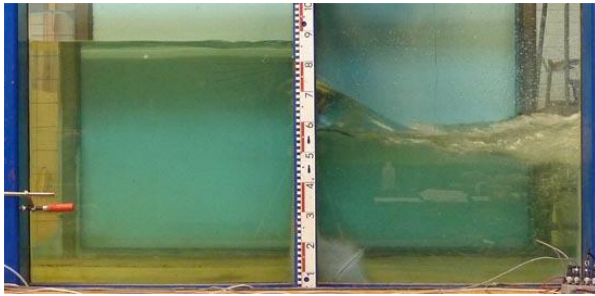
$h_U = 607.1 \text{ mm}$, $Q_A = 281.2 \text{ l/s}$, $Q_T = 456.6 \text{ l/s}$
 $h_D = 242.6 \text{ mm}$, $h_D^* = 140 \text{ mm}$



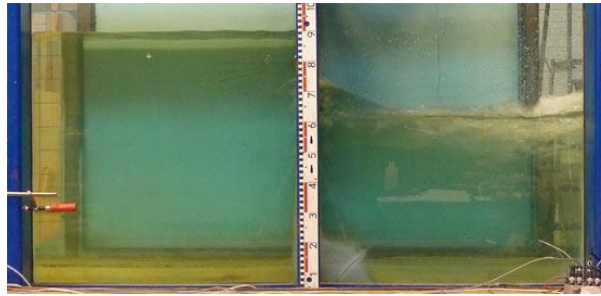
$h_U = 615.7 \text{ mm}$, $Q_A = 280.8 \text{ l/s}$, $Q_T = 450.7 \text{ l/s}$
 $h_D = 286.0 \text{ mm}$, $h_D^* = 210 \text{ mm}$



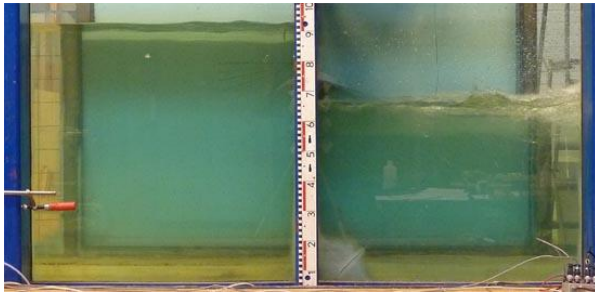
$h_U = 630.0 \text{ mm}$, $Q_A = 281.8 \text{ l/s}$, $Q_T = 444.6 \text{ l/s}$
 $h_D = 333.7 \text{ mm}$, $h_D^* = 250 \text{ mm}$



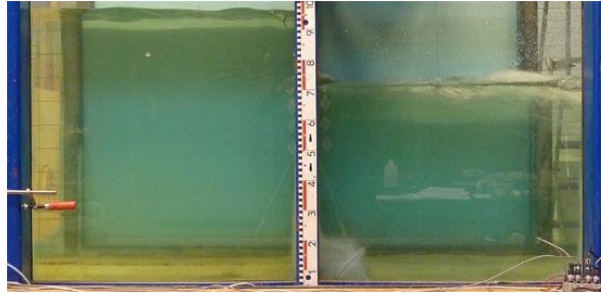
$h_U = 681.5 \text{ mm}$, $Q_A = 281.5 \text{ l/s}$, $Q_T = 427.7 \text{ l/s}$
 $h_D = 445.4 \text{ mm}$, $h_{D^*} = 380 \text{ mm}$



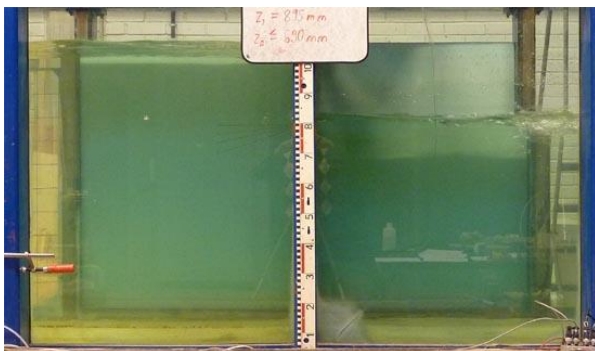
$h_U = 711.2 \text{ mm}$, $Q_A = 281.5 \text{ l/s}$, $Q_T = 420.2 \text{ l/s}$
 $h_D = 492.0 \text{ mm}$, $h_{D^*} = 425 \text{ mm}$



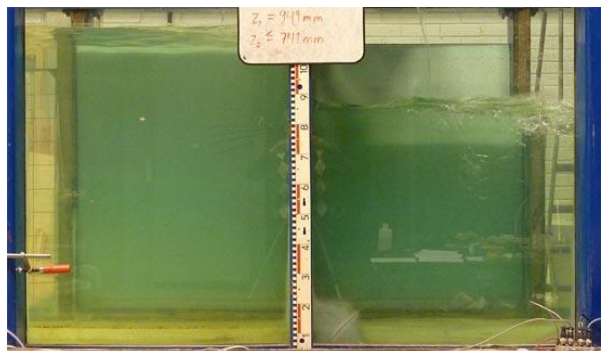
$h_U = 746.5 \text{ mm}$, $Q_A = 281.9 \text{ l/s}$, $Q_T = 413.8 \text{ l/s}$
 $h_D = 538.5 \text{ mm}$, $h_{D^*} = 470 \text{ mm}$



$h_U = 787.1 \text{ mm}$, $Q_A = 280.7 \text{ l/s}$, $Q_T = 409.5 \text{ l/s}$
 $h_D = 584.9 \text{ mm}$, $h_{D^*} = 515 \text{ mm}$



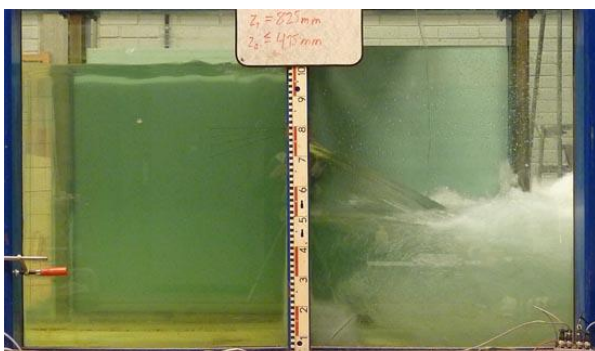
$h_U = 893.6 \text{ mm}$, $Q_A = 280.3 \text{ l/s}$, $Q_T = 410.7 \text{ l/s}$
 $h_D = 690.4 \text{ mm}$, $h_{D^*} > 600 \text{ mm}$



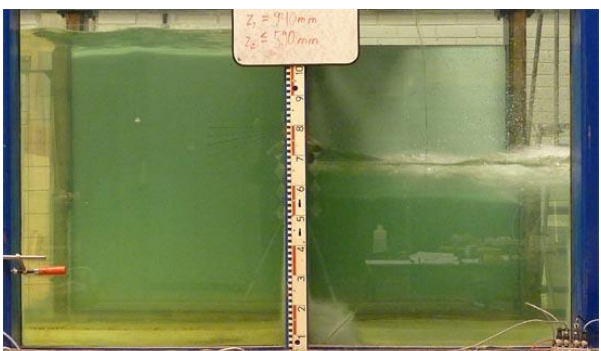
$h_U = 947.3 \text{ mm}$, $Q_A = 281.1 \text{ l/s}$, $Q_T = 414.8 \text{ l/s}$
 $h_D = 740.0 \text{ mm}$, $h_{D^*} > 600 \text{ mm}$

A.5. Test case V6

Partly submerged orifice flow through a full-scale manhole with the actual discharge of approximately $Q_A = 363 \text{ l/s}$. The velocity head was not included in the theoretical discharge computations. The displayed Q_T values are computed with method 2.



$h_U = 822.9 \text{ mm}$, $Q_A = 364.2 \text{ l/s}$, $Q_T = 563.5 \text{ l/s}$
 $h_D = 418.1 \text{ mm}$, $h_{D^*} = 300 \text{ mm}$



$h_U = 936.0 \text{ mm}$, $Q_A = 364.5 \text{ l/s}$, $Q_T = 537.2 \text{ l/s}$
 $h_D = 588.2 \text{ mm}$, $h_{D^*} = 480 \text{ mm}$

A.6. Test case I1

Free flow through a full-scale manhole inclined 20° from upright position towards the upstream. The velocity head was included in the theoretical discharge computations.



$h_U = 120.8 \text{ mm}$, $Q_A = 18.8 \text{ l/s}$, $Q_T = 32.2 \text{ l/s}$



$h_U = 144.5 \text{ mm}$, $Q_A = 25.8 \text{ l/s}$, $Q_T = 45.3 \text{ l/s}$



$h_U = 299.2 \text{ mm}$, $Q_A = 93.3 \text{ l/s}$, $Q_T = 168.5 \text{ l/s}$



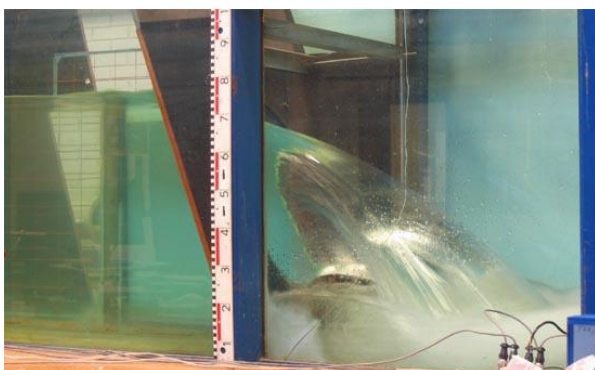
$h_U = 376.8 \text{ mm}$, $Q_A = 138.1 \text{ l/s}$, $Q_T = 249.1 \text{ l/s}$



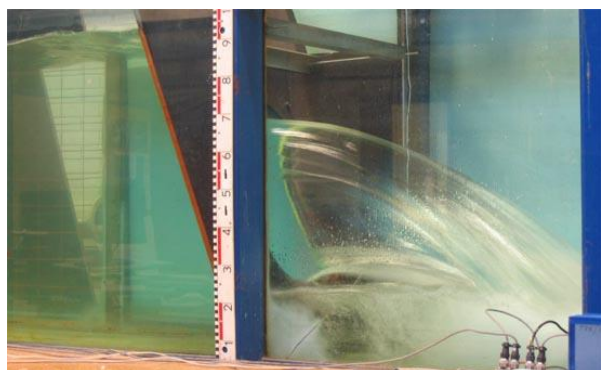
$h_U = 447.5 \text{ mm}$, $Q_A = 183.1 \text{ l/s}$, $Q_T = 331.1 \text{ l/s}$



$h_U = 528.2 \text{ mm}$, $Q_A = 238.0 \text{ l/s}$, $Q_T = 428.2 \text{ l/s}$



$h_U = 597.5 \text{ mm}$, $Q_A = 281.9 \text{ l/s}$, $Q_T = 500.3 \text{ l/s}$



$h_U = 768.0 \text{ mm}$, $Q_A = 365.6 \text{ l/s}$, $Q_T = 631.5 \text{ l/s}$

A.7. Test case I2

Submerged weir flow through a full-scale manhole inclined 20° from upright position towards the upstream with the actual discharge of approximately $Q_A = 93$ l/s. The velocity head was not included in the theoretical discharge computations. The displayed theoretical discharge Q_T values are computed with method 2.



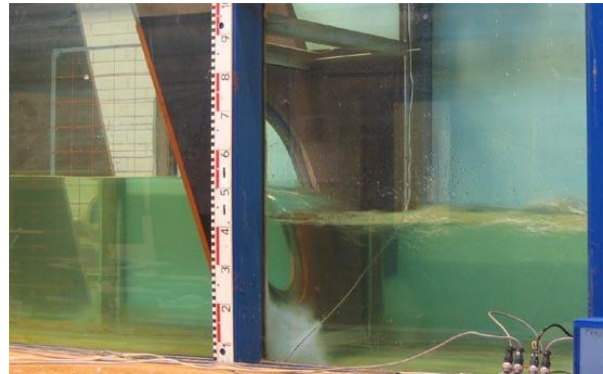
$h_U = 299.0$ mm, $Q_A = 92.8$ l/s, $Q_T = 167.0$ l/s
 $h_D = < 0$ mm, $h_D^* = < 0$ mm



$h_U = 303.2$ mm, $Q_A = 92.8$ l/s, $Q_T = 164.1$ l/s
 $h_D = 112.8$ mm, $h_D^* = 75$ mm



$h_U = 310.5$ mm, $Q_A = 92.7$ l/s, $Q_T = 162.5$ l/s
 $h_D = 154.2$ mm, $h_D^* = 120$ mm



$h_U = 344.0$ mm, $Q_A = 92.5$ l/s, $Q_T = 154.1$ l/s
 $h_D = 255.0$ mm, $h_D^* = 230$ mm



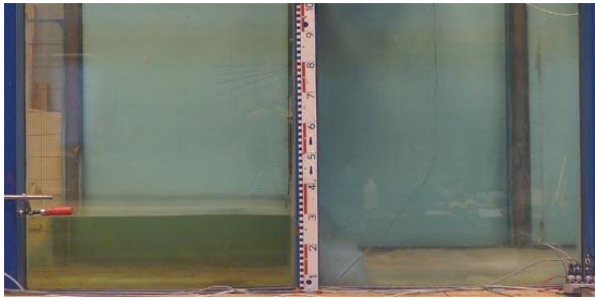
$h_U = 400.6$ mm, $Q_A = 92.7$ l/s, $Q_T = 142.5$ l/s
 $h_D = 352.3$ mm, $h_D^* = 340$ mm



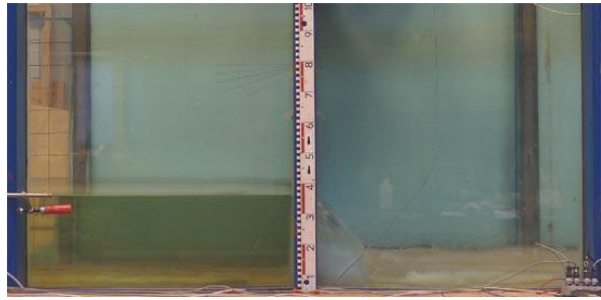
$h_U = 493.3$ mm, $Q_A = 92.9$ l/s, $Q_T = 134.6$ l/s
 $h_D = 466.8$ mm, $h_D^* = 455$ mm

A.8. Test case H1

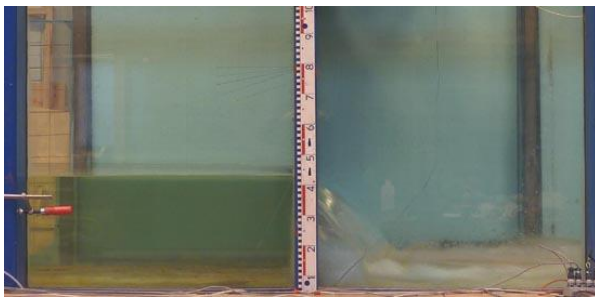
Free flow through a full-scale manhole in horizontal position. The velocity head was included in the theoretical discharge computations.



$h_U = 82.3 \text{ mm}$, $Q_A = 18.5 \text{ l/s}$, $Q_T = 27.8 \text{ l/s}$



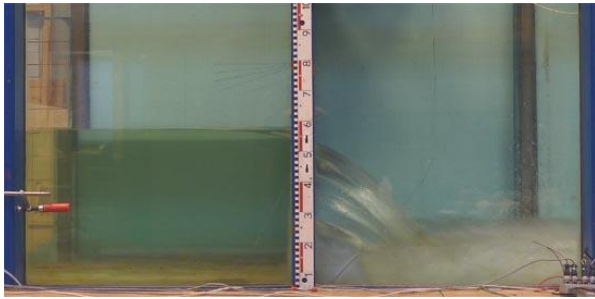
$h_U = 148.9 \text{ mm}$, $Q_A = 49.1 \text{ l/s}$, $Q_T = 78.0 \text{ l/s}$



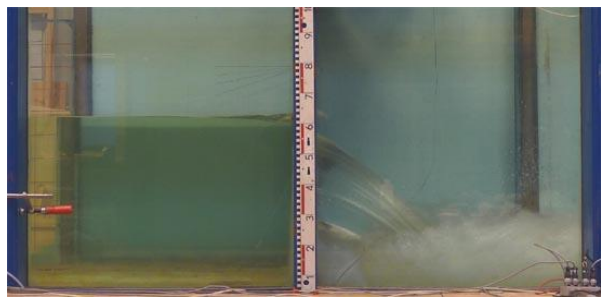
$h_U = 220.4 \text{ mm}$, $Q_A = 94.0 \text{ l/s}$, $Q_T = 153.3 \text{ l/s}$



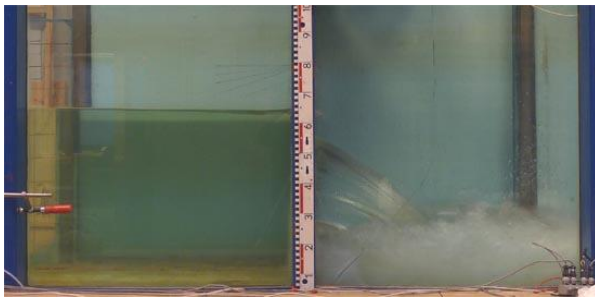
$h_U = 297.2 \text{ mm}$, $Q_A = 152.1 \text{ l/s}$, $Q_T = 252.2 \text{ l/s}$



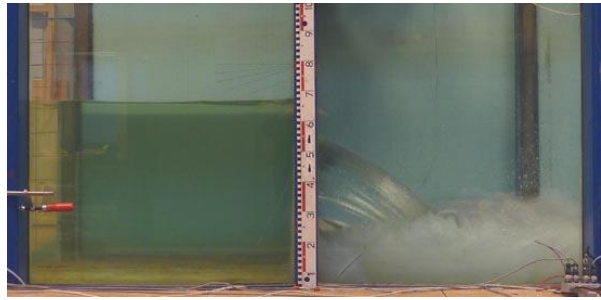
$h_U = 368.0 \text{ mm}$, $Q_A = 211.1 \text{ l/s}$, $Q_T = 351.8 \text{ l/s}$



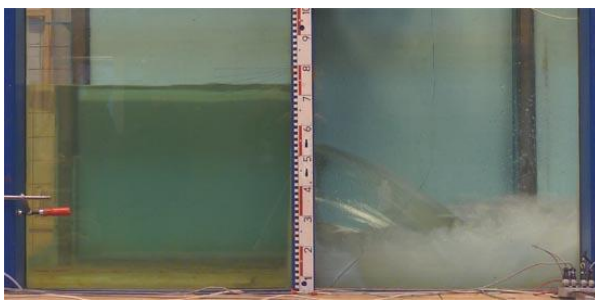
$h_U = 431.2 \text{ mm}$, $Q_A = 259.6 \text{ l/s}$, $Q_T = 431.0 \text{ l/s}$



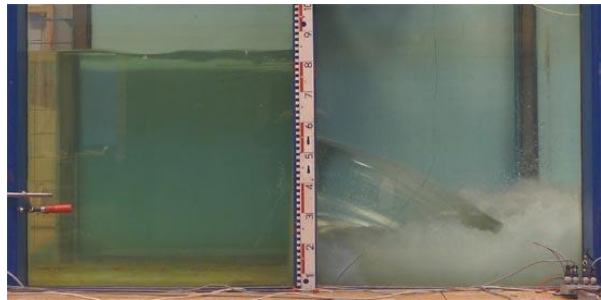
$h_U = 449.3 \text{ mm}$, $Q_A = 269.5 \text{ l/s}$, $Q_T = 449.3 \text{ l/s}$



$h_U = 470.8 \text{ mm}$, $Q_A = 281.1 \text{ l/s}$, $Q_T = 469.9 \text{ l/s}$



$h_U = 544.9 \text{ mm}$, $Q_A = 318.1 \text{ l/s}$, $Q_T = 533.5 \text{ l/s}$



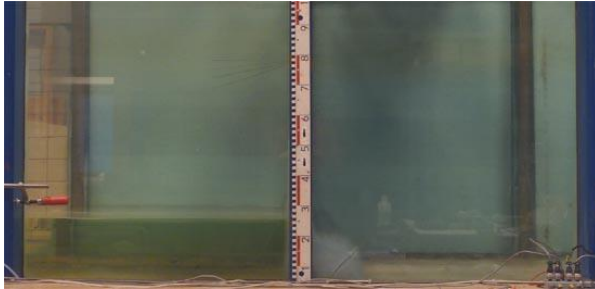
$h_U = 652.5 \text{ mm}$, $Q_A = 362.5 \text{ l/s}$, $Q_T = 612.7 \text{ l/s}$

B. 1:2 scale model manhole

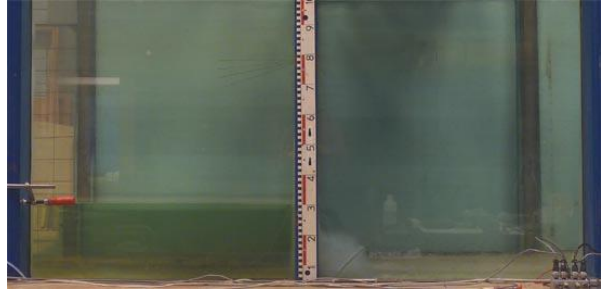
All scale model dimension values have been translated into corresponding full-scale values. The velocity head was not included in the computed theoretical discharges.

B.1. Test case HM1

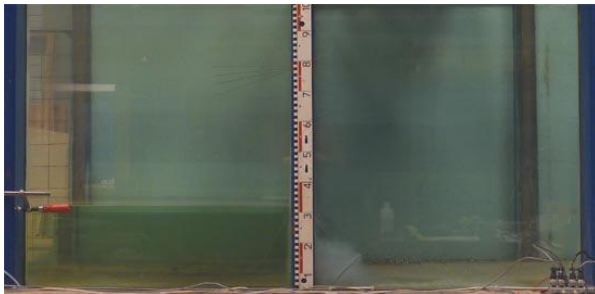
Free flow through a 1:2 scale model manhole in horizontal position.



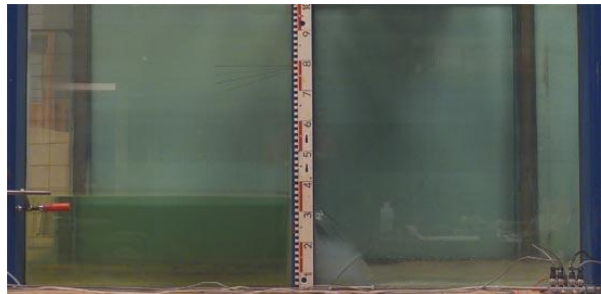
$h_U = 90.3 \text{ mm}$, $Q_A = 20.6 \text{ l/s}$, $Q_T = 32.4 \text{ l/s}$



$h_U = 194.3 \text{ mm}$, $Q_A = 75.0 \text{ l/s}$, $Q_T = 121.8 \text{ l/s}$



$h_U = 227.4 \text{ mm}$, $Q_A = 96.7 \text{ l/s}$, $Q_T = 158.9 \text{ l/s}$



$h_U = 286.1 \text{ mm}$, $Q_A = 139.5 \text{ l/s}$, $Q_T = 232.6 \text{ l/s}$



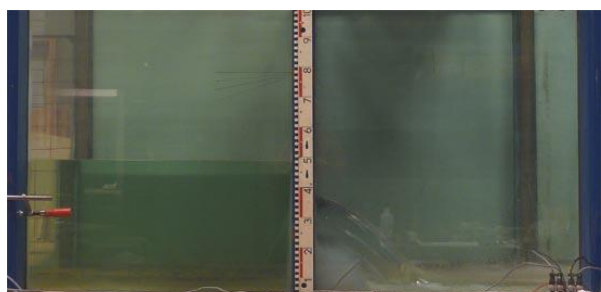
$h_U = 341.4 \text{ mm}$, $Q_A = 183.7 \text{ l/s}$, $Q_T = 307.1 \text{ l/s}$



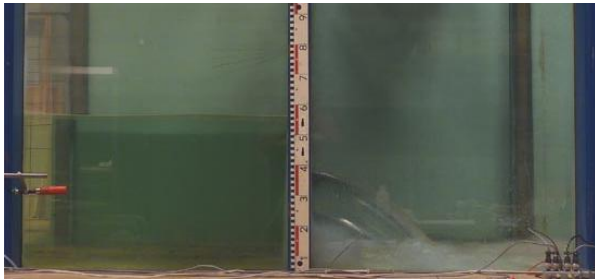
$h_U = 393.0 \text{ mm}$, $Q_A = 227.3 \text{ l/s}$, $Q_T = 378.6 \text{ l/s}$



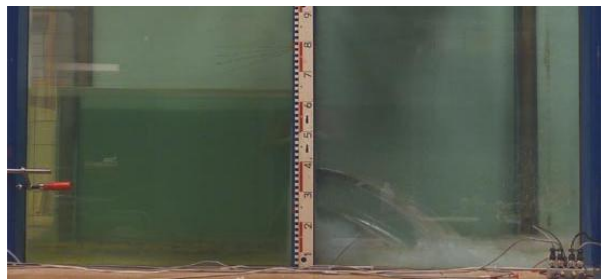
$h_U = 471.5 \text{ mm}$, $Q_A = 282.8 \text{ l/s}$, $Q_T = 463.7 \text{ l/s}$



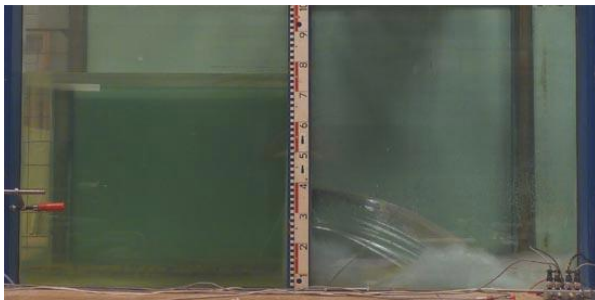
$h_U = 576.8 \text{ mm}$, $Q_A = 333.8 \text{ l/s}$, $Q_T = 552.4 \text{ l/s}$



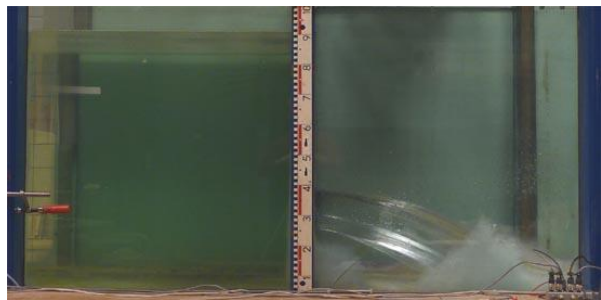
$h_U = 735.0 \text{ mm}$, $Q_A = 403.8 \text{ l/s}$, $Q_T = 661.9 \text{ l/s}$



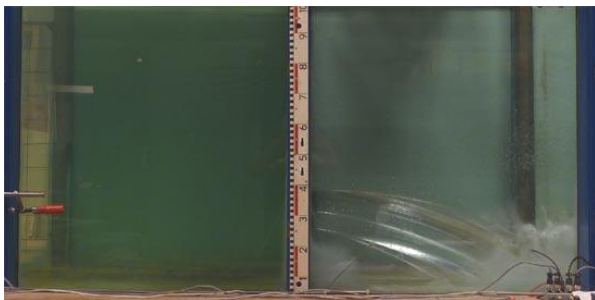
$h_U = 905.0 \text{ mm}$, $Q_A = 459.4 \text{ l/s}$, $Q_T = 761.5 \text{ l/s}$



$h_U = 1143.4 \text{ mm}$, $Q_A = 530.8 \text{ l/s}$, $Q_T = 882.0 \text{ l/s}$



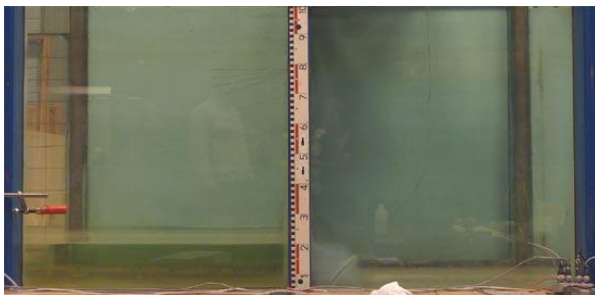
$h_U = 1447.8 \text{ mm}$, $Q_A = 610.2 \text{ l/s}$, $Q_T = 1015.2 \text{ l/s}$



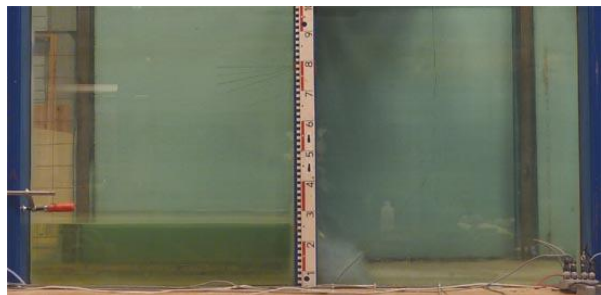
$h_U = 1845.0 \text{ mm}$, $Q_A = 699.6 \text{ l/s}$, $Q_T = 1166.0 \text{ l/s}$

B.2. Test case VM1

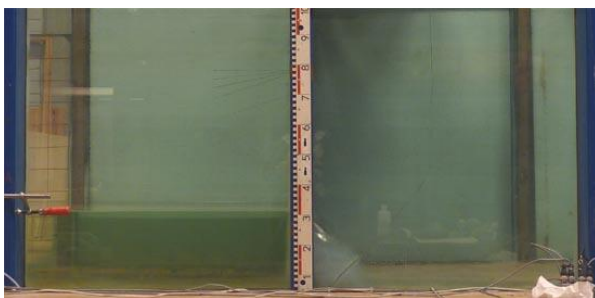
Free flow through a 1:2 scale model manhole in vertical position.



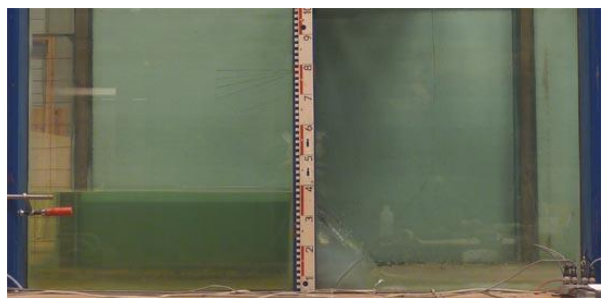
$h_U = 72.0 \text{ mm}$, $Q_A = 7.7 \text{ l/s}$, $Q_T = 10.8 \text{ l/s}$



$h_U = 196.3 \text{ mm}$, $Q_A = 46.0 \text{ l/s}$, $Q_T = 73.2 \text{ l/s}$



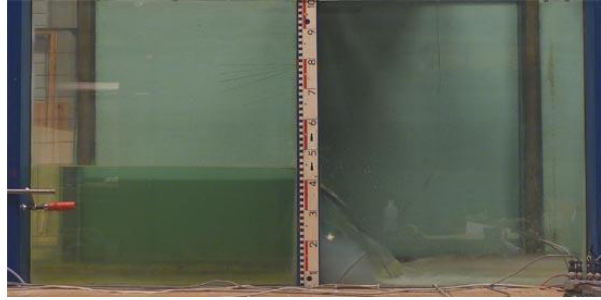
$h_U = 303.7 \text{ mm}$, $Q_A = 96.7 \text{ l/s}$, $Q_T = 159.5 \text{ l/s}$



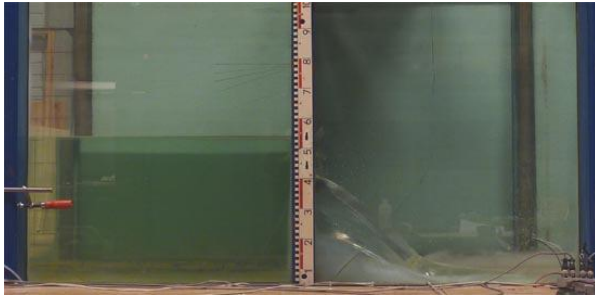
$h_U = 445.1 \text{ mm}$, $Q_A = 181.1 \text{ l/s}$, $Q_T = 303.1 \text{ l/s}$



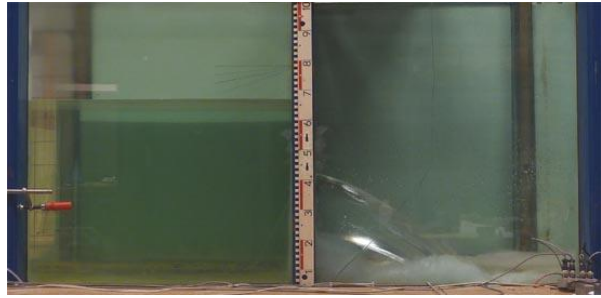
$h_U = 508.5 \text{ mm}$, $Q_A = 224.3 \text{ l/s}$, $Q_T = 376.5 \text{ l/s}$



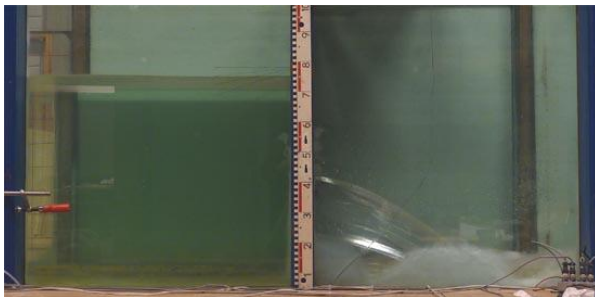
$h_U = 583.7 \text{ mm}$, $Q_A = 276.4 \text{ l/s}$, $Q_T = 461.9 \text{ l/s}$



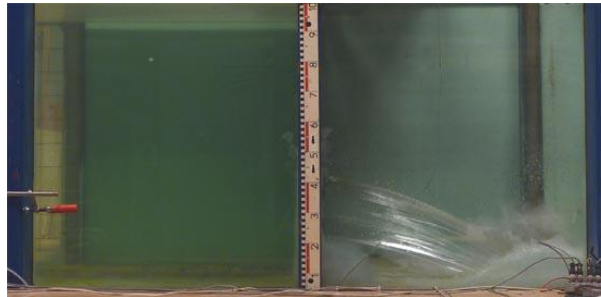
$h_U = 785.4 \text{ mm}$, $Q_A = 380.4 \text{ l/s}$, $Q_T = 626.5 \text{ l/s}$



$h_U = 1060.9 \text{ mm}$, $Q_A = 478.0 \text{ l/s}$, $Q_T = 791.0 \text{ l/s}$



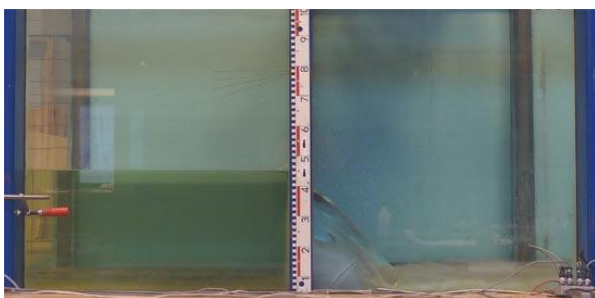
$h_U = 1233.9 \text{ mm}$, $Q_A = 528.5 \text{ l/s}$, $Q_T = 877.7 \text{ l/s}$



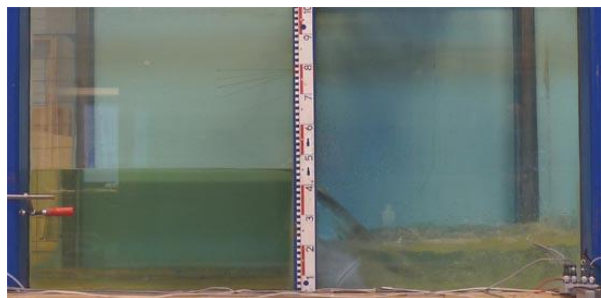
$h_U = 1806.1 \text{ mm}$, $Q_A = 670.1 \text{ l/s}$, $Q_T = 1116.6 \text{ l/s}$

B.3. Test case VM2

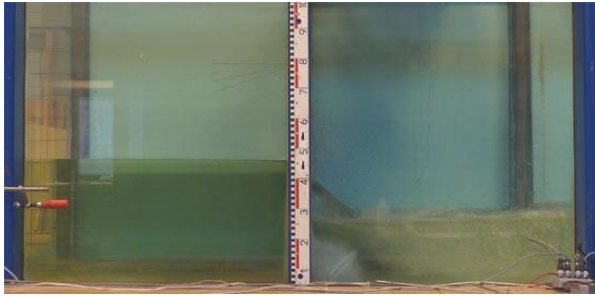
Partly and completely submerged orifice flow through 1:2 scale model manhole with the actual discharge of approximately $Q_A = 290 \text{ l/s}$ (51.2 l/s).



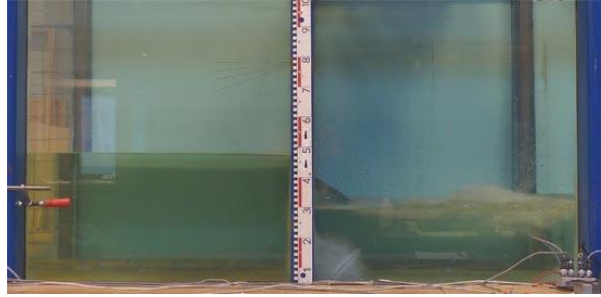
$h_U = 605.9 \text{ mm}$, $Q_A = 289.6 \text{ l/s}$, $Q_T = 483.6 \text{ l/s}$
 $h_D < 0 \text{ mm}$, $h_D^* < 0 \text{ mm}$



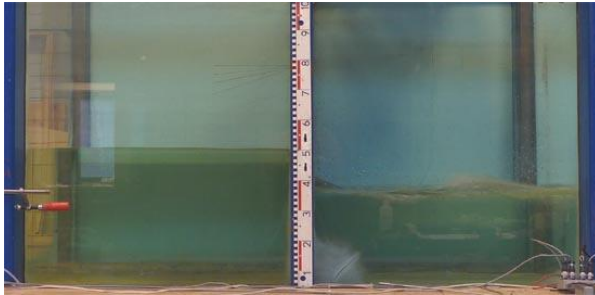
$h_U = 608.8 \text{ mm}$, $Q_A = 289.8 \text{ l/s}$, $Q_T = 482.3 \text{ l/s}$
 $h_D = 122.6 \text{ mm}$, $h_D^* = 80 \text{ mm}$



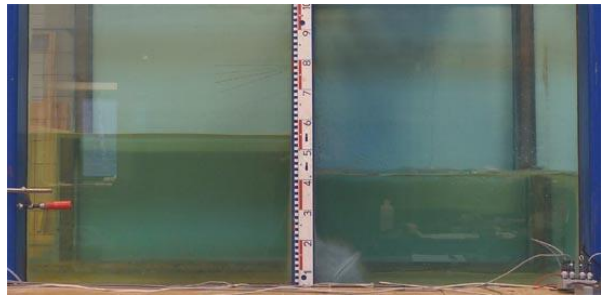
$h_U = 621.7 \text{ mm}$, $Q_A = 290.0 \text{ l/s}$, $Q_T = 476.3 \text{ l/s}$
 $h_D = 225.5 \text{ mm}$, $h_D^* = 190 \text{ mm}$



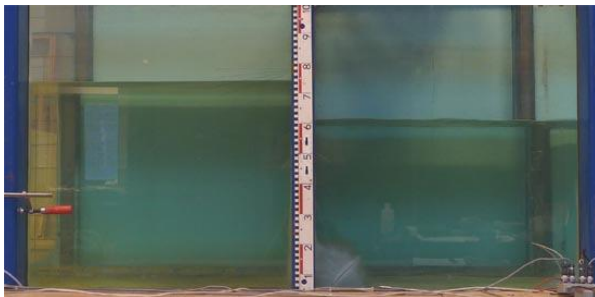
$h_U = 656.1 \text{ mm}$, $Q_A = 290.4 \text{ l/s}$, $Q_T = 472.9 \text{ l/s}$
 $h_D = 327.8 \text{ mm}$, $h_D^* = 290 \text{ mm}$



$h_U = 716.5 \text{ mm}$, $Q_A = 290.1 \text{ l/s}$, $Q_T = 461.9 \text{ l/s}$
 $h_D = 444.2 \text{ mm}$, $h_D^* = 420 \text{ mm}$



$h_U = 812.0 \text{ mm}$, $Q_A = 290.4 \text{ l/s}$, $Q_T = 448.6 \text{ l/s}$
 $h_D = 569.3 \text{ mm}$, $h_D^* = 550 \text{ mm}$



$h_U = 1214.1 \text{ mm}$, $Q_A = 289.8 \text{ l/s}$, $Q_T = 457.1 \text{ l/s}$
 $h_D = 962.4 \text{ mm}$, $h_D^* = 950 \text{ mm}$

C. Girder test cases G1-G7

Most tests with the 1:3 scale model girder were conducted in submerged flow conditions, which means that there is not much to observe visually.



The stiffeners were pointing downstream in test case G3.



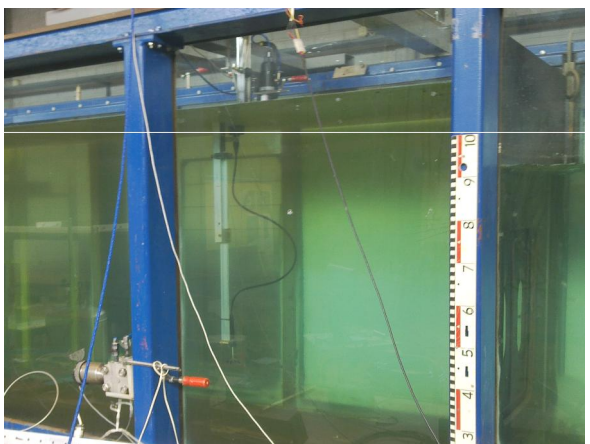
The stiffeners were pointing upstream in test case G4.



The hydrostatic pressure bends the model girder, which is made of 6 mm thick plywood (test case G3).



The downstream water surface was quite turbulent with low downstream water levels (G4).



The velocity field on the upstream side of the girder was measured with a 3D ADV device.



The velocities on the downstream side of the girder was measured with a Prandtl tube.

D. Cross-duct



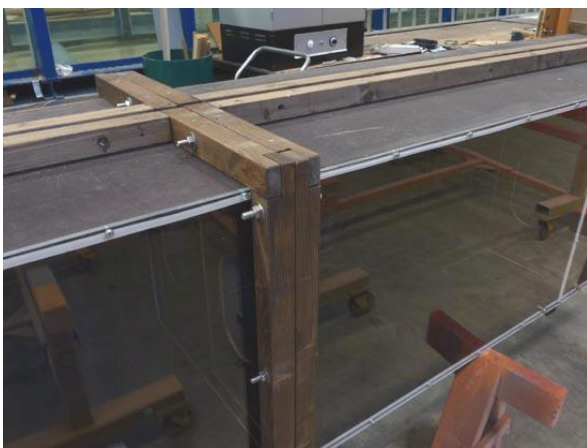
The cross-duct model before test case C1.



The end girder of the cross-duct modules were equipped with band seals in order to make joints waterproof.



There was an opening on the top of the cross-duct for the web frame plates. The opening was sealed with a plywood plate during the tests.



The cross-duct modules were attached to each other with bolts through the supporting wooden frame.



Test case C1.



Test case C1. The downstream water level was raised with a tailgate.



The downstream end of the cross-duct during test case C1.



The upstream end of the cross-duct with the dam plate during test case C1.



After test case C1, the plexus glass was removed and model stiffeners were added into the compartments and girders. The plexus glass was then fastened again.



Inside view of a cross-duct compartment with stiffeners attached to the bed, roof and girders.



The stiffeners in the compartment roof were made of two parts in order to leave space for the web- frame plate.



Two cross-duct modules with stiffeners in place and bolted together before test case C2.



Test case C2.



Some leakage was observed between the web-frame plate and the roof of the cross-duct.



Test case C2.



The web-frame plate is fitted in place.



In test case C4 the cross-duct was inclined 7° towards the upstream side. The flow range was very limited due to the flume height. The picture is taken before the test.



The downstream end of the cross-duct during test case C4.



The cross-duct model consisted of just one module in test case C5.



All three cross-duct modules were used in test case C6.